ATLAS PUB Note

ATL-PHYS-PUB-2017-005

Multi-Boson Simulation for 13 TeV ATLAS Analyses

The ATLAS Collaboration

2nd May 2017
Revised: 1st February 2018

This note describes the Monte Carlo setup used by ATLAS to model multi-boson processes in 13 TeV pp collisions. The baseline Monte Carlo generators are compared with each other in key kinematic distributions of the processes under study. Sample normalisation and assignment of systematic uncertainties are discussed.

Figures 1, 2, 3 and 19 have been updated to correct an error in the dressing of leptons in the analysis which affected only the Sherpa predictions in these figures.
The text in Subsection 4.1.2 has been adjusted to state the actual scale choice.

ATL-PHYS-PUB-2017-005
07/05/2018

Contents

1 Introduction

Measurements of multi-boson production at the Large Hadron Collider (LHC) provide an excellent test of the electroweak sector in the Standard Model (SM). The production of multiple heavy gauge bosons V ($= W^{\pm}, Z$) opens up a multitude of potential decay channels categorised according to the number of charged leptons in the final state. Numerous Monte Carlo (MC) tools exist to simulate the various multi-boson production processes involving additional jets.

This note documents the Monte Carlo setup used by ATLAS to model multi-boson processes in proton-proton collisions at a centre-of-mass energy of 13 TeV. The note is organised as follows: The baseline generators employed throughout are first introduced in Section 2. The fully leptonic diboson processes are described in Section 3, followed by diboson processes involving electroweak dijet production (such as vector boson scattering) in Section 4. Loop-induced diboson processes are covered in Section 5 and semi-leptonic diboson processes are discussed in Section 6. Triboson production processes (VVV) are

dealt with in Section 7, followed by $V\gamma$ production Section 8. Finally, the Conclusions are given in Section 9.

2 Baseline generators

Several samples described in the following are generated using the Sherpa and PowhegBox generators. This section collects general information about the versions and configurations of these generators used, while process-specific information about the samples and information about further generators used can be found in the relevant sections.

2.1 Sherpa

Sherpa [1] is a parton shower Monte Carlo generator simulating additional hard parton emissions [2] that are matched to a parton shower based on Catani-Seymour dipoles [3]. The NLO+PS matching [4] is employed for different jet multiplicities which are then merged into an inclusive sample using the MEPS@NLO approach [5]. For NLO matrix elements, virtual QCD corrections are provided by the OpenLoops library [6] using the Collier tensor integral reduction library [7].

The following versions and configurations of Sherpa have been employed:

Sherpa v2.1.1 The default setup provided by the Sherpa authors is used and includes a tuning based on CT10NLO PDFs [8]. The following particle properties have been set to more recent PDG values than in the default Sherpa release:

- $m_t = 172.5$ GeV, $m_Z = 91.1876$ GeV, $m_W = 80.399$ GeV
- $\Gamma_Z = 2.4952$ GeV, $\Gamma_W = 2.085$ GeV, $\Gamma_\tau = 2.26735 \cdot 10^{-12}$ GeV

Sherpa v2.2.1 The default setup provided by the Sherpa authors is used and includes a tuning based on NNPDF3.0 NNLO parton density functions [9]. In addition to the PDG modifications given above the top width was also adjusted to $\Gamma_t = 1.32$ GeV.

To assess systematic uncertainties, all ATLAS samples generated with Sherpa v2.2.1 and later are set up to include on-the-fly variation event weights accounting for a 7-point scale variation and PDF variations in the matrix elements. For the scale variations, the factorisation and renormalisation scales are varied independently by factors of 0.5 and 2 but avoiding opposite factors. For the nominal PDF set weights for 100 variation replicas are included, as well as the $\alpha_S = 0.117$ and $\alpha_S = 0.119$ variations. Additionally, weights using the central values of the CT14NNLO [10] and MMHT2014NNLO [11] PDF sets are stored.

Unless otherwise stated in the process-specific sections, electroweak parameters are specified in the over-constrained scheme EW_SCHEME=0, enforcing an effective weak mixing angle $\sin^2\theta_w = 0.23113$ instead of the one given by LO tree-level relations.

Sherpa v2.2.2 The only relevant difference with respect to `v2.2.1` is a bug fix in the bookkeeping of process groups, where lepton flavours were wrongly mapped in the subtracted real-emission contribution of NLO matrix elements, thus leading to a wrong flavour composition if multiple lepton flavours were generated simultaneously in one sample. This affected only the fully leptonic diboson samples described in Sec. 3 and will have only a negligible impact on the modelling of the observables shown there.

All configuration options are identical to the ones given above for `v2.2.1`.

2.2 PowhegBox

`PowhegBox` [12–14] provides a general framework for implementing NLO QCD calculations with shower Monte Carlo programs based on the `Powheg` method. A library of processes is available which can be interfaced with shower Monte Carlo programs through the Les Houches Interface [15, 16]. In this note, `PowhegBox v2` interfaced to `PYTHIA v8.212` [17] for parton showering is used. All samples utilise the G_μ scheme with m_W, m_Z and G_μ as electroweak input parameters. Generally, the following PDG [18] values are used in VV samples: $m_W = 80.399$ GeV, $m_Z = 91.1876$ GeV, $G_\mu = 1.166364 \times 10^{-5}\,\mathrm{GeV}^{-2}$. The electroweak $W^\pm W^\pm jj$ samples use an older set of input parameters from PDG [19], which should have no significant impact on the studies presented here.

In addition, other dedicated generators have been used for certain signatures. These will be introduced in the relevant sections.

3 Fully leptonic diboson processes

This section describes processes of four-lepton production including all lepton and neutrino flavors, where τ leptons subsequently can decay leptonically or hadronically. The processes are grouped according to the number of charged leptons, giving rise to the following final states: 4ℓ, $3\ell\nu$, $2\ell 2\nu$, $\ell 3\nu$ and 4ν. Note that the lepton charges in the $2\ell 2\nu$ are of opposite sign. A dedicated sample for the $2\ell 2\nu jj$ final state, where the two lepton charges are of equal sign, has been generated as well. An overview of the accuracy achieved with the chosen generators is given in Table 1.

Table 1: Overview of process accuracies for the generators.

	$VV + 0j$	$VV + 1j$	$VV + 2j$	$VV + 3j$	$VV + \geq 4j$
Sherpa v2.2	NLO	NLO	LO	LO	PS
PowhegBox+PYTHIA8 /HERWIG++	NLO	LO	PS	PS	PS
MadGraph5_aMC@NLO +PYTHIA8	NLO	NLO	LO	PS	PS
MC@NLO +HERWIG	NLO	LO	PS	PS	PS

3.1 Generator setup

3.1.1 Sherpa

Event samples for the fully leptonic diboson processes have been generated using Sherpa v2.2 with up to three additional partons in the matrix element, including up to one additional parton at NLO accuracy. A generator-level cut of 5 GeV on the transverse momentum of the two highest-p_{T} leptons is imposed for these samples. Furthermore, the dilepton invariant mass $m_{\ell\ell}$ is required to exceed 4 GeV. The $2\ell 2\nu$ final state has been generated without bottom quarks in the hard scattering process, to avoid contributions from top-quark mediated processes.

EXCLUSIVE_CLUSTER_MODE has been enabled for all samples (including same-sign $2\ell 2\nu$), ensuring that only QCD splittings are inverted by the clustering algorithm, thus allowing for the leptons to be associated with the core process. The factorisation and renormalisation scales were set using the STRICT_METS scale setter with a core scale of $\mu = m_{\mathrm{VV}}$.

3.1.2 PowhegBox

PowhegBox is used to generate the WW, WZ and ZZ [20, 21] processes to NLO precision in QCD. The samples are split according to the charged lepton multiplicity (4ℓ, $3\ell\nu$, $2\ell 2\nu$, $\ell 3\nu$, 4ν) of the final state. However, each sample is inclusive regarding the lepton flavor. All final states include the effect of off-shell singly resonant amplitudes, and the WZ and ZZ samples include the effects of Z/γ^* interference. Interference effects due to identical leptons in the final state are included as well, but are ignored between WW and ZZ for the common decay mode to same-flavor opposite-charge leptons and a pair of neutrinos – a negligible effect at Born level [20].

Samples are generated using PowhegBox v2, base revision r3033. The specific PowhegBox process version is r2819 for each diboson (WW, WZ, ZZ) sample. Events are generated using the CT10 NLO [8] PDF and then showered with PYTHIA8 using the AZNLO [22] tune and the CTEQ6L1 [23] PDF for the shower.

The EvtGen [24] afterburner is used to ensure that heavy quarks are properly decayed. The dynamic scale of the mass of the boson pair is used for both the factorisation and renormalisation scales. The withdamp and bornzerodamp flags were set in PowhegBox for each sample to ensure that any phase-space region in which the Born cross section vanishes is properly handled.

Samples with alternative parton shower modeling are generated by showering PowhegBox matrix elements with HERWIG ++ v2.3.3 [25]. Unlike the p_{T} ordering of parton showers employed in the PYTHIA8, HERWIG makes use of the angular ordering of parton showers. The PowhegBox+HERWIG samples are generated using CT10 NLO PDF for matrix elements and UE-EE-5 tune with CTEQ6L1 PDF for PS.

A matrix element level generator cut is placed on the Z boson decay products in the case that they are charged leptons, requiring the mass of the charged lepton pair to be greater than 4 GeV. If there are two Z bosons decaying to like-flavored charged leptons, the cut is applied to the two possible pairings.

3.1.3 MadGraph5_aMC@NLO

MadGraph5_aMC@NLO [26] v2.3.3 is used to generate fully leptonic diboson processes corresponding to the decay modes 4ℓ, $3\ell\nu$ and $2\ell 2\nu$. Their matrix elements are simulated in association with up-to one additional parton with NLO precision, thus diagrams with two additional partons in the final state are included at LO. As for the samples generated with Sherpa, bottom quarks are not included in the hard scattering process and both the factorisation and renormalisation scales are set dynamically per event using the scalar p_{T} sum of all final state particles generated at the matrix element stage.

Events are generated using the PDF set NNPDF3.0 with $\alpha_S = 0.118$ and the PYTHIA8 A14 shower tune [27]. Here, a generator level cut is set to the invariant mass of all oppositely-signed same-flavour lepton pairs, such that events are vetoed if their $m_{\ell\ell}^{SF}$ is below a threshold of 4 GeV.

Overlaps between identical partonic final states generated at the matrix element and the parton shower stage are removed using the FxFx merging [28], where the merging scale qcut and the scale at which the matrix elements are regularised qcutME are set to 20 GeV and 10 GeV, respectively.

3.1.4 MC@NLO

MC@NLO 4.0 [29] is used to generate the WZ and WW processes with $3\ell\nu$ and $2\ell 2\nu$ decay modes accordingly. The matrix elements are calculated at NLO precision in QCD, using the CT10 PDF set. MC@NLO is interfaced with HERWIG and JIMMY [30] for the simulation of the parton shower, hadronisation and underlying event using AUET2 CT10 tune.

These samples are particularly interesting due to the inclusion of event-by-event weights for anomalous couplings [31]. They can be reweighted to any arbitrary value and combination of anomalous couplings, reproducing the differential distributions of anomalous WZ and WW production without the need to generate and simulate several samples. For the validity of anomalous coupling studies, it is important that the Standard Model distributions are well-described.

3.2 Systematic uncertainties

3.2.1 Uncertainties due to choice of QCD scale

The MCFM [32, 33] Monte Carlo program allows the evaluation of NLO cross section predictions for a variety of processes at hadron colliders as well as LO "Les Houches event" (LHE) [16] generation for a subset of these processes. The NLO cross sections for 13 TeV WW, WZ and ZZ production with fully leptonic decay modes are evaluated using MCFM v7.0.1 with CT10 NLO PDF and a dynamic scale of $m_{VV}/2$ for renormalisation and factorisation scales. The Z boson mass range evaluated is 66 – 116 GeV, and non-resonant $gg \to WW$ and $gg \to ZZ$ production is included at LO. Scale uncertainties are derived using the maximum and minimum values when varying renormalisation and factorisation scales independently by factors of two. The resulting uncertainties are found to be at the 4–5 % level, depending on the process under study. CT10 PDF uncertainties are derived from the eigenvector error sets as described in Reference [34] and scaled to 68 % CL, yielding an $\approx$ 2% uncertainty for the processes studied. Adding both uncertainties in quadrature, a (conservative) uncertainty of 6 % is used for the total NLO WW, WZ and ZZ production cross sections.

The MCFM cross sections are only used to evaluate the systematic uncertainties as detailed above and not to normalise the samples discussed in this section. Since the generators of these samples already have NLO accuracy themselves, their native cross sections are used. On the other hand prediction of NNLO QCD accuracy [35–38] exceed for some processes and phase space regions the NLO cross section and its uncertainty. Therefore comparisons to those calculations are performed in some cases as well.

3.2.2 On-the-fly variations for the Sherpa samples

Perturbative generator uncertainties can be estimated in Sherpa v2.2 using its variation framework [39]. The event weights due to scale and PDF variations are generated on-the-fly and stored with each event. They include 7-point scale variations of the factorisation and the renormalisation scales, two α_S variations by ± 0.02 around the nominal value of 0.118 as well as a PDF uncertainty estimated using the NNPDF3.0nnlo replicas.

3.2.3 On-the-fly variations for the PowhegBox samples

To enable studies of systematic uncertainties due to PDF and scale variations, the PowhegBox samples were generated including weights corresponding to:

- independent variations of renormalisation and factorisation scales by a factor of two (nine variations including the nominal scale settings),
- PDF variations for the CT10 NLO [8] eigenvector error sets (52 variations) and central values of MSTW2008 NLO [40], NNPDF3.0 [9] PDFs.

3.3 Generator comparisons

In the following we provide validation plots with different object definitions and event selections. Where jets are used, they are reconstructed using the anti-k_t clustering algorithm [41] with a jet-radius parameter of $R = 0.4$. The jet transverse momentum is required to be greater than 30 GeV. The distance between jets and leptons is required to be $\Delta R_{\ell j} = \sqrt{\Delta\eta_{\ell j} + \Delta\phi_{\ell j}} > 0.1$ in η-ϕ space[1]. In case of overlap, the jet is removed if $E_\ell / E_{\text{jet}} > 0.5$, otherwise the lepton is removed. Leptons four-vectors are built by adding the four-vector of photons in a cone of $\Delta R_{\ell j} < 0.1$ centred on the lepton. Photons originating from decays of hadrons are ignored. Moreover, photons are assigned to their nearest lepton in η-ϕ space in order to avoid double counting. Further details of the selections are given in the respective subsections.

3.3.1 4ℓ final state

This section summarises some basic generator validation for ZZ diboson production with subsequent decay into charged leptons. Moreover, there are attempts presented which are followed to incorporate high order effects beyond the generator accuracy. There is a detailed discussion on the advantages, disadvantages and compromises coming along when this additional modeling is applied. Even though loop-induced production of Z boson pairs is part of the process at next-to-next-to-leading order it can be encapsulated because of its pure gluon initial state. Following this distinction it is not part of this section, however, more explicit explanations can be found in Section 5.

The generator comparison is performed in the fiducial phase space of the ATLAS Higgs analyses [42, 43] which is more inclusive than the one used in the Standard Model analysis [44] as the Z boson is allowed to be more off-shell. The selection criteria for the charged leptons and eventually the events are given in Table 2.

At first there is a general shape comparison between `PowhegBox` and `Sherpa v2.2` shown in Figure 1. The distributions are normalised to the samples' cross section and there is no reweighting applied. The four-lepton invariant mass, which is an observable quite insensitive to higher-order QCD effects, shows good agreement above the ZZ threshold between the two generators. The deviations below this threshold can be related to differences in both the QCD and the electroweak shower which is fully based on `PYTHIA8` in case of `PowhegBox` while `Sherpa` uses its own shower model. Distributions explicitly sensitive to QCD effects like the transverse momentum of the four-leptons system or the ϕ distance between the two Z bosons show growing deviations for higher values as expected. These differences are likely due to `Sherpa` including up to one jet at NLO, and two or three jets at LO, while `PowhegBox` includes only one jet at LO accuracy.

In addition to the QCD effects mentioned above, higher-order electroweak corrections can also significantly affect several observables, particularly in the tails of the distributions. In Figure 2 the default `Sherpa` prediction is compared to its prediction reweighted to take next-to-leading order weak effects into account. The corrections are based on recent calculations for different flavor [45] and same flavor leptons [46] in the final state. In this case special care is taken to match the electroweak scheme used in `Sherpa` and the calculation. Finally, since for example final state photon radiation is already modeled by

[1] ATLAS uses a right-handed coordinate system with its origin at the nominal interaction point (IP) in the centre of the detector and the z-axis along the beam pipe. The x-axis points from the IP to the centre of the LHC ring, and the y-axis points upward. Cylindrical coordinates (r, ϕ) are used in the transverse plane, ϕ being the azimuthal angle around the z-axis. The pseudorapidity is defined in terms of the polar angle θ as $\eta = -\ln\tan(\theta/2)$.

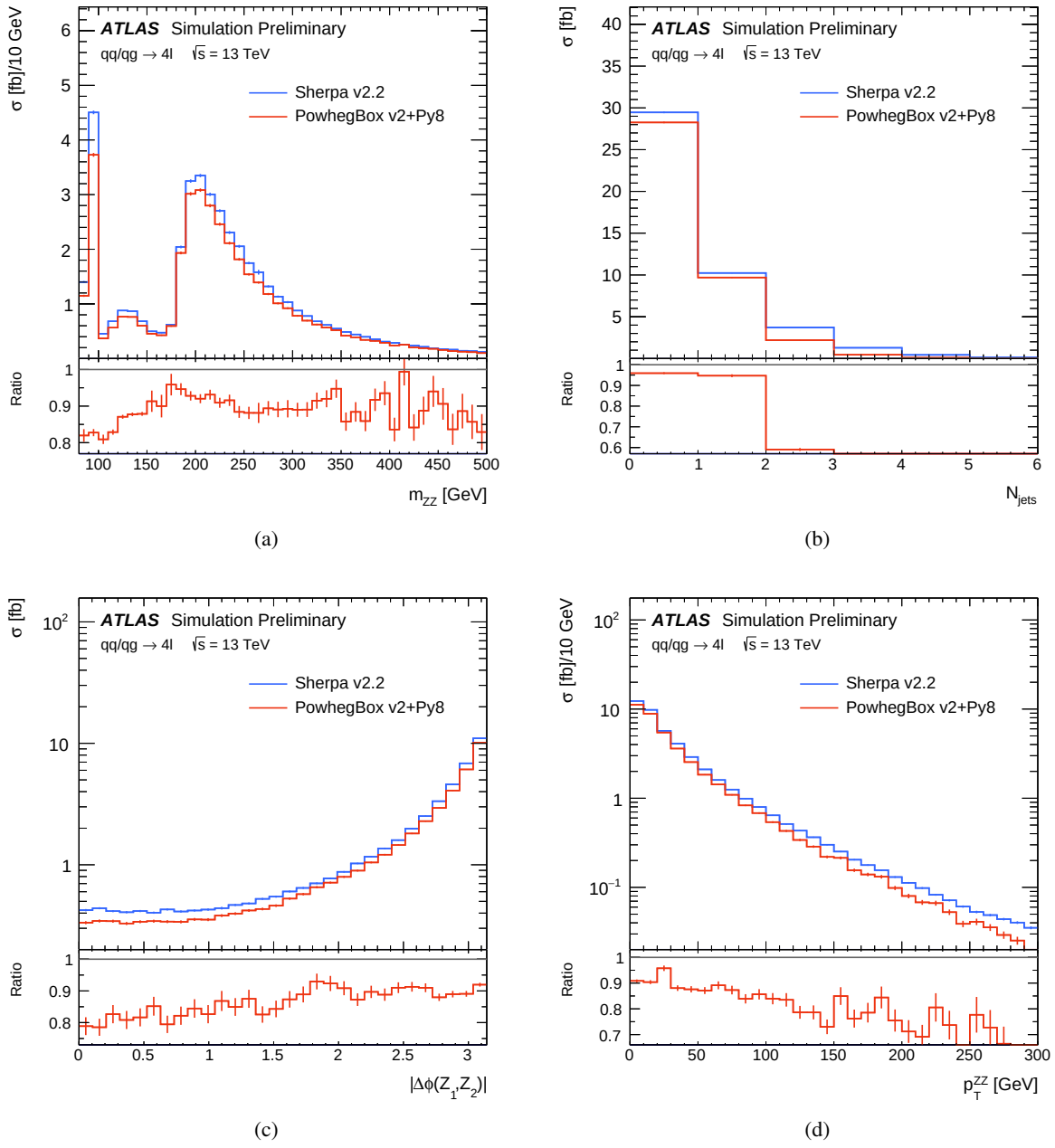

Figure 1: Comparison of shapes normalised to the samples' cross section and combining all four channels, namely $4e$, 4μ, $2e2\mu$ and $2\mu2e$, as predicted by `PowhegBox` and `Sherpa`. While for the four-lepton invariant mass (a) there is good agreement because it is not strongly sensitive to higher-order QCD effects, there is a difference in the jet multiplicity (b), the distance in ϕ of the two Z bosons (c) and the transverse momentum of the four lepton system (d). The ratio in the lower panels is taken with respect to the `Sherpa` prediction.

Table 2: Definitions of the event selection employed for studies of $ZZ \to 4\ell$ and $ZZ \to 2\ell 2\ell'$ final states. In these definitions, ℓ/ℓ' are the charged leptons from the decays $Z \to e^+e^-$ and $Z \to \mu^+\mu^-$. The primary Z boson (Z_1) is the same-flavor opposite-charge lepton pair with invariant mass $m(\ell^+, \ell^-)$ closest to the Z mass $m_Z = 91.1876\,\text{GeV}$ while the secondary Z boson (Z_2) is a remaining same-flavor opposite-charge leptons pair with $m(\ell^+, \ell^-)$ next-closest to m_Z.

lepton selection

electrons	$E_\text{T} > 7\,\text{GeV}$, $\lvert\eta\rvert < 2.47$
muons	$p_\text{T} > 6\,\text{GeV}$, $\lvert\eta\rvert < 2.7$
lepton separation	$\Delta R(\ell, \ell) > 0.1$ for same flavor $\Delta R(\ell, \ell') > 0.2$ for different flavor
ordered p_T requirement	$p_\text{T}^3 > 10\,\text{GeV}$, $p_\text{T}^2 > 15\,\text{GeV}$, $p_\text{T}^1 > 20\,\text{GeV}$

event selection

J/Ψ veto	no same-flavor opposite-charge lepton pair with $m(\ell^+, \ell^-) < 5\,\text{GeV}$		
on-shell requirement			$50 < \frac{m(Z_1)}{\text{GeV}} < 106$
sliding mass selection	$m(4\ell) < 140\,\text{GeV}$	:	$12 < \frac{m(Z_2)}{\text{GeV}} < 115$
	$140 < \frac{m(4\ell)}{\text{GeV}} < 190$	:	$12 + \left(\frac{m(4\ell)}{\text{GeV}} - 140\right) \cdot 0.76 < \frac{m(Z_2)}{\text{GeV}} < 115$
	$m(4\ell) > 190\,\text{GeV}$	:	$50 < \frac{m(Z_2)}{\text{GeV}} < 115$

the shower, the calculation explicitly exclude higher-order QED effects to avoid potential double counting. Higher-order electroweak effects are rather sensitive to lepton and event selection criteria, and are therefore calculated separately for each of the four channels $4e$, 4μ, $2e2\mu$ and $2\mu 2e$. Even though all the distributions in this figure are reweighted based on the four-lepton invariant mass, it is more appropriate to calculate reweighting factors per observable to avoid mis-modeling caused by an incomplete description of the full event kinematics when just reweighting in the invariant mass. This is in particular important for analyses aiming for triple gauge couplings by studying for example the transverse momentum of the more energetic Z boson.

A comparison of modeled differential cross sections predicted by `Sherpa` and `PowhegBox` is shown in Figure 3. While the predictions of both generators are similarly corrected for higher-order electroweak effects, there is an additional reweighting applied for `PowhegBox` intended to bring it from NLO to approximately NNLO QCD accuracy [38]. The correction is based on k-factors calculated in a inclusive setup only including loose constraints on the Z bosons' masses and differential in the four-lepton invariant mass. With the `Sherpa` approach of back-clusterisation of jets to the NLO matrix element it is de facto of the same accuracy for one and two jets and even more accurate for three jets. The NNLO QCD calculation is only of higher precision if no jets are present. While additional accuracy could be obtained by merging the NNLO prediction for zero-jet events with the higher-accuracy NLO predictions for one or more jets, this is not done here. Except for the deviations below the ZZ threshold mentioned earlier there is reasonable agreement of the four-lepton invariant mass inclusive in higher-order QCD effects as predicted by the fully-modeled `PowhegBox` and partially-reweighted `Sherpa`.

Following the described approaches to include higher-order corrections assumes the factorisation of QCD

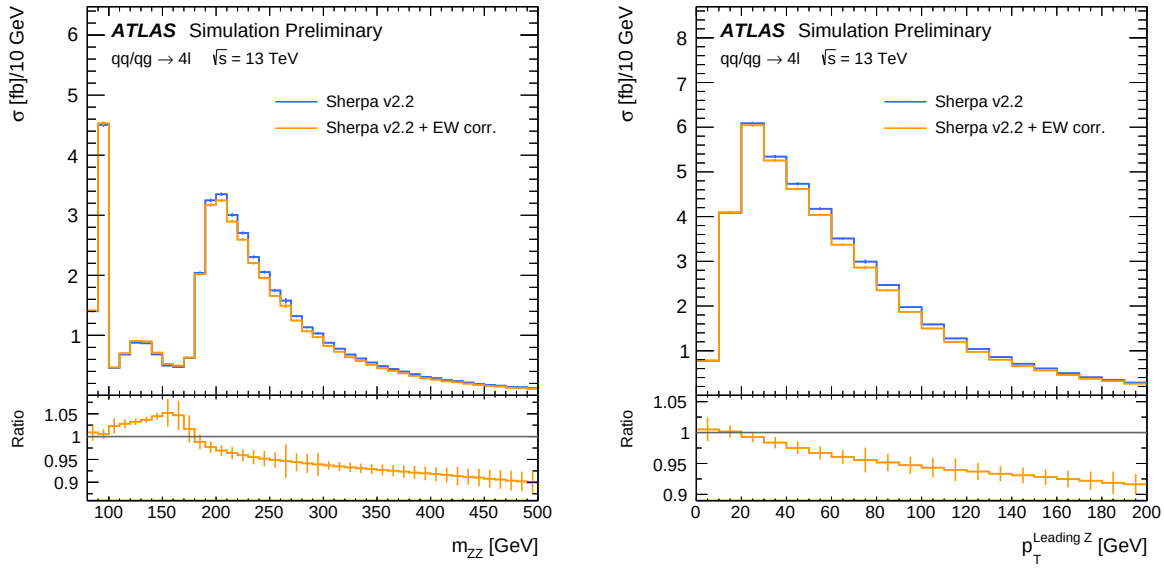

(a) (b)

Figure 2: Comparison of the default Sherpa prediction and its modeling to take higher-order electroweak effects into account. The reweighting is based on per channel k-factors calculated for the four lepton invariant mass which is shown for all channels combined in (a). There is also the transverse momentum of the more energetic Z boson shown (b).

and electroweak effects. As this assumption is not valid in general, physics analyses incorporate another systematic uncertainty following the procedure described in [47]. Based on a quantity in first order sensitive to QCD effects and related to the planarity of the ZZ system the full electroweak correction is considered as uncertainty after its application.

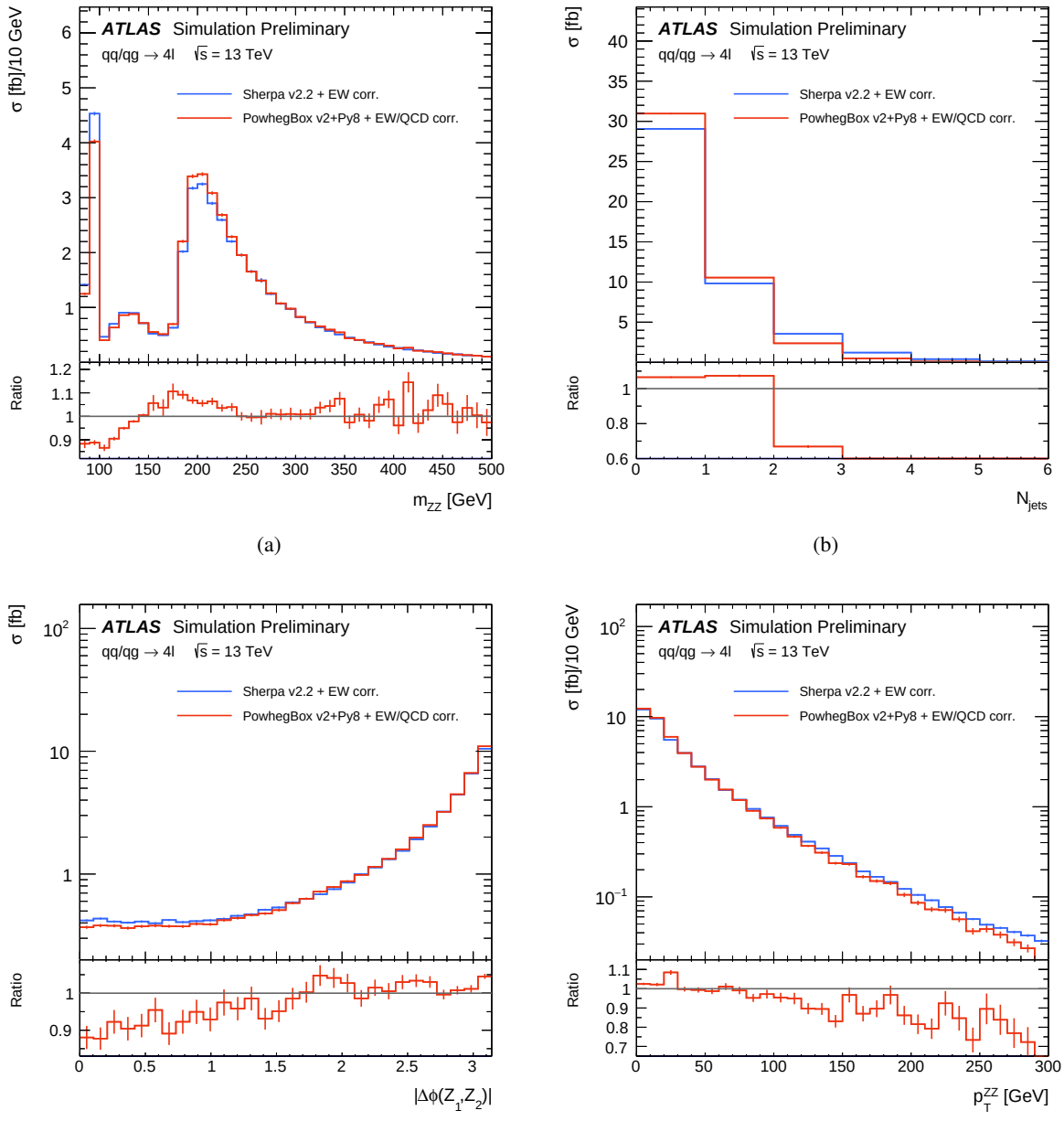

Figure 3: Differential cross section predictions of `Sherpa` and `PowhegBox` both corrected for higher-order electroweak effects and additional incorporation of QCD effects in `PowhegBox`. The four-lepton invariant mass (a) rather insensitive to higher-order QCD effects shows rather good agreement while there are visible differences in the jet multiplicity (b), the distance in Φ of the two Z bosons (c) and the transverse momentum of the four lepton system (d).

3.3.2 $3\ell\nu$ final state

In this section, MC generators are compared to the ATLAS measurements of $W^{\pm}Z$ boson pair-production cross section at 13 TeV [48, 49]. The measurements are performed in the $3\ell\nu$ final state, where the gauge bosons decay to electrons or muons. The comparison is presented in two phase spaces - fiducial and total, formed by the requirements summarised in Table 3. The fiducial phase space is defined to closely follow the detector-level kinematic selection of the measurements. The fiducial cross section is extrapolated to the total phase space and corrected for the leptonic branching fractions of the W and Z bosons. The total phase space is constrained only by a requirement on the invariant mass of the lepton pair associated with the Z boson. For the jet multiplicity distribution, particle-level jets are reconstructed from stable particles excluding muons, electrons, neutrinos and photons associated with the W and Z boson decays. In the presented comparison jets are required to have a p_{T} above 25 GeV and $|\eta|$ below 4.5.

Table 3: Fiducial and total phase space definitions for the $W^{\pm}Z \to 3\ell\nu$ ATLAS measurements.

Fiducial Phase-Space
$\lvert m_{Z\to\ell\ell} - m_Z\rvert < 10$ GeV
$m_{\mathrm{T}}^{W} > 30$ GeV
Z leptons: $p_{\mathrm{T}}^{\ell} > 15$ GeV
W lepton: $p_{\mathrm{T}}^{\ell} > 20$ GeV
$\lvert\eta_{\ell}\rvert < 2.5$ for all three leptons
$\Delta R(\ell,\ell) > 0.3$ between W and Z leptons
$\Delta R(\ell,\ell) > 0.2$ between Z leptons
Total Phase-Space
$66 < m_{Z\to\ell\ell} < 116$ GeV

Table 4 shows the comparison between the measured fiducial and total $W^{\pm}Z$ cross section with various MC generators. `PowhegBox+PYTHIA8` , `PowhegBox+HERWIG` and `MC@NLO+HERWIG` predictions are lower than the measured cross section by $15-18\%$, while the `Sherpa` calculations show better agreement with the data due to its incorporation of multi-jet matrix elements. The recent calculations of the $W^{\pm}Z$ cross section at NNLO QCD made with MATRIX are also included in the comparison, the details of the calculations are described in Ref. [35, 36]. Since the MATRIX predictions do not include effects of QED FSR, correction factors of 0.972 for the total cross section and of 1.04 for the fiducial cross section, estimated from `PowhegBox+PYTHIA8` , are applied. A comparison of the measured exclusive jet multiplicity with the MC generators is shown in Figure 4. The shape of the measured distribution is well described by `Sherpa`, where up to three jets are included in the matrix-element calculation, while in the `PowhegBox+PYTHIA8` prediction only the leading jet is included and the higher jet multiplicities are described by the parton shower jets. Figure 5 shows a comparison of the measured differential cross sections as a function of the transverse momentum of the reconstructed Z boson (p_{T}^{Z}) and the transverse mass variable m_{T}^{WZ} for the $W^{\pm}Z$ system. The variable m_{T}^{WZ} is reconstructed as

$$m_{\mathrm{T}}^{WZ} = \sqrt{\left(\sum_{\ell=1}^{3} p_{\mathrm{T}}^{\ell} + E_{\mathrm{T}}^{\mathrm{miss}}\right)^2 - \left[\left(\sum_{\ell=1}^{3} p_x^{\ell} + E_x^{\mathrm{miss}}\right)^2 + \left(\sum_{\ell=1}^{3} p_y^{\ell} + E_y^{\mathrm{miss}}\right)^2\right]}. \quad (1)$$

These distributions are particularly interesting due to their sensitivity to possible new physics effects. Specifically, the presence of anomalous triple gauge couplings would manifest itself as an increased yield of events at high values of p_{T}^{Z} and m_{T}^{WZ}. A reasonable description of the measured distributions is provided by all generators, while the highest rates are predicted by Sherpa.

Table 4: Comparison of the measured at $\sqrt{s}$ = 13 TeV combined fiducial cross section for a single leptonic channel and the cross section extrapolated to the total phase space with PowhegBox+PYTHIA8 , PowhegBox+HERWIG , Sherpa and MC@NLO+HERWIG predictions. The cross sections are additionally compared to the MATRIX calculations at NNLO QCD corrected for QED FSR effects.

Fiducial cross section	
$\sigma_{\mathrm{W^{\pm}Z}}^{\mathrm{ATLAS,\ fid.}}$	63.2 ± 3.2 (stat.) ± 2.6 (sys.) ± 1.5 (lumi.) fb
Sherpa	62.7 ± 0.05 (stat.) fb
PowhegBox+PYTHIA8	51.2 ± 0.01 (stat.) fb
PowhegBox+HERWIG	53.4 ± 0.02 (stat.) fb
MC@NLO+HERWIG	52.9 ± 0.01 (stat.) fb
MATRIX	66.6 ± 0.03 (stat.) fb
Total cross section	
$\sigma_{\mathrm{W^{\pm}Z}}^{\mathrm{ATLAS,\ tot.}}$	50.6 ± 2.6 (stat.) ± 2.0 (sys.) ± 0.9 (th.) ± 1.2 (lumi.) pb
Sherpa	50.5 ± 0.01 (stat.) pb
PowhegBox+PYTHIA8	42.2 ± 0.00 (stat.) pb
PowhegBox+HERWIG	48.0 ± 0.01 (stat.) pb
MC@NLO+HERWIG	42.7 ± 0.00 (stat.) pb
MATRIX	48.1 ± 0.06 (stat.) pb

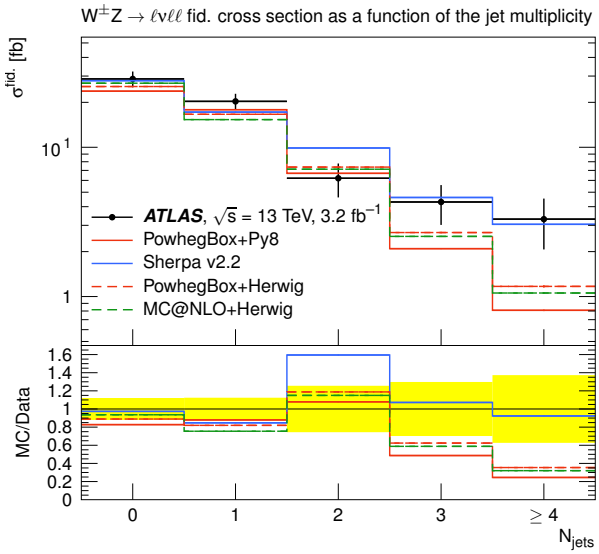

Figure 4: Comparison of the measured at $\sqrt{s}$ = 13 TeV exclusive jet multiplicity with various MC generators.

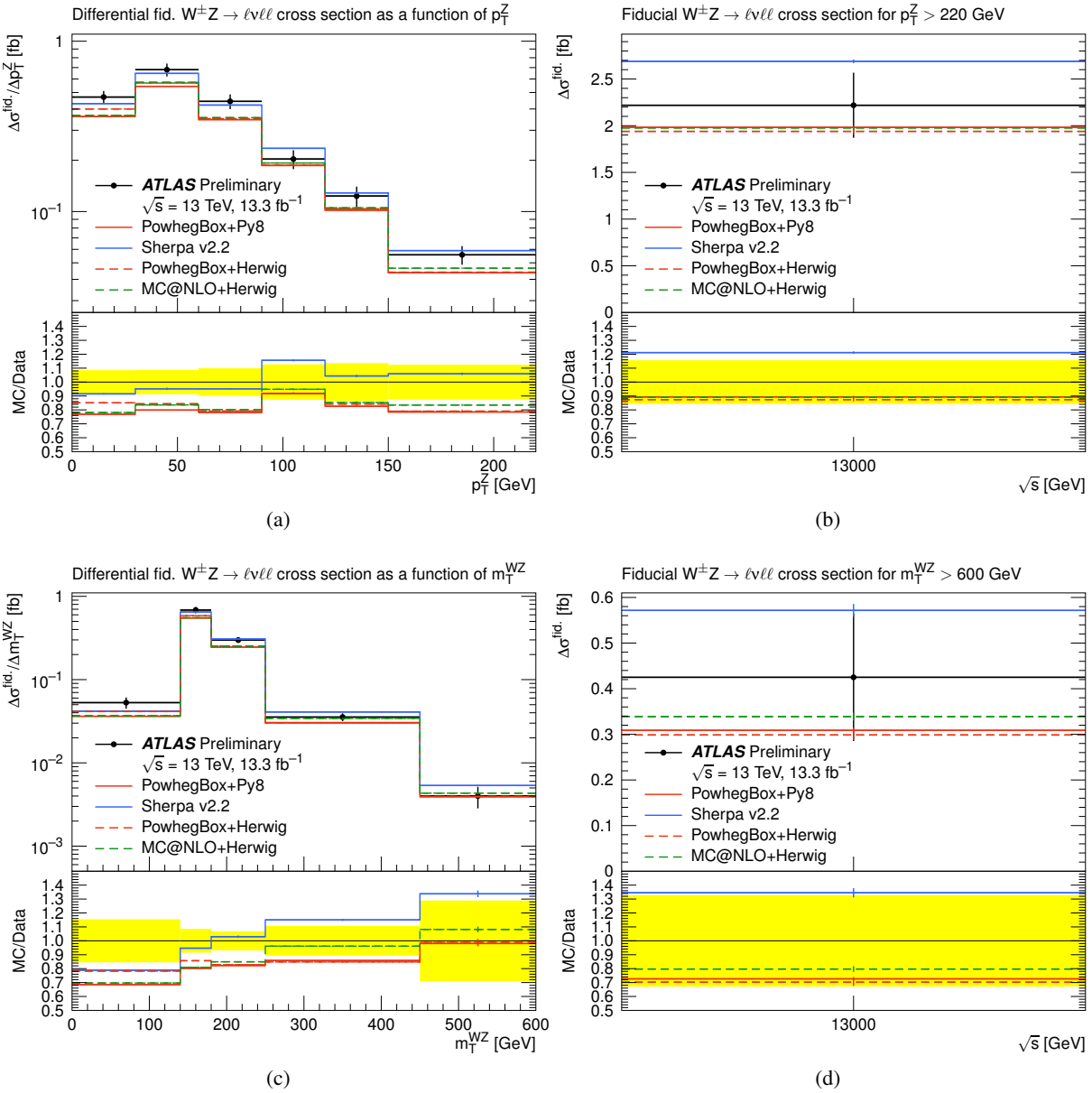

Figure 5: Comparison of the measured at $\sqrt{s} = 13$ TeV differential $W^{\pm}Z$ cross section as a function of transverse momentum of the reconstructed Z boson p_{T}^{Z} (a,b) and as a function of the transverse mass variable m_{T}^{WZ} for the $W^{\pm}Z$ system (c,d) with `PowhegBox+PYTHIA8` , `PowhegBox+HERWIG` , `Sherpa` and `MC@NLO+HERWIG` predictions. The left plots show the cross section normalised to the bin width, while in the right plots the cross section is shown for the tails of the kinematic distributions and is not normalised.

Table 5: Definitions of the event selection employed for studies of $WW \to \ell\nu\ell\nu$ final states [50]. In these definitions, ℓ is the charged lepton from the decays $W \to e\nu$ and $W \to \mu\nu$, and $\sin(\Delta\phi_\ell)$ is the minimum difference in azimuthal angle between the vector sum of the momenta of the neutrinos and any of the selected generator-level charged leptons. The quantity $E^{\text{miss}}_{\text{T, Rel}}$ is defined as $|\mathbf{\Sigma p}^{\nu_i}_{\text{T}}|$ for $\Delta\phi_\ell > \pi/2$ and $|\mathbf{\Sigma p}^{\nu_i}_{\text{T}}| \times \sin(\Delta\phi_\ell)$ in case of $\Delta\phi_\ell < \pi/2$. Furthermore $p^{\text{miss}}_{\text{T}}$ describes the transverse magnitude of the vectorial sum of all neutrinos, $|\mathbf{\Sigma p}^{\nu_i}_{\text{T}}|$.

	$e\mu$
p^{ℓ}_{T} (leading/sub-leading)	> 25 / 20 GeV
$\lvert\eta^{\ell}\rvert$	$\lvert\eta^{\mu}\rvert < 2.4$ and $\lvert\eta^{e}\rvert < 2.47$, excluding $1.37 < \lvert\eta^{e}\rvert < 1.52$
$m_{\ell\ell}$	> 10 GeV
Number of jets with $p_{\text{T}} > 25$ GeV, $\lvert\eta\rvert < 4.5$	either 0 (Figure 6) or 1 (Figure 7) or any number of jets (Figure 8)
$E^{\text{miss}}_{\text{T, Rel}}$	> 15 GeV
$p^{\text{miss}}_{\text{T}}$	> 20 GeV

3.3.3 $e\nu\mu\nu$ final state

In the following we examine WW diboson production decaying fully leptonically and in particular the $e\nu\mu\nu$ final state. Since so far there are no differential WW cross section measurements available at a centre-of-mass energy of $\sqrt{s} = 13$ TeV, only comparison plots for four different generators are provided using the baseline event selection for the measurement carried out using data taken in 2012 [50]. All of the distributions are normalised to unity. The event selection is based on this measurement, but differs slightly: The jet transverse momentum is required to be greater than 25 GeV and jets are required to fall into a pseudorapidity of $|\eta| < 4.5$. The distance between jets and leptons is required to be $\Delta R_{\ell j} > 0.3$ in η-ϕ space, otherwise the jet is removed, no other overlap removal is performed. Only events with one electron and one muon ($e\mu$ final states) are considered. Table 5 summarises the other event selection criteria, which include requirements on the p_{T} and η of the leptons, the invariant mass of the dilepton system as well as on the missing transverse momentum. Of particular interest is WW production in association with jets, as a jet veto is often used to for example suppress backgrounds like $t\bar{t}$. The uncertainty of such jet vetoes depends on resummation effects, which may degrade the accuracy of theory predictions and lead to deviations from the measurements. Hence, three different sets of jet requirements are applied, requiring either zero, exactly one, or any number of jets to pass the event selection to investigate different aspects of WW production.

Differential distributions are shown in Figure 6 for events with zero jets. The event selection is based on Table 5 and the distributions are the same as in Ref. [50] and they have been normalised to unity to allow for a better comparison of the shapes predicted by the different generators. The distributions considered are: the transverse momentum of the leading lepton, $p^{\text{lead}}_{\text{T}}$; the invariant mass of the dilepton system, $m_{\ell\ell}$; and its transverse momentum, $p_{\text{T}}(\ell\ell)$; the difference in azimuthal angle between the decay leptons, $\Delta\phi_{\ell\ell}$;

their combined rapidity, $|y_{\ell\ell}|$; as well as $|\cos(\theta^*)|$ being defined as:

$$\left|\cos(\theta^*)\right| = \left|\tanh\left(\frac{\Delta\eta_{\ell\ell}}{2}\right)\right|. \tag{2}$$

The upper panel shows the normalised distributions as predicted by PowhegBox+PYTHIA8 , MC@NLO, Sherpa 2.1 and 2.2, MadGraph5_aMC@NLO and PowhegBox+HERWIG , the lower panel displays the ratios of the different predictions using PowhegBox+PYTHIA8 as a reference. In general, Sherpa 2.1 and 2.2 exhibit excellent agreement and are in the following commonly referred to as Sherpa. The most striking differences are present for the observables related to energy and mass, namely $p_{\mathrm{T}}^{\mathrm{lead}}$, $p_{\mathrm{T}}(\ell\ell)$ and $m_{\ell\ell}$. Both, MC@NLO and Sherpa exhibit a small slope with respect to PowhegBox+PYTHIA8 and predict a 5-10% larger cross-section at higher energies or masses, whilst PowhegBox+HERWIG predicts a 10% lower cross section, presumably caused by the different parton shower. The differences are in general of the order of a few percent and do not exceed 10%. The angular variables $\Delta\phi_{\ell\ell}$, $|y_{\ell\ell}|$ and $|\cos(\theta^*)|$ agree much better for all of the generators and agree within 5-7%. Only for $|\cos(\theta^*)|$ there is a small trend visible especially for Sherpa, which prefers a softer $|\cos(\theta^*)|$ distribution. Unsurprisingly, MC@NLO prefers a slightly larger cross-section for large values of $\Delta\phi_{\ell\ell}$ which is correlated with larger $p_{\mathrm{T}}(\ell\ell)$.

To study properties of jets produced in association with the diboson system, the same event selection is applied but requesting exactly one jet to pass the above cuts. This is the same selection as applied in Ref. [51] which reports the fiducial cross-section of WW production in associated with a jet. Here, the transverse momentum of the jet, $p_{\mathrm{T}}^{\mathrm{jet}}$, and its pseudorapidity, η^{jet}, as well as the distance between the jet and the dilepton system given as $\Delta\phi_{\ell\ell,\mathrm{jet}}$ and $\Delta\eta_{\ell\ell,\mathrm{jet}}$ are investigated for the different generators.

As shown in Figure 7, the differences between MC@NLO, Sherpa, PowhegBox+HERWIG and PowhegBox+PYTHIA8 are much larger than for the lepton variables in the WW+0-jet case. PowhegBox+PYTHIA8 predicts the hardest jet-p_{T} spectrum compared to the other generators. All other generators are very close and predict about 15-20% fewer events at 150 GeV. Large difference are also apparent for η^{jet} where MC@NLO, MadGraph5_aMC@NLO and Sherpa predict a much large cross-section in the forward region compared to the other generators. Also the differences in the distance in pseudo-rapidity, $\Delta\eta_{\ell\ell,\mathrm{jet}}$ are substantial, MC@NLO, MadGraph5_aMC@NLO and Sherpa predict the dilepton system and the jet to be much further apart. Sherpa and MadGraph5_aMC@NLO predict the angle between the dilepton system and the jet, $\Delta\phi_{\ell\ell,\mathrm{jet}}$, to much smaller by up to 10%, whereas in MC@NLO dilepton system and jet are much more likely to be back-to-back than in the reference PowhegBox+PYTHIA8 generator.

Further distributions related to jets produced in association with the WW system are shown in Figure 8. The number of jets in the central region ($|\eta| < 2.5$) and in the full acceptance region ($|\eta| < 4.5$) is compared for the four generators. Sherpa and PowhegBox+HERWIG predict much higher jet multiplicities than PowhegBox+PYTHIA8 and MC@NLO. The higher jet multiplicity in Sherpa can be explained by the fact that it is a multi-leg generator with up to 4 jets generated by the matrix element in the final state. Also shown is the fiducial cross section as a function of the p_{T}-requirement used in the jet veto. While there are up to 4% differences between the predictions at low $p_{\mathrm{T}}^{\mathrm{jet}}$, this reduces to less than 2% at higher $p_{\mathrm{T,jet}}^{\mathrm{veto}}$. Sherpa and MadGraph5_aMC@NLO show smaller cross sections for low $p_{\mathrm{T,jet}}^{\mathrm{veto}}$ compared to the PowhegBox+PYTHIA8 reference, whilst their predicted cross section is up to 2% larger at higher values of the veto. For the n PowhegBox+PYTHIA8 and MC@NLO the situation is reversed: for low $p_{\mathrm{T,jet}}^{\mathrm{veto}}$ they predict a 2-3% larger cross section, whilst for high $p_{\mathrm{T,jet}}^{\mathrm{veto}}$ it is lower by 2%.

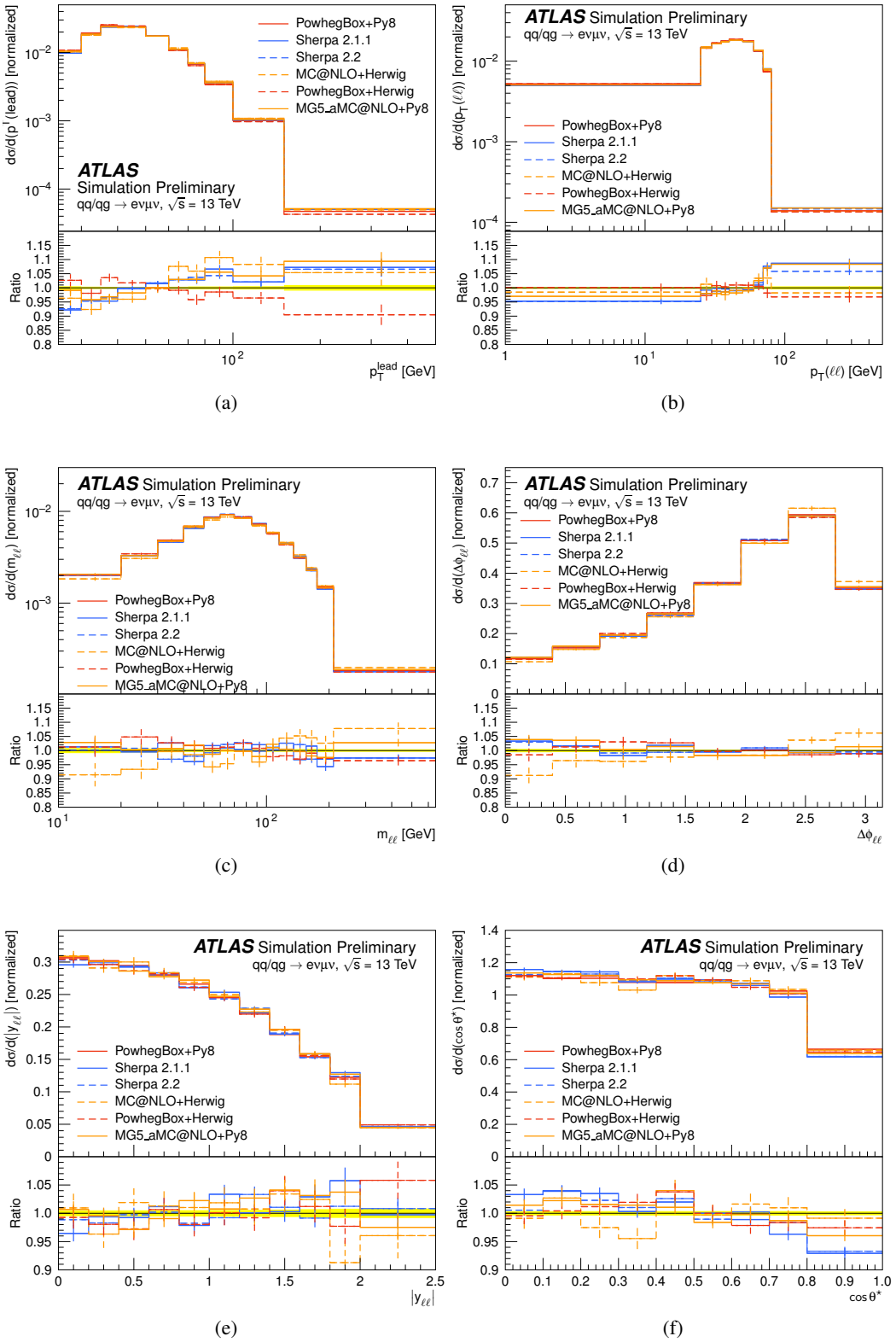

Figure 6: Differential normalised distributions of WW production in the $e\mu$ final state for the transverse momentum of the leading lepton, $p_{\mathrm{T}}^{\mathrm{lead}}$, the invariant mass, $m_{\ell\ell}$, and the transverse momentum of the dilepton system, $p_{\mathrm{T}}(\ell\ell)$, as well as the difference in azimuthal angle between the decay leptons, $\Delta\phi_{\ell\ell}$, their combined rapidity, $|y_{\ell\ell}|$, and the observable $|\cos(\theta^*)|$. All of the distributions have been normalised to unity. The lower panels show the ratio with respect to the PowhegBox+PYTHIA8 sample.

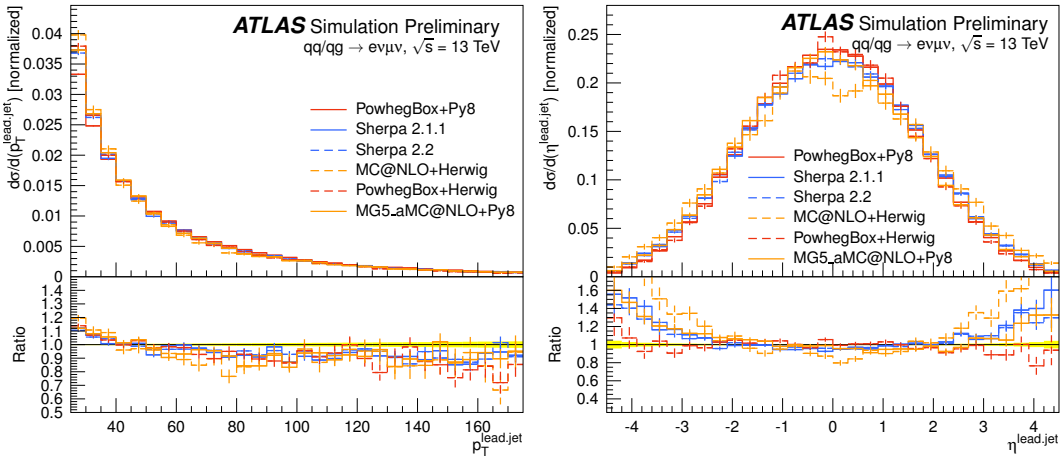

(a) (b)

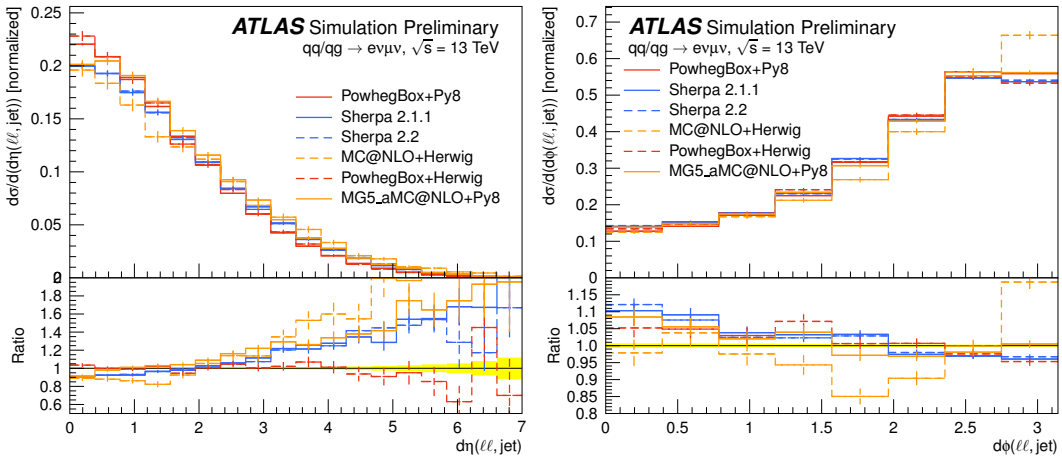

(c) (d)

Figure 7: Normalised differential cross sections of WW production in the $e\mu$ final state with exactly one associated jet for the transverse momentum of the jet, $p_{\mathrm{T}}^{\mathrm{jet}}$, its pseudorapidity, η^{jet}, the distance between the jet and the dilepton system in the pseudorapidity, $\Delta\eta_{\ell\ell,\mathrm{jet}}$ and in the polar angle, $\Delta\phi_{\ell\ell,\mathrm{jet}}$. All of the distributions have been normalised to unity. The lower panels show the ratio with respect to the `PowhegBox+PYTHIA8` sample.

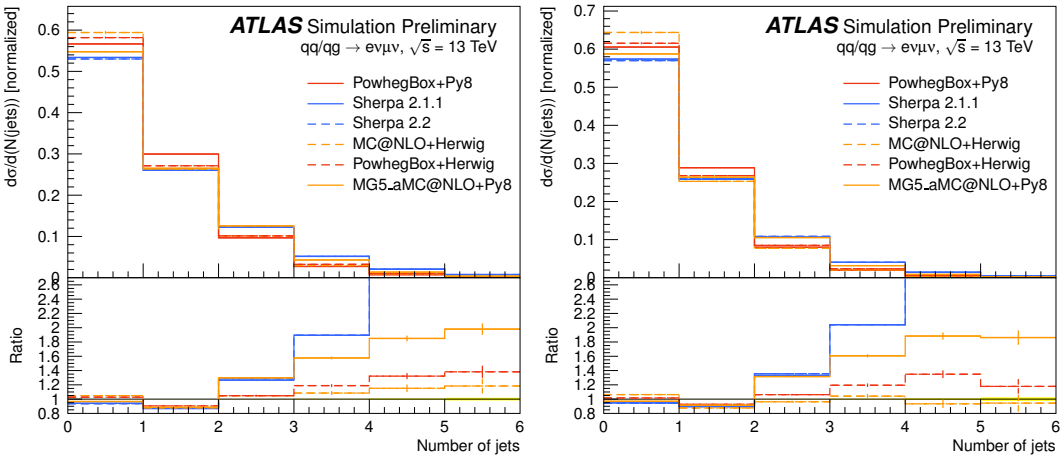

(a) (b)

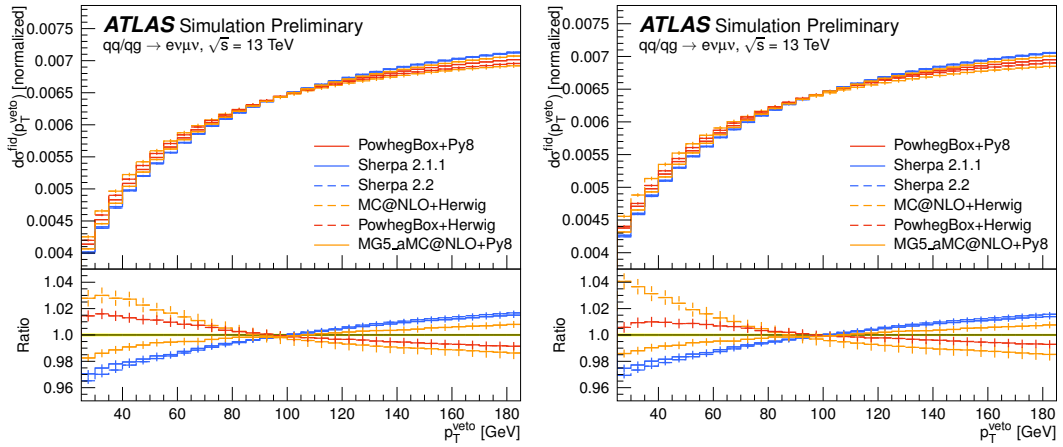

(c) (d)

Figure 8: Number of jets in the central region ($|\eta| < 2.5$) and in the full acceptance region ($|\eta| < 4.5$) as predicted by the different generators and the fiducial cross section as function of the p_{T}-requirement used in the jet veto. All of the distributions have been normalised to unity. The lower panels show the ratio with respect to the PowhegBox+PYTHIA8 sample.

3.3.4 $e\nu\mu\nu$ final state with FxFx merging

Fully leptonic final states of diboson processes are among the main background sources for e.g. Higgs-boson measurements in the $H \to WW^* \to \ell\nu\ell\nu$ or $H \to ZZ^* \to \ell\ell\ell\ell$ decay channels. In order to obtain precise measurements of these processes, a good modelling of the diboson backgrounds is essential.

With the high integrated luminosity recorded during the Run-2 data taking, studies of Higgs-boson production in association with several jets become more and more sensitive. As measurements of these production modes can be sensitive to new physics phenomena, the modelling of the main backgrounds as e.g. diboson production in association with several jets gains importance as well.

The `MadGraph5_aMC@NLO` generator is capable to produce diboson events in association with several jets at NLO precision in the matrix element, for example fully leptonic $\ell\nu\ell\nu$, $\ell\nu\ell\ell$ or $\ell\ell\ell\ell$ final states. In the following samples with NLO precision of events with up-to one jet at the matrix element are studied. These new samples are compared to predictions from `PowhegBox` and `Sherpa` in phase spaces that are relevant to measurements of Higgs-bosons decaying via $H \to VV$ into a system of four leptons.

The definition of leptons and jets as well as the overlap-removal procedure are chosen to be exactly the same to those of the previously stated WW cross section measurements via the $e\nu\mu\nu$ final state (except for the requirement of the minimum p_T of the sub-leading lepton which is set to 15 GeV instead). The full event selection requirements that have been previously used in studies of $H \to WW^* \to \ell\nu\ell\nu$ events and that are now used to compare the predictions of `MadGraph5_aMC@NLO` to those of `PowhegBox` and `Sherpa` are summarised in Table 6. In total three disjoint event categories are defined according to the jet multiplicity. In the $N^{\text{jets}} = 0$ category, cuts are applied on the invariant mass and transverse momentum of the dilepton system $m_{\ell\ell}$ and $p_T^{\ell\ell}$, the inner angle between the two leptons $\Delta\Phi_{\ell\ell}$ and the angle in the transverse plane between the combined dilepton vector and the missing momentum $\Delta\Phi(\ell\ell, E_T^{\text{miss.}})$. Cuts on the $m_{\ell\ell}$ and $\Delta\Phi_{\ell\ell}$ are also applied in the $N^{\text{jets}} = 1$ and $N^{\text{jets}} \geq 2$ categories as well as vetos for b-jets and τ-pair topologies (leptonic τ decays are not considered as signal contribution). In order to perform the veto of $\tau\tau$ events, the quantity $m_{\tau\tau}$ is used which is defined via

$$m_{\tau\tau} = \frac{m_{\ell\ell}}{\sqrt{x_1 \cdot x_2}}$$

with

$$x_1 = \frac{p_x^{\ell_1} \cdot p_y^{\ell_2} - p_y^{\ell_1} \cdot p_x^{\ell_2}}{p_y^{\ell_2} \cdot E_x^{\text{miss}} - p_x^{\ell_2} \cdot E_y^{\text{miss}} + p_x^{\ell_1} \cdot p_y^{\ell_2} - p_y^{\ell_1} \cdot p_x^{\ell_2}}$$

and

$$x_2 = \frac{p_x^{\ell_1} \cdot p_y^{\ell_2} - p_y^{\ell_1} \cdot p_x^{\ell_2}}{p_x^{\ell_1} \cdot E_y^{\text{miss}} - p_y^{\ell_1} \cdot E_x^{\text{miss}} + p_x^{\ell_1} \cdot p_y^{\ell_2} - p_y^{\ell_1} \cdot p_x^{\ell_2}},$$

in which the x- and y-component of the missing transverse momentum is determined by the four-vector sum of all neutrinos in the event. In the $N^{\text{jets}} = 1$ category, there is an additional selection requirement on the maximum of the two transverse W-boson mass values $m^1_{\text{T},W}$ and $m^2_{\text{T},W}$, which are defined via

$$m^i_{\text{T},W} = \sqrt{2 p^{\ell_i}_{\text{T}} E^{\text{miss}}_{\text{T}} \left(1 - \cos\phi(\ell_i, E^{\text{miss}}_{\text{T}})\right)}$$

and are evaluated separately for the leading and second leading lepton.

Table 6: Event selection requirements previously used in studies of $H \to WW^* \to \ell\nu\ell\nu$ decays [52]. Three disjoint phase spaces are defined according to the jet multiplicity of the studied events.

	$N^{\text{jets}} = 0$	$N^{\text{jets}} = 1$	$N^{\text{jets}} = 2$
p_T^{ll}	> 30 GeV	—	—
$\Delta\Phi(\ell\ell, E_T^{\text{miss.}})$	> 1.57	—	—
$m_{W,T}^{\text{max}}$	—	> 50 GeV	—
$\Delta\Phi_{\ell\ell}$	< 1.8	< 1.8	< 1.8
$m_{\ell\ell}$	< 55 GeV	< 55 GeV	< 60 GeV
$\lvert m_{\tau\tau} - m_Z \rvert$	—	> 25 GeV	> 25 GeV
$N^{\text{b-tags}}$	—	0	0

Comparisons of these new `MadGraph5_aMC@NLO` samples and the predictions of `Sherpa v2.2`, `Sherpa v2.1.1` and `PowhegBox` are presented in the Figures 9, to 11. Distributions of the leading and sub-leading lepton p_T and the transverse mass of the WW system m_T are shown for both the $N^{\text{jets}} = 0$ and $N^{\text{jets}} = 1$ channels in Figure 9, where the variations between these four generators is below 10% for most part of the studied phase spaces. Even the transverse momentum and the pseudorapidity distribution for jets in the $N^{\text{jets}} = 1$ channel (as depicted in Figure 10 a) and b)) show a very reasonable agreement for all these generators. However, significantly larger discrepancies can be seen for the predictions in the $N^{\text{jets}} \geq 2$ phase space. Distributions of the leading and second leading jet p_T and η as well as several comparisons for properties of the di-jet system (as the invariant di-jet mass, the rapidity gap ΔY_{jj} and the inner angle $\Delta\Phi_{jj}$ between the two leading jets) are shown in Figures 10 c-f) and Figures 11 a-f). In particular, the predictions of the `PowhegBox` generator, for which the second jet is emulated by the parton shower, vary strongly from the predictions of the other generators. The differences of the `PowhegBox` predictions range up-to 70% in some parts of the studied phase space. Indeed, also the predictions of `MadGraph5_aMC@NLO` vary significantly from the `Sherpa` predictions, where again the jet p_T or m_{jj} spectra are softer than the corresponding spectra predicted by `Sherpa`. Nevertheless, these differences are significantly smaller than the difference between `PowhegBox` and `Sherpa`.

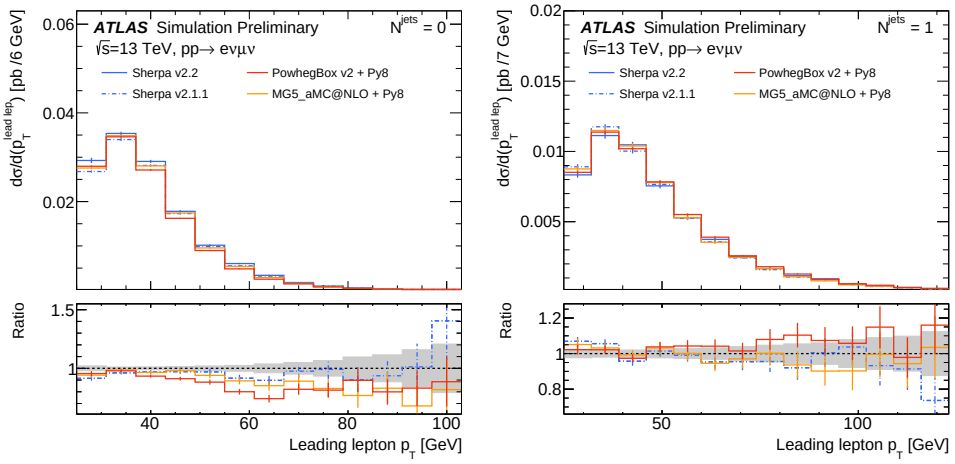

(a)

(b)

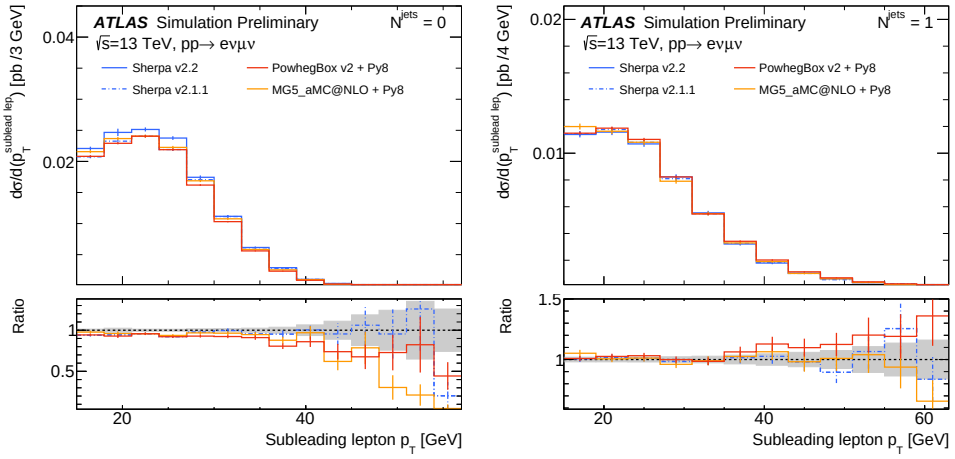

(c)

(d)

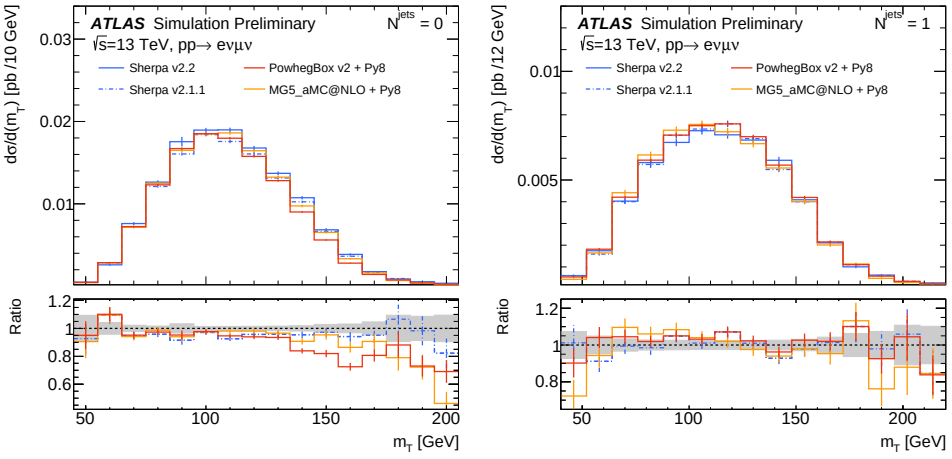

(e)

(f)

Figure 9: Differential production cross sections in the $N^{\text{jets}} = 0$ (left column) and $N^{\text{jets}} = 1$ (right column) phase spaces that are dedicated for measurements of Higgs-bosons decaying via $H \to WW^* \to e\nu\mu\nu$. The predictions of the `MadGraph5_aMC@NLO`, `Sherpa v2.1.1` and `PowhegBox` generators are compared with respect to the predictions of `Sherpa v2.2`.

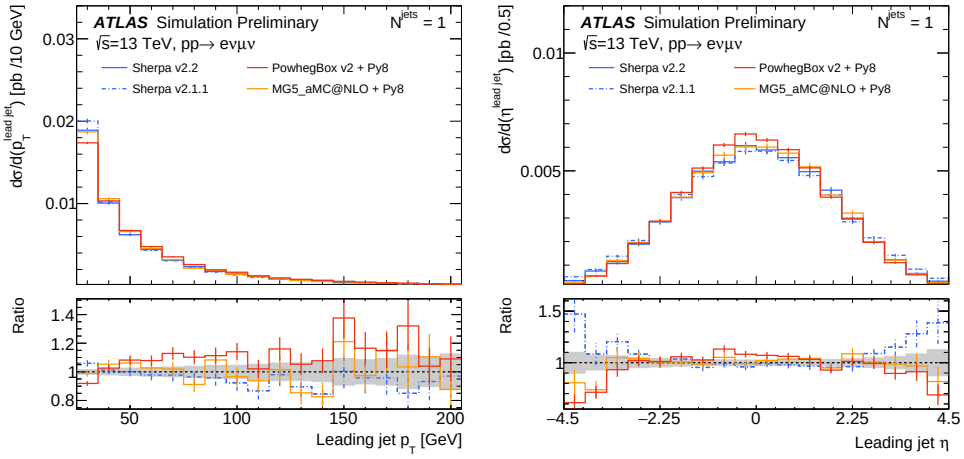

(a) (b)

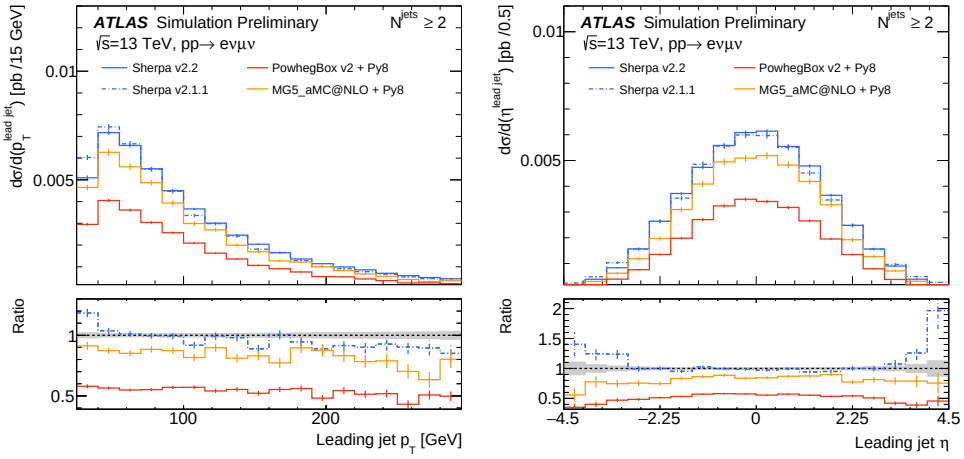

(c) (d)

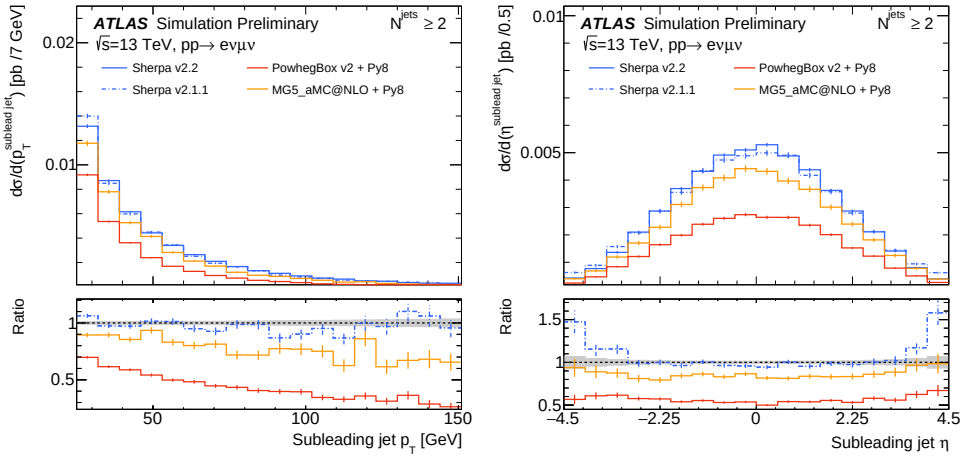

(e) (f)

Figure 10: Differential production cross sections in the $N^{\text{jets}} = 1$ (first row) and $N^{\text{jets}} \geq 2$ (second and third row) phase spaces that are dedicated for measurements of Higgs-bosons decaying via $H \to WW^* \to e\nu\mu\nu$. The predictions of the `MadGraph5_aMC@NLO`, `Sherpa v2.1.1` and `PowhegBox` generators are compared with respect to the predictions of `Sherpa v2.2`.

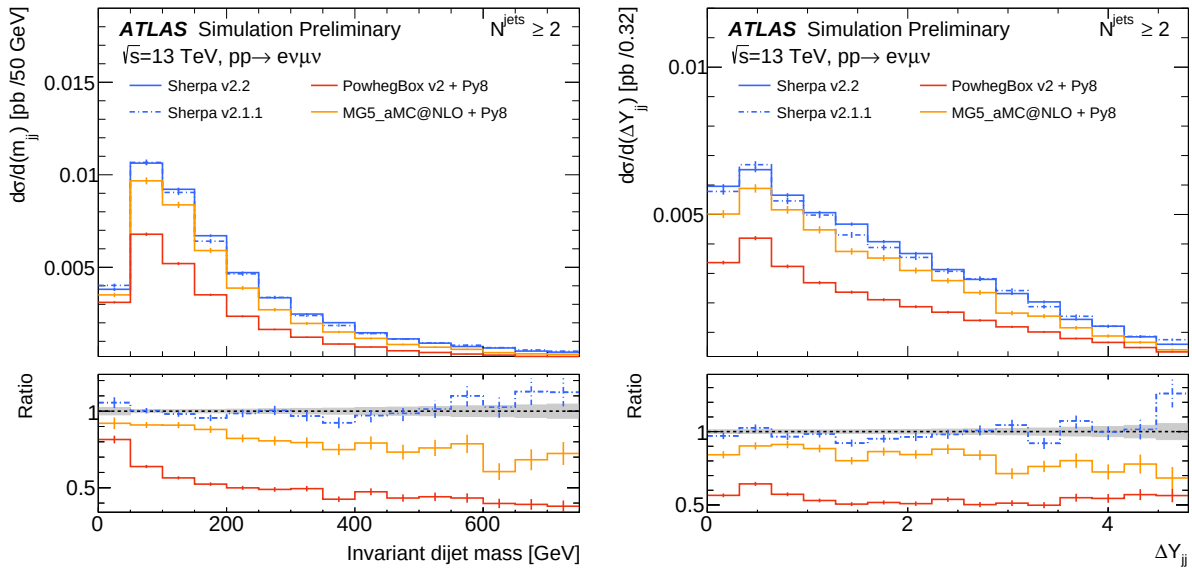

(a) (b)

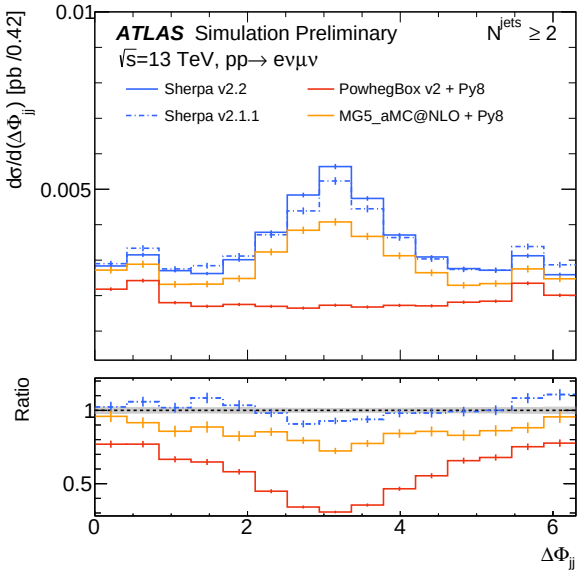

(c)

Figure 11: Differential production cross sections in the $N^{\text{jets}} \geq 2$ phase spaces that is dedicated for measurements of Higgs-bosons decaying via $H \to WW^* \to e\nu\mu\nu$. The predictions of the `MadGraph5_aMC@NLO`, `Sherpa v2.1.1` and `PowhegBox` generators are compared with respect to the predictions of `Sherpa v2.2.1`.

4 Electroweak diboson production with jets

Electroweak diboson production with at least two jets includes vector boson scattering (VBS) diagrams, where the two "tagging" jets recoil against the (heavy) gauge bosons, and involves an extra two electroweak couplings compared to the $VVjj$ processes presented in Sections 3 and 6. The resulting leptonic final states include the $4\ell jj$, as well as the $2\ell 2\nu jj$ final states, where the two lepton charges can be of equal or opposite sign. Semi-leptonic processes lead to $\ell\ell/\ell\nu/\nu\nu jj\ jj$ final states. An overview of the accuracy achieved with the chosen generators is given in Table 7.

Table 7: Accuracies of the chosen generators for the listed electroweak processes.

		$VV+2j$	$VV+3j$	$VV+\geq 4j$
$VVjj = \ell^{\pm}\ell^{\mp}2\nu jj$	VBFNLO+PYTHIA8	LO	PS	PS
	MadGraph5_aMC@NLO+PYTHIA8	LO	PS	PS
$VVjj = \ell^{\pm}\ell^{\pm}2\nu jj$	Sherpa	LO	PS	PS
	PowhegBox+PYTHIA8	NLO	LO	PS
$VVjj = \ell\ell/\ell\nu/\nu\nu jj\ jj$	Sherpa	LO	PS	PS
	MadGraph5_aMC@NLO+PYTHIA8	LO	PS	PS
$Z\gamma jj = 2\ell\gamma jj$	Sherpa	LO	PS	PS
	VBFNLO+PYTHIA8	LO	PS	PS
	MadGraph5_aMC@NLO+PYTHIA8	LO	PS	PS

4.1 Generator setup

4.1.1 Sherpa

Matrix elements for the electroweak $2\ell\gamma jj$ process and opposite-sign as well as same-sign $2\ell 2\nu jj$ processes have been generated at LO accuracy using Sherpa v2.1.1. The $2\ell\gamma jj$ process was studied as well with Sherpa v2.2 at LO, also with no extra parton in the final state. The nominal factorisation scale has been set to the invariant mass of the diboson system. Further details of the general Sherpa setup are provided in Section 2.

4.1.2 PowhegBox

PowhegBox v2 is used to produce electroweak $W^{\pm}W^{\pm}jj \rightarrow \ell^{\pm}\nu\ell^{\pm}\nu jj$ events at NLO QCD [53]. These events are produced at the matrix-element level (LHE) with the NNPDF3.0 NLO PDF and need to be showered by a showering Monte Carlo such as PYTHIA8 (used in the samples shown in this note) or HERWIG. The PowhegBox base revision used to produce the integrations and LHE events is r3208 and the process-specific (vbf_wp_wp) revision is r3178. The sample is inclusive in regards to the leptonic decay flavors from the W bosons from the hard scatter. The vbf_wp_wp process does not include non-WW diboson contributions that would produce a similar final state (e.g. semi-leptonic WWW). The renormalisation and factorisation scales are set to m_W.

The withdamp and bornzerodamp flags were set in PowhegBox for each sample to ensure that any singularity in the integrated phase-space is handled properly. No other generator level cuts are applied.

All events are showered with PYTHIA8 using the AZNLO tune and the CTEQ6L1 PDF for the shower. We ensure that heavy flavor hadron decays are properly handled by processing them with EvtGen and QED radiative corrections in decays of any resonances are handled by Photos++.

4.1.3 MadGraph5_aMC@NLO

Matrix elements for the electroweak $2\ell\gamma jj$ process have been generated at LO accuracy using MadGraph5_aMC@NLO 2.3.3 with no extra parton in the final state. The nominal factorisation scale has been set to the invariant mass of the diboson system. The NNPDF30_lo_as_0118 PDF was used for the generation. The events are hadronised using PYTHIA8. Similar generator configurations are used to model the electroweak $VVjj$ leptonic ($\ell\ell\nu\nu jj$) and semi-leptonic ($\ell\ell/\ell\nu/\nu\nu jj\ jj$) processes, except that the transverse mass of the VV system is used for the QCD scales.

4.1.4 VBFNLO

Matrix elements for the electroweak $2\ell\gamma jj$ and $\ell\ell\nu\nu jj$ processes have been generated at LO accuracy using VBFNLO 3.0.0 beta 3 with no extra parton in the final state. The nominal factorisation scale has been set to the invariant mass of the diboson system. The NNPDF30_lo_as_0118 PDF was used for the generation. The events are hadronised using PYTHIA8.

4.2 Cross sections

4.2.1 Generator cross sections

This section summarises the cross sections for the various samples used. It should be noted that the cross sections are *not* necessarily expected to agree across generators for any given process since different diagrams may be included and/or a different phase space sampled. To be able to compare the different generator cross-sections on more equal footing one should refer to the comparisons of fiducial cross-sections given in Subsection4.4.

A summary of the cross sections predicted by Sherpa v2.1.1 for leptonic $VVjj$ final states is given in Table 8 and in Table 9 for PowhegBox. The normalisation of the Sherpa v2.1.1 predictions includes a correction to account for different electroweak schemes. Sherpa v2.1.1 is using an electroweak parameter scheme were $\alpha_{\mathrm{QED}}(m_Z)$ and the boson masses are used as input and the other parameters are calculated from the corresponding tree-level relations. This can lead to values of e.g. the weak mixing angle which deviate from the PDG values, or also differences to the α_{QED} calculated in the G_μ scheme. Since the inclusive cross section of the $VVjj$ samples with their *six* electroweak vertices is particularly affected by this discrepancy, it has been decided to scale down the Sherpa predictions by a factor of 0.87 which accounts for this global difference due to the EW couplings.

The cross sections obtained in the $2\ell\gamma jj$ for the different MC generators are given in Table 10.

The cross sections for electroweak and strong $VVjj$ semi-leptonic ($\ell\ell/\ell\nu/\nu\nu jj\ jj$) processes are shown in Table 11. Only on-shell boson production is considered.

Table 8: Summary of the generator cross sections at $\sqrt{s} = 13$ TeV predicted by Sherpa v2.1.1 for electroweak diboson dijet final states.

Final state	Sherpa prediction [pb]
$\ell^{\pm}\ell^{\mp}2\nu jj$	0.175
$\ell^{\pm}\ell^{\pm}2\nu jj$	0.037

Table 9: Summary of the generator cross sections at $\sqrt{s} = 13$ TeV predicted by PowhegBox for electroweak $W^{\pm}W^{\pm}jj$ final states ($\ell = e, \mu, \tau$).

Final state	PowhegBox prediction [pb]
$\ell^{-}\ell^{-}2\nu jj$	7.81×10^{-3}
$\ell^{+}\ell^{+}2\nu jj$	20.9×10^{-3}

Table 10: Summary of the generator cross sections for electroweak $\ell\ell\gamma jj$ final states (e, μ) at $\sqrt{s} = 13$ TeV predicted by Sherpa v2.2, MadGraph5_aMC@NLO and VBFNLO.

Generator	prediction [pb]
Sherpa	0.213
MadGraph5_aMC@NLO	0.095
VBFNLO	0.055

Table 11: Summary of the generator cross sections at $\sqrt{s} = 13$ TeV predicted by MadGraph5_aMC@NLO for electroweak and strong production of diboson dijet semi-leptonic final states.

process	EWK [pb]	QCD [pb]
$ZZ(\to \ell\ell jj)jj$	0.0078	0.2889
$ZZ(\to \nu\nu jj)jj$	0.0181	0.7298
$ZW(\to \ell\ell jj)jj$	0.0180	0.7850
$ZW(\to \nu\nu jj)jj$	0.0413	1.1956
$WZ(\to \ell\nu jj)jj$	0.0512	2.2841
$WW(\to \ell\nu jj)jj$	0.8206	10.0384

4.3 Systematic uncertainties

4.3.1 PowhegBox

The systematic variations for events generated with PowhegBox are derived using the PowhegBox internal reweighting scheme. The resulting weights include renormalisation scale, factorisation scale, and PDF variations. There are eight scale variations corresponding to factors of $\frac{1}{2}$ or 2 applied independently to the renormalisation and factorisation scales. We also include the 100 eigenvector error sets for the nominal PDF (NNPDF3.0 NLO) and the central values of the CT14 NLO and MMHT2014 NLO PDFs. These variations are not normalised to the nominal event weight and as such, each varied distribution must be normalised to their respective cross-section.

Figure 12 illustrates the impact of variations of scales, α_S in the central PDF as well as the impact of changing the central PDF on key distributions in the $\ell^{\pm}\nu\ell^{\pm}\nu jj$ final state.

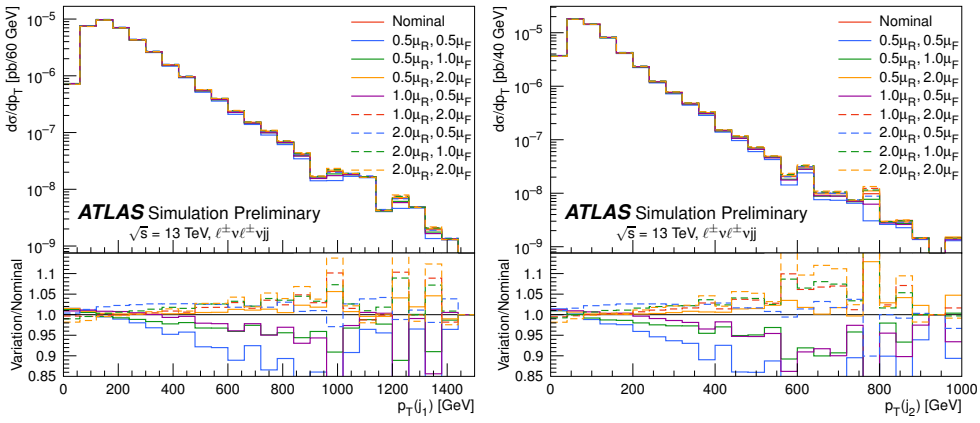

(a) $p_T(j_1)$ (b) $p_T(j_2)$

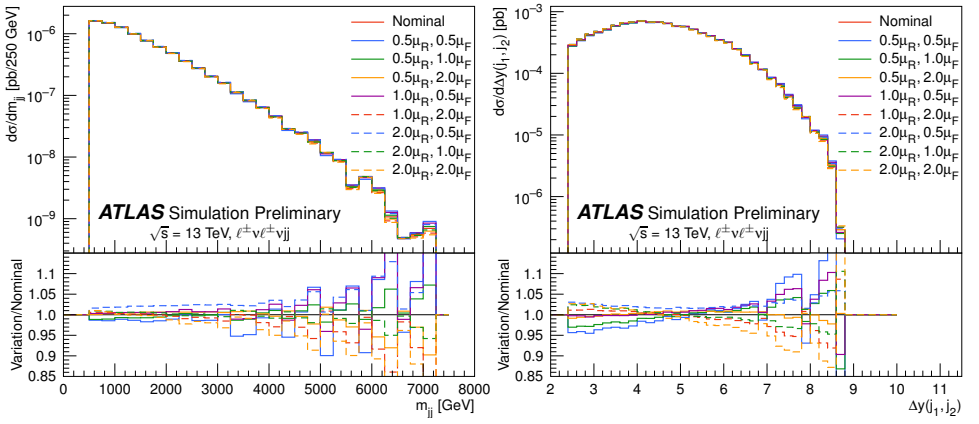

(c) m_{jj} (d) $\Delta y(j_1, j_2)$

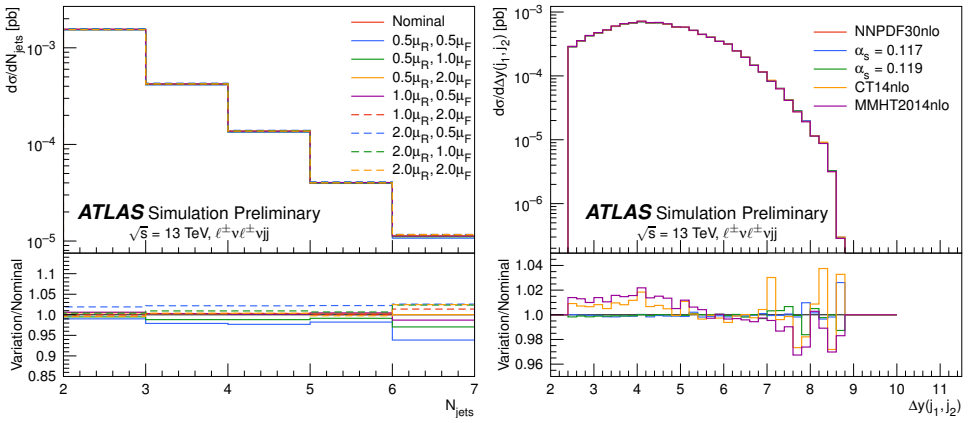

(e) Jet Multiplicity (f) $\Delta y(j_1, j_2)$

Figure 12: Impact of scale variations on (a), (b) the p_{T} distributions of the two highest p_{T} jets, (c), (d) dijet invariant mass m_{jj} and rapidity separation $\Delta y(j_1, j_2)$ for the two leading jets and (e) jet multiplicity N_{jets} in PowhegBox $\ell^{\pm}\nu\ell^{\pm}\nu jj$ events ($\ell = e, \mu$) in the fiducial region defined in Table 15. (f) is the same as (d), but showing the impact of PDF variations.

4.4 Generator comparisons

In the following we provide validation plots with different object definitions and event selections. Jets are reconstructed using the anti-k_t clustering algorithm [41] with a jet-radius parameter of $R = 0.4$. Further details of the selections are given in the respective subsections.

4.4.1 $\ell^{\pm}\ell^{\mp}\nu\nu jj$

The EWK production of the $\ell^{\pm}\ell^{\mp}\nu\nu jj$ final state can be modeled using various Monte Carlo generators, and in this note, the expected yields and kinematic distributions of the EWK process in a given fiducial phase space are compared between `MadGraph5_aMC@NLO` and `VBFNLO`. The details of the generator versions and configurations are summarised below in Table 12. The fiducial phase space is defined in Table 13 and corresponds to a typical selection of the EWK signal process. The cross-sections reported by the generators as well as the fiducial cross-sections obtained after applying the fiducial selections to the generated MC samples are reported in Table 14. One should note that the cross-sections calculated from the `MadGraph5_aMC@NLO` generator are scaled by a factor of three to account for all $\ell^{\pm}\ell^{\mp}\nu\nu jj$ processes with three neutrino flavors. Differences in the generator-level cross-sections are expected due to the difference in the included processes and generator cuts. The predicted fiducial cross-section from `VBFNLO` is lower than that from `MadGraph5_aMC@NLO`, due to missing processes and differences in QCD scales. Although there are differences in the predicted cross-sections from the compared generators, their kinematic distributions after the fiducial selection are found to be similar, as shown in Figures 13 and 14.

Table 12: Generator configurations for the EWK production of the $\ell^{\pm}\ell^{\mp}\nu\nu jj$ process.

	`MadGraph5_aMC@NLO`	`VBFNLO`
Version	`MadGraph5_aMC@NLO v2.3.3`	`VBFNLO 3.0.0` beta 2
Precision	LO QCD + PS, QED <= 6, QCD = 0	
Process	$pp \to \ell\ell\nu\nu jj; \ell = e,\mu; \nu = \nu_\tau$	$pp \to ZZjj \to \ell\ell\nu\nu jj; \ell = e,\mu; \nu = \nu_{e,\mu,\tau}$
QCD Scales	$m_T^{\ell\ell\nu\nu}$	$m^{\ell\ell\nu\nu}$
PDF	`NNPDF3.0` leading order with $\alpha_S = 0.118$	
Generator Cuts	$p_T^j > 15$ GeV, $\lvert y^j\rvert < 5$, $p_T^\ell > 5$ GeV, $\lvert y^\ell\rvert < 2.8$, $m^{\ell\ell} > 40$ GeV, $p_T^{\nu\nu} > 10$ GeV	
Parton Shower	`PYTHIA8 A14 NNPDF2.3 LO EvtGen`	

Table 13: Fiducial phase space definition for the study of EWK production of the $\ell^{\pm}\ell^{\mp}\nu\nu jj$ process.

2 leptons with $p_{\mathrm{T}} > 10$ GeV and $\|\eta\|$ <2.5
leading lepton $p_{\mathrm{T}} > 30$ GeV, sub-leading lepton $p_{\mathrm{T}} > 20$ GeV
$p_{\mathrm{T}}^{\nu\nu} > 90$ GeV
$76 < m_{\ell\ell} < 106$ GeV
≥ 2 jets with $p_{\mathrm{T}} > 25$ GeV and $\|\eta\|$ <4.5; use two highest p_{T} jets
$m_{jj} > 500$ GeV
$\|\Delta\eta(jj)\| > 3$

Table 14: Comparison of the reported generator-level cross-sections and the fiducial cross-sections from `MadGraph5_aMC@NLO` and `VBFNLO`.

	`MadGraph5_aMC@NLO`	`VBFNLO`
Generator σ [fb]	4.1	2.4
Fiducial σ [fb]	0.42	0.35

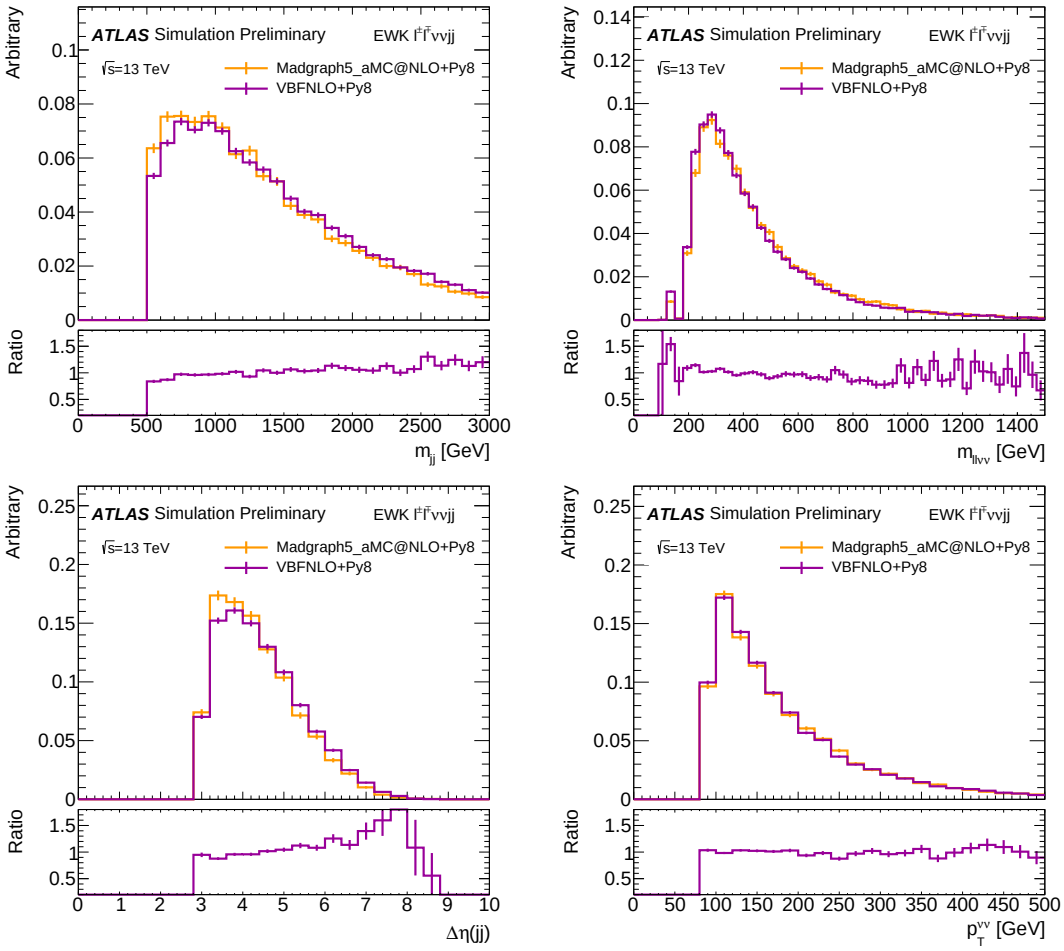

Figure 13: Comparison of predicted kinematic distributions in the fiducial phase space from `MadGraph5_aMC@NLO` and `VBFNLO`, both showered with `PYTHIA8`, for m_{jj} (top left), $m_{\ell\ell\nu\nu}$ (top right), $|\Delta\eta(jj)|$ (bottom left), and $p_{\mathrm{T}}^{\nu\nu}$ (bottom right). All the distributions are normalised to the same area, and the shown uncertainties are statistical only.

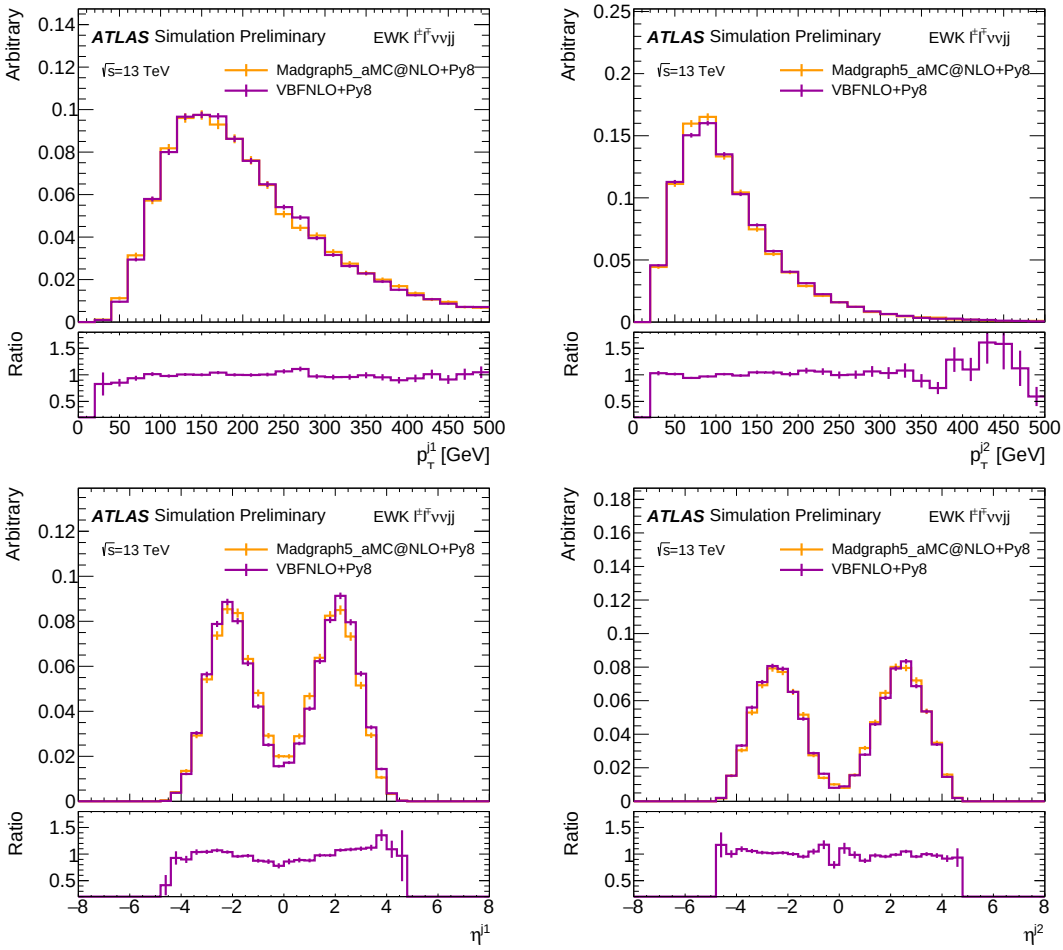

Figure 14: Comparison of predicted kinematic distributions in the fiducial phase space from `MadGraph5_aMC@NLO` and `VBFNLO`, both showered with `PYTHIA8`, for leading jet p_{T} (top left), sub-leading jet p_{T} (top right), leading jet η (bottom left), and sub-leading jet η (bottom right). All the distributions are normalised to the same area, and the shown uncertainties are statistical only.

Table 15: Particle-level event selection used in $\ell^{\pm}\nu\ell^{\pm}\nu jj$ final states. These are implemented in a Rivet analysis.

Lepton pre-selection	$\ell \in e, \mu$ && $p_T > 15$ GeV && $\lvert\eta\rvert < 2.5$ photon dressing $\Delta R = 0.1$
Jet pre-selection	anti$-k_t$ $R = 0.4$ && $[(p_T > 30$ GeV && $\lvert\eta\rvert < 4.5)$ || $(p_T > 25$ GeV && $\lvert\eta\rvert < 2.4)]$ $N_{jets} \geq 2$
Overlap removal	loop over jets: $\Delta R(j, \ell) > 0.2$ loop over leptons: $\Delta R(\ell, j) > 0.4$
Selected leptons	$\ell^{\pm}\ell^{\pm}$ with $p_T > 27$ GeV $\lvert\eta\rvert < 1.37$ if $\ell \equiv e$ $\Delta R(\ell, \ell) > 0.3$ $N_{leps} == 2$ with same charge $M_{\ell\ell} > 20$ GeV
Tau veto	Veto event if selected lepton comes from τ
Drell-Yan cut	If $\ell^{\pm}\ell^{\pm} = e^{\pm}e^{\pm}$ then $\lvert M_Z - M(e, e)\rvert > 15$ GeV
Missing E_T cut	$E_{\mathrm{T}}^{\mathrm{miss}} > 30$ GeV
Dijet mass	$m_{jj} > 500$ GeV
B-jet veto	$N_{bjets} == 0$
Rapidity cut	$\lvert\Delta y(j, j)\rvert > 2.4$

4.4.2 $\ell^{\pm}\nu\ell^{\pm}\nu jj$

We present a generator comparison of $\ell^{\pm}\nu\ell^{\pm}\nu jj$ final states between `PowhegBox` (NLO) and `Sherpa` (LO) samples at $\sqrt{s} = 13$ TeV. The `Sherpa` sample includes all contributions to the final state $\ell^{\pm}\nu\ell^{\pm}\nu jj$ for the given order, while for `PowhegBox` the number of intermediate gauge bosons is restricted to two. The event selection in Table 15 is chosen to maximise $W^{\pm}W^{\pm} \rightarrow \ell^{\pm}\nu\ell^{\pm}\nu$ contributions and models a fiducial volume used in the $W^{\pm}W^{\pm}jj$ analysis [54].

We can see in Figure 15 that the `PowhegBox` jet distributions are overall softer than what is seen in `Sherpa`. Discrepancies are also present in the dijet distributions: we see that the rapidity separation between the two leading jets is smaller in `Sherpa` than in `PowhegBox` which leads to a softer m_{jj} spectrum. The difference between the two setups regarding diagrams included in the calculation is most likely irrelevant for this discrepancy as the event selection is requiring a high $m_{jj} > 500$ GeV. In the future it will be interesting to study upgraded `Sherpa` samples with LO accuracy for the 3-jet process to see whether the discrepancy persists. We observe good kinematic agreement between the two generators for the selected leptons, which are hence not shown in a separate figure. Table 16 shows the common fiducial cross section for the region defined in Table 15. The `PowhegBox` prediction gives a 36% larger cross section than `Sherpa` in this phase space.

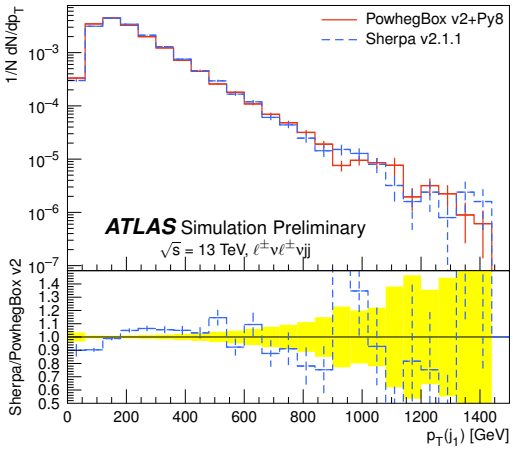

(a) $p_T(j_1)$

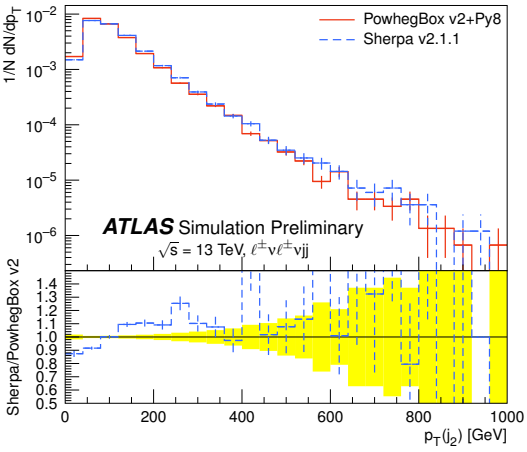

(b) $p_T(j_2)$

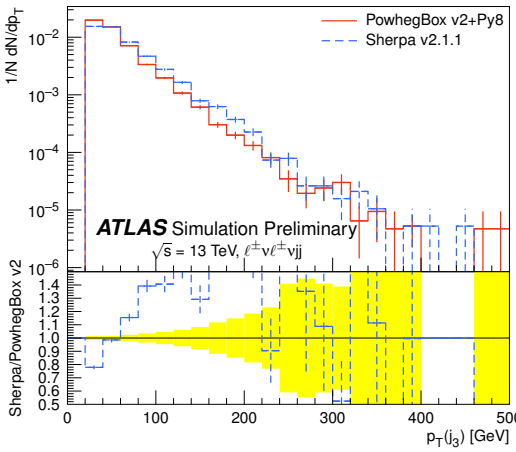

(c) $p_T(j_3)$

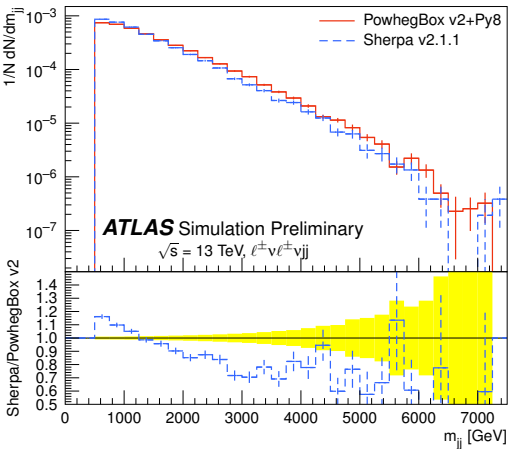

(d) m_{jj}

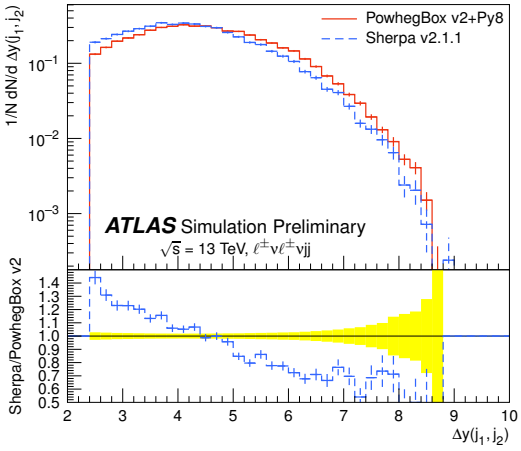

(e) $\Delta y(j_1, j_2)$

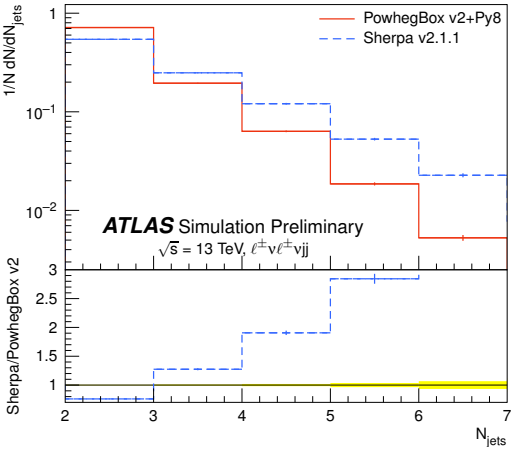

(f) Jet Multiplicity

Figure 15: (a)-(c) p_{T} distributions for the three highest p_{T} jets, (d), (e) dijet invariant mass m_{jj} and rapidity separation $\Delta y(j_1, j_2)$ for the two leading jets and (f) jet multiplicity N_{jets} in $\ell^{\pm}\nu\ell^{\pm}\nu jj$ events ($\ell = e, \mu$) in the fiducial region defined in Table 15. The yellow band is the statistical uncertainty of the PowhegBox sample.

Table 16: Summary of the generator fiducial region cross sections at $\sqrt{s} = 13$ TeV predicted by PowhegBox and Sherpa for electroweak $W^{\pm}W^{\pm}jj$ final states ($\ell = e, \mu, \tau$).

Generator	σ_{fid} [fb]
Sherpa	1.587
PowhegBox	2.163

Table 17: Particle-level event selection used in $\ell^{\pm}\ell^{\mp}\gamma jj$ final states.

Inclusive selection	Leptons	$p_{\mathrm{T}} > 15$ GeV and $\lvert\eta\rvert < 2.5$
	Di-Leptons	$N(\ell) \geq 2$, $m_{\ell\ell} > 40$ GeV and $\Delta R_{\ell\ell} > 0.1$
	Photons	$N(\gamma) \geq 1$, $\mathrm{E}_T > 15$ GeV and $\lvert\eta\rvert < 2.5$
	Jets	$N(\mathrm{jets}) \geq 2$, $p_{\mathrm{T}} > 20$ GeV, $\lvert\eta\rvert < 5.5$, $\Delta R_{j\ell} > 0.4$, and $\Delta R_{jg} > 0.4$
VBS selection	Pre-selection	Inclusive selection
	Three body	$m_{\ell\ell\gamma} + m_{\ell\ell} > 182$ GeV
	Jets	$p_{\mathrm{T}j1} > 30$ GeV, $p_{\mathrm{T}j1} > 25$ GeV, $\lvert\eta\rvert < 4.9$
	Di-Jets	$m_{jj} > 500$ GeV

4.4.3 $\ell^{\pm}\ell^{\mp}\gamma jj$

Only $Z \to ee\gamma$ events are shown in the following. The smooth photon isolation [55] with $n = 2$, $\epsilon = 0.025$, $\delta = 0.3$ is used in all cases. Electrons are selected if they are stable (HEPMC status 1), and they are dressed with photons contained in a cone of $\Delta R = 0.1$ around the lepton. The comparison has been done in two phase spaces defined in Table 17. The first one is designed such that it allows for a direct comparison of the three generators. The second phase space mimics a VBS search region to enhance the VBS $Z\gamma$ signal compared to the QCD processes. The different generators are normalised with their respective production-cross section obtained at LO in QCD. The cross-sections predicted in the VBS search region fiducial volume are given in Table 18. In all distributions only statistical uncertainties on the events generated are shown.

Table 18: Summary of the generator VBS fiducial region cross-sections at $\sqrt{s} = 13$ TeV predicted by Sherpa, MadGraph5_aMC@NLO and VBFNLO for electroweak $\ell\ell\gamma jj$ final states ($\ell = e, \mu$).

Generator	σ_{fid} [fb]
Sherpa	4.6
MadGraph5_aMC@NLO	4.2
VBFNLO	4.3

Figure 16 shows the distributions obtained in the inclusive phase space for the invariant mass of the two leading jets, and the $m_{\ell\ell\gamma}$ distributions; and in the VBS phase space for the $\ell\ell\gamma$ centrality,

$$\frac{y(Z\gamma) - 0.5 \times (y(j1) + y(j2))}{(y(j1) - y(j2))},$$

and the two leading jets' $\Delta\eta_{jj}$ distributions. The upper panel shows the normalised distributions as pre-

dicted by MadGraph5_aMC@NLO, Sherpa and VBFNLO, the lower panel displays the ratios of the different predictions using MadGraph5_aMC@NLO as a reference. In the inclusive phase space, the largest differences are observed for VBFNLO. These are due to the fact that the $ZV\gamma$ diagrams are not included in the event generation, while they are for MadGraph5_aMC@NLO and Sherpa, as can be seen in the m_{jj} distribution. When going to the VBS phase space, hence cutting away the low m_{jj} distribution, the agreement between VBFNLO and the other generators is restored. A good agreement between the leptons and photon distributions is observed, which are therefore not shown here.

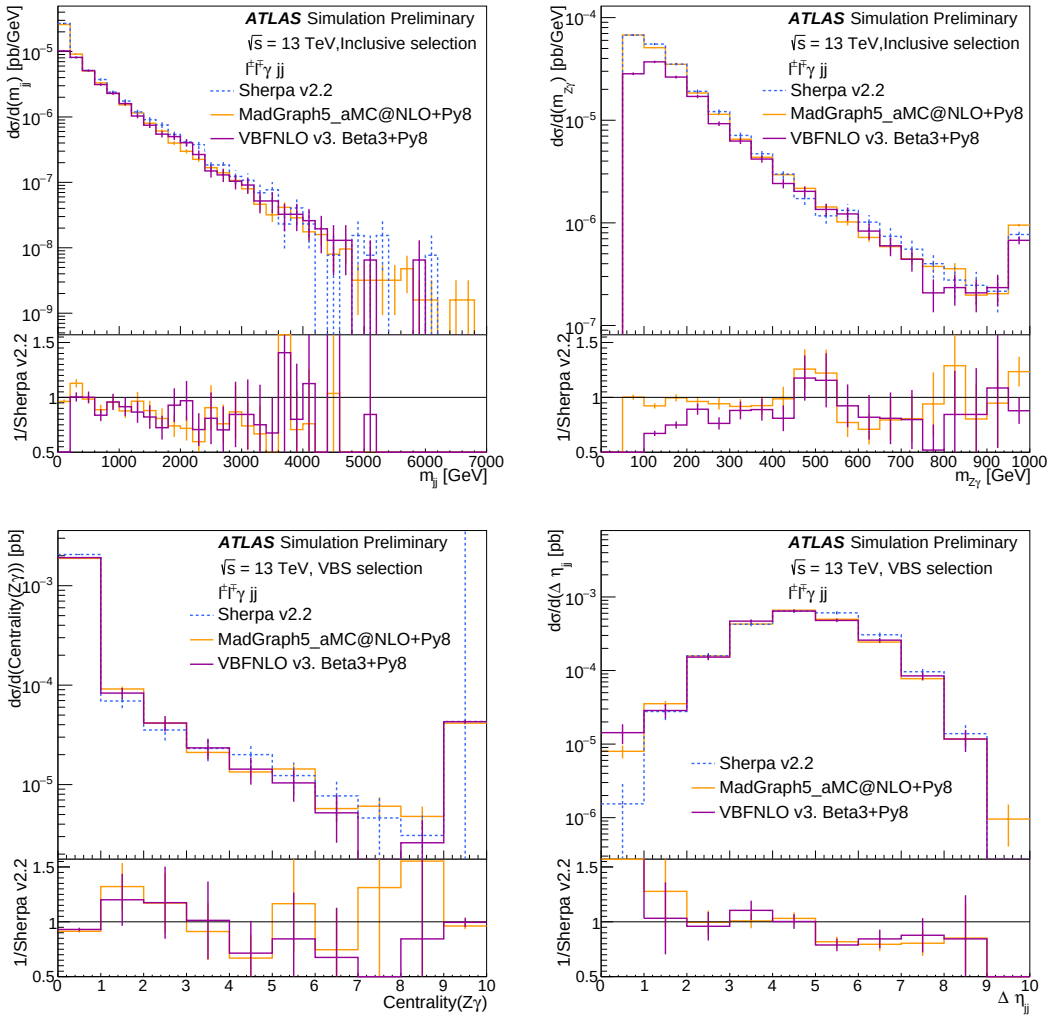

Figure 16: Differential normalised distributions of $\ell\ell\gamma + 2j$ production in the inclusive phase space for the invariant mass of the two leading jets, and the $m_{\ell\ell\gamma}$; and in the VBS phase space for the $\ell\ell\gamma$ centrality, and the two leading jets' $\Delta\eta_{jj}$.

4.4.4 Semileptonic $VVjj$

For electroweak $VVjj$ semi-leptonic ($VV(\to \ell\ell/\ell\nu/\nu\nu jj)jj$) processes, a generator comparison between `MadGraph5_aMC@NLO` and `Sherpa v2.2` is performed. By way of example for all the semi-leptonic electroweak processes, the process $ZZ(\to \ell\ell jj)jj$ is used for the comparison between `MadGraph5_aMC@NLO` and `Sherpa v2.2`.

A fiducial phase space is defined for the comparison study as shown in Table 19.

Table 19: Fiducial phase space for the $ZZ(\to \ell\ell jj)jj$ comparison study.

2 leptons with $p_{\mathrm{T}} > 20\,\mathrm{GeV}$ and $\lvert\eta\rvert < 2.5$
Jets overlapping with a selected lepton with $\Delta R < 0.2$ are removed
≥ 4 jets with $p_{\mathrm{T}} > 20$ GeV and $\lvert\eta\rvert < 4.5$

Comparisons of kinematic distributions between the two generators, such as the invariant mass and pseudorapidity separation of the tagging jets (m_{jjtag}, $\Delta\eta_{jjtag}$) and lepton transverse momenta, are shown in Figure 17. Table 20 shows the fiducial cross-sections for the phase space defined in Table 19.

Table 20: Summary of the fiducial region cross-sections at $\sqrt{s} = 13$ TeV predicted by `MadGraph5_aMC@NLO` and `Sherpa v2.2` for electroweak $ZZ(\to \ell\ell jj)jj$ production.

Generator	σ_{fid} [fb]
`MadGraph5_aMC@NLO`	5.61
`Sherpa`	5.45

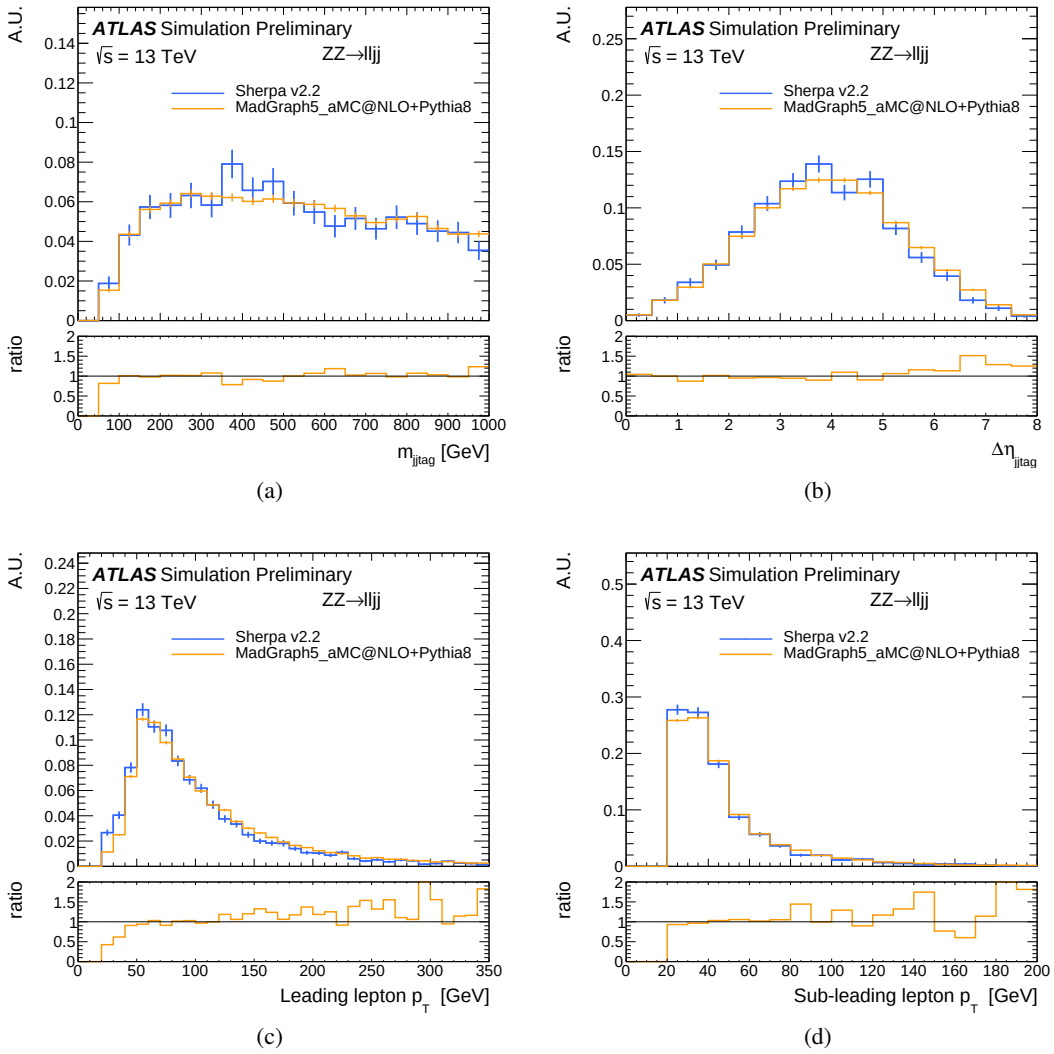

Figure 17: Dijet (a) invariant mass and (b) $\Delta\eta$ distributions of the tag jets and (c), (d) lepton transverse momentum distributions for electroweak $ZZ(\to \ell\ell jj)jj$ production.

5 Loop-induced diboson production

This section describes the loop-induced production of W or Z boson pairs, $gg(\to H/H^*) \to VV$ with a subsequent decay of V into neutral or charged leptons (including all lepton flavors, where τ leptons subsequently can decay leptonically or hadronically). The actual final states generated are 4ℓ, $2\ell 2\nu$ and $\ell\nu\ell\nu$. These processes are part of diboson production at NNLO QCD. However, due to the pure gluon initial state it can be calculated separated and split from other NNLO QCD predictions. Depending on the invariant mass of the diboson system the process is dominated either by continuum VV production via a quark box or resonant VV production via a H boson in the s-channel, both illustrated in Figure 18. Furthermore the interference of these two components varies with the invariant mass, and, additionally, with properties of the H boson observed at about 125 GeV as well as potential higher mass resonances. Eventually the different scopes of the various physics analyses require these contributions to be modeled

either independently or all together, and with different accuracy.

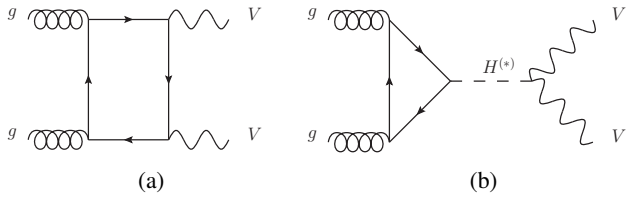

Figure 18: Feynman diagrams of loop-induced continuum (a) and resonant diboson production (b). The V indicates the electroweak gauge bosons Z or W.

5.1 Generator setup and cross sections

Event generation is performed at LO using `gg2VV` for ZZ and WW with subsequent leptonic decay of the bosons, or MCFM just for ZZ with the decay of the Z bosons into charged leptons. For this final state, `Sherpa` is also used. It generates events at LO accuracy, but includes one jet merged back from parton shower. Separate predictions for VV continuum production and VV resonant production provided by these three generators enter physics analyses as well as their predictions for the combined production including all off-shell and interference effects.

Table 21: Overview of process accuracies for the chosen generators. The precisions marked with an asterisk are not reached for all initial states [56].

		$VV+0j$	$VV+1j$	$VV+\geq 2j$
$VV \to 4\ell$	`Sherpa v2.1.1`	LO	LO	PS
	`gg2VV +PYTHIA8`	LO	PS	PS
	`MCFM +PYTHIA8`	LO	PS	PS
	`PowhegBox+PYTHIA8` $(2e2\mu)$	NLO*	LO*	PS
$VV \to 2\ell 2\nu$	`Sherpa v2.1.1`	LO	LO	PS
	`gg2VV +PYTHIA8`	LO	PS	PS

5.1.1 `gg2VV`

The generator `gg2VV v3.1.6` [57, 58] is used to produce samples with the final states 4ℓ, $2\ell 2\nu$ and $\ell\nu\ell\nu$, where τ leptons subsequently decay leptonically or hadronically. The matrix element is calculated at leading order either including or excluding the Standard Model Higgs as intermediate particle. If the Higgs is considered in the s-channel, the width predicted by the Standard Model is used and off-shell effects are taken into account properly. Furthermore, all possible interferences, like the final-state-lepton interference or the ZZ/WW interference in the $2\ell 2\nu$ final state are incorporated. For some application, the latter is avoided by requiring on matrix element level the neutrinos to be of different flavor than the charged leptons. The corresponding cross section is subsequently scaled by 1.5 to account for the missing final state. These samples are mainly used to enhance statistics in analyses studying ZZ production and

requiring the invariant mass of the charged lepton pair to be strongly consistent with an on-shell Z boson what reduces the interference to a negligible level.

Commonly the generator is configured to use the CT10 PDF set, and the dynamic renormalisation and factorisation scale is set to be the invariant mass of the diboson system, $m(VV)$. For special purposes, there are deviations from this baseline configuration. Beside predictions for the full process with interferences there are dedicated samples with exclusive continuum VV production and resonant VV production only.

Finally the subsequent shower is performed with PYTHIA8 using the A14 tune and the NNPDF2.3LO PDF set. The EvtGen afterburner is used to ensure that heavy quarks are properly decayed. Studies of jet distributions showed a harder spectrum for the common PYTHIA8 setup used by ATLAS. This is related to the fact that the matrix element is evaluated at leading order rather than next-to-leading order which is what the shower is tuned for. Therefore the so called "wimpy shower" configuration (SpaceShower:pTmaxMatch = 1) is enabled.

Regardless of ZZ or WW the invariant mass of all possible same-flavor opposite-charge leptons pairs are required to be greater than 4 GeV on generator level. In case of $gg(\to H/H^*) \to WW$ there is no further selection applied. To enhance statistics the four lepton invariant mass is required to be more than 100 GeV for ZZ continuum production decaying into 4ℓ. Further selections at the generator level are applied for $gg(\to H/H^*) \to ZZ \to 2\ell 2\nu'$ in which case the charged leptons are required to be within $|\eta| < 5$, to have a transverse momentum of at least 3 GeV each and a combined transverse momentum above 2 GeV. The corresponding cross sections of these predictions is summarised in Table 22.

Table 22: Summary of the generator cross sections at $\sqrt{s} = 13$ TeV predicted by gg2VV for various loop-induced diboson processes. Details on the generator selection criteria are given in the text.

process	gg2VV (fb)
$gg \to ZZ \to 4\ell$ (with $\ell/ = e, \mu$)	2.70
$gg \to ZZ \to 2e2\mu$	2.75
$gg(\to H/H^*) \to ZZ2\ell 2\nu_{\ell'}$	31.7
$gg(\to H/H^*) \to WW \to e^+\nu\mu^-\nu$	398

5.1.2 MCFM

MCFM version 8.0 configured with the CT10 NNLO PDF set and the dynamic renormalisation and factorisation scale set equal to half of the invariant mass of the diboson system was used to generate predictions for the process $gg(\to H/H^*) \to ZZ \to 4\ell$ with leading order accuracy. Similar to gg2VV, all interference effects including final state lepton interference in case of four same-flavor leptons are included properly. There are different samples for ZZ continuum and resonant production as well as the full process. The shower was configured following the same prescription as for gg2VV.

At generator level same-flavor opposite-sign lepton pairs are required to have an invariant mass greater than 4 GeV. Moreover, there needs to be one lepton with transverse momentum above 5 GeV and another one with transverse momentum above 2 GeV. Both of them have to be within $|\eta| < 3$. To increase statistics samples were generated with additional requirements on the four lepton invariant mass. A summary of the calculated cross sections is given in Table 23

Table 23: Summary of the generator cross sections at $\sqrt{s} = 13\,\text{TeV}$ predicted by MCFM for various loop-induced diboson processes. Details on the generator selection criteria are given in the text.

process	further selection	MCFM (fb)
$gg \to ZZ \to 4e$	$m(4\ell) > 100\,\text{GeV}$	1.25
$gg \to ZZ \to 2e2\mu$	$m(4\ell) > 100\,\text{GeV}$	2.52
$gg(\to H/H^*) \to ZZ \to 4e$	$m(4\ell) > 130\,\text{GeV}$	1.14
$gg(\to H/H^*) \to ZZ \to 2e2\mu$	$m(4\ell) > 130\,\text{GeV}$	2.29

5.1.3 Sherpa

Matrix elements for the loop-induced diboson processes have been generated using OpenLoops within Sherpa v2.1.1 with up to one additional parton in the final state. The matrix elements are LO accurate and the gauge boson decay is fully incorporated, i.e. off-shell effects and interferences are fully taken into account [59]. Besides dedicated samples with just continuum VV production or VV production exclusively via an s-channel Higgs boson, there are predictions including all components and related interferences. The EXCLUSIVE_CLUSTER_MODE option was enabled for all samples, ensuring that only QCD splittings are inverted by the clustering algorithm, thus allowing for the leptons to be associated with the core process. This core process is then used to set the core scale to $\mu = m(VV)/2$ within the scale setting approach used by Sherpa. Commonly the generator was configured with the CT10 NLO PDF set.

The inclusive cross section predicted by Sherpa is scaled by a flat k-factor of 0.91 to be roughly consistent with prediction calculated with the G_μ electroweak scheme. Per default the mentioned Sherpa version uses an electroweak parameter scheme which takes the boson masses and $\alpha_{\text{QED}}(m_Z)$ as input and calculates the remaining parameters from using tree-level relations. This can introduce differences of $\alpha_{\text{QED}}(m_Z)$ with respect to the one evaluated in the G_μ scheme or lead to deviations from the PDG value for e.g. the weak mixing angle. Because of the four electroweak vertices in continuum ZZ and WW production these samples are particularly affected.

Predictions for the 4ℓ and the $2\ell2\nu$ final state are produced. In the latter case always both, WW and ZZ, and their interference are included. Dedicated cuts on the dilepton respectively neutrino pair got imposed for some samples to enhance the statistics for ZZ production. Furthermore there are predictions only above a certain four charged lepton invariant mass to increase the statistics in the tail. Common selections is applied on all samples requiring a minimum of 10(2) GeV invariant mass for all same-flavor opposite-sign lepton pairs for the $4\ell(2\ell2\nu)$ final state. Finally, there are separate predictions just including VV continuum or VV resonant production as well as for the full process with all interferences. A summary of the calculated cross sections by Sherpa are given in Table 24.

Table 24: Summary of the generator cross sections at $\sqrt{s} = 13\,\text{TeV}$ predicted by Sherpa for various loop-induced diboson processes. Details on the generator selection criteria are given in the text.

process	Sherpa (fb)
$gg \to ZZ \to 4\ell/2\ell2\ell'$ (with $\ell/\ell' = e,\mu,\tau$)	11.2
$gg(\to H/H^*) \to ZZ \to 4\ell/2\ell2\ell'$ (with $\ell/\ell' = e,\mu,\tau$)	20.7
$gg(\to H/H^*) \to ZZ \to 4\ell/2\ell2\ell'$ (with $\ell/\ell' = e,\mu,\tau$ and $m(4\ell) > 100\,\text{GeV}$)	16.2
$gg(\to H/H^*) \to VV \to \ell\nu\ell'\nu/2\ell2\nu$ (with $\ell/\ell' = e,\mu,\tau$ and $V = Z, W$)	854

5.1.4 PowhegBox

For ZZ continuum production and subsequent decay to $2e2\mu$ it is possible to produce event samples at NLO QCD accuracy merged with parton shower following the Powheg approach [56]. A trial version of this process is provided by the authors and used with PowhegBox v2, base revision r3333. The generator is configured with the NNPDF3.0 NLO PDF set and the dynamic renormalisation and factorisation scale $\mu_{r/f} = m(VV)$ as central scale. The subsequent shower is performed with PYTHIA8 using the A14 tune and the NNPDF2.3 LO PDF set as well as the EvtGen afterburner to ensure proper decays of heavy flavor quarks. This step and the full detector simulation are done mimicking official ATLAS work-flows. At generator level the two same-flavor opposite-charge lepton pairs are required to have an invariant mass within [4; 200] GeV and a combined transverse momentum above 0.05 GeV. To enlarge statistics by keeping the computing time sensible the four lepton invariant mass is required to be within [100; 300] GeV. The predicted cross section and its scale variation and prediction with more precise PDF set can be found in Table 25.

Table 25: Summary of the generator cross sections at $\sqrt{s} = 13$ TeV predicted by Sherpa for various loop-induced diboson processes. Details on the generator selection criteria are given in the text.

process	configuration	PowhegBox (fb)
$gg \to ZZ \to 2e2\mu$	$\mu_{r/f} = m(VV)$	4.88
$gg \to ZZ \to 2e2\mu$	$\mu_{r/f} = 2 \cdot m(VV)$	4.44
$gg \to ZZ \to 2e2\mu$	$\mu_{r/f} = 0.5 \cdot m(VV)$	5.30
$gg \to ZZ \to 2e2\mu$	$\mu_{r/f} = m(VV)$; NNPDF3.0 NNLO PDF set	4.66

5.2 Systematic uncertainties and reweighting to higher accuracy

Recent theory results suggest a sizeable enhancement with respect to the LO prediction caused by higher-order QCD effects. NLO QCD corrections were calculated for continuum VV production assuming a heavy top quark [60] or mass-less quarks [61, 62] in the loop. Furthermore, the latter predictions got matched to parton shower using the Powheg approach [56]. However, a complete calculation in particular view of the simultaneous treatment of all quark masses is not yet available. The contribution to diboson production through an off-shell Standard Model Higgs H^* and the interference with the continuum production is known beyond NLO QCD and calculated using various approximations [63–67]. Depending on the physics analysis it would be useful to model all three components separately and even per jet multiplicity as long as there is no actual event generator available. Especially in the context of jet multiplicity and parton shower matching, there are unfortunately some difficulties as mentioned in Reference [56]. Considering the results of all listed references, the predictions of the earlier-mentioned leading order generators are scaled by a flat k-factor of 1.7 with an conservative uncertainty of 60%. This procedure applies also for Sherpa, which in principle includes parts of the NLO QCD effects, but which would be in significant disagreement with NLO predictions without scaling. At higher invariant masses of the system Sherpa is expected to approach the full calculation and has the advantage of fully included top quark mass effects. In particular Higgs analyses [43, 68] are sensitive to a good modeling of this process and therefore apply the scaling.

5.3 Generator comparisons

In particular at the resonance peak at about 125 GeV only continuum VV production matters as the production via an s-channel Higgs is generated by dedicated programs and the interference is minimal. Figure 19 shows the `gg2VV`, MCFM and `Sherpa` samples scaled to include NLO QCD effects with respect to the shower matched NLO QCD result of the `PowhegBox` test version. The plotted `Sherpa` prediction is corrected for the electroweak scheme. The explicit process under study is ZZ production in the $2e2\mu$ final state and the applied selection follows the Higgs fiducial definition detailed in Section 3.3.1. The agreement is well within the conservative 60% uncertainty. At higher invariant masses starting from the ZZ threshold the negative interference begins to become non-negligible and top quark mass effects appear to be sizeable above about 340 GeV. Both effects are not presented explicitly because the `PowhegBox` predictions do not incorporate them. Given the very good agreement for continuum production and the only very mild slope of QCD effects for inclusive observables like m_{VV} the flat k-factor is assumed to be valid also there, in particular if the conservative uncertainty is applied. In the region above the ZZ threshold the predictions of MCFM and `Sherpa` for the full process including continuum and resonant production as well as their interference are displayed in Figure 19 as well. For this high invariant mass region all channels, namely $4e$, 4μ, $2e2\mu$ and $2\mu2e$, are summed up and the flat k-factor of 1.7 is applied. The flat ratio indicates the only mild dependence of this observable on higher-order QCD effects as the description by `Sherpa` is more accurate. On the other hand quantities like the transverse momentum of jets or the ZZ system show significant deviations. The off-set between `MCFM` and `Sherpa` is caused by the different scale and PDF set choices.

A comparison of `Sherpa` and `gg2VV` for the process $gg \to WW \to e\nu\mu\nu$ which does not interfere with intermediate ZZ bosons is presented in Figure 20. The fiducial selection of the events entering this figure are detailed in Section 3.3.3. While the prediction by `gg2VV` is pure leading order with subsequent parton shower by `PYTHIA8` configured with the "wimpy shower" option, the `Sherpa` predictions have the first jet clustered back to the matrix element. As expected there are only mild differences for the fairly inclusive invariant mass of the dilepton system. On the other hand the transverse momentum of the leading lepton shows more sizeable deviations in particular for higher values as there is sensitivity to higher-order effects.

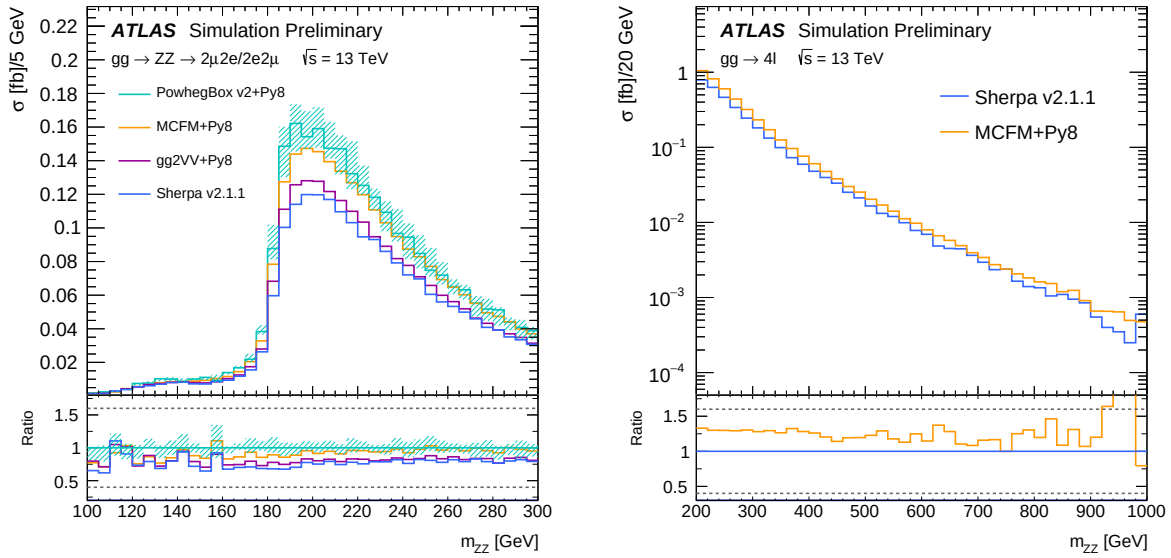

(a) (b)

Figure 19: Invariant mass distribution of the ZZ system for fully simulated continuum production in the $2e2\mu$ final state predicted by `gg2VV`, MCFM and `Sherpa` compared to NLO QCD `PowhegBox` (a). The shaded band indicates the NLO QCD scale uncertainty. In the high mass (b) region where `PowhegBox` is not valid anymore the prediction for the invariant mass of the ZZ system for all final state channels and including continuum and resonant production as well as the interference is compared between `MCFM` and `Sherpa`. The fiducial selection of the Standard Model Higgs analysis is used and a flat k-factor of 1.7 is applied for all except the `PowhegBox` prediction. Furthermore `Sherpa` is scaled by 0.91 to account for the different electroweak scheme. In both plots the dashed lines indicate the 60% systematic uncertainties mentioned above.

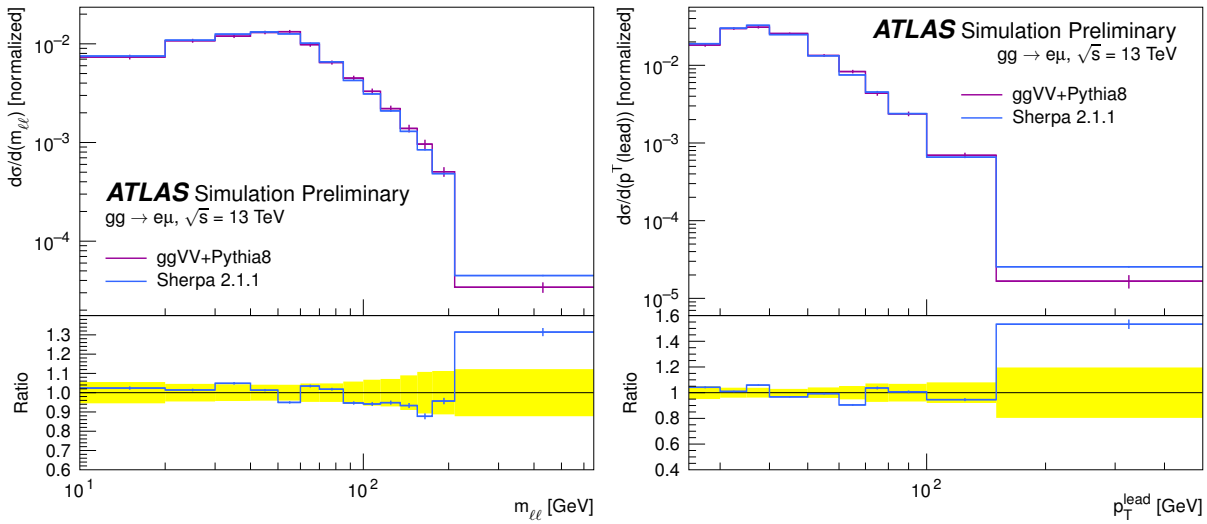

(a) (b)

Figure 20: Comparison on the invariant dilepton mass $m_{\ell\ell}$ (a) and the leading lepton transverse momentum (b) predicted by `gg2VV` and `Sherpa` for the process $gg \to e\nu\mu\nu$. All of the distributions have been normalised to unity.

6 Semi-leptonic diboson processes

6.1 Generator setup

Table 26: Overview of process accuracies for the chosen generators.

		$VV + 0j$	$+1j$	$+2j$	$+3j$	$+ \geq 4j$
$VV = WW, WZ$	Sherpa v2.1.1	NLO	LO	LO	LO	PS
	Sherpa v2.2	NLO	NLO	LO	LO	PS
	PowhegBox+PYTHIA8 /HERWIG++	NLO	LO	PS	PS	PS
$VV = ZZ$	Sherpa v2.1.1	NLO	NLO	LO	LO	PS
	Sherpa v2.2	NLO	NLO	LO	LO	PS
	PowhegBox+PYTHIA8 /HERWIG++	NLO	LO	PS	PS	PS

6.1.1 Sherpa v2.1.1

Samples for semileptonic diboson production are generated with Sherpa v2.1.1 in a factorised approach: boson pairs are produced on-shell according to the accuracies given in Table 26. The vector boson decays are then generated a posteriori in a decay module, which also generates a Breit-Wigner mass distribution of the decaying boson. All decay channel combinations involving one hadronically decaying vector boson and one vector boson decaying into charged leptons or neutrinos are generated as separate samples, using branching ratios calculated at LO.

The factorisation and renormalisation scales were set using the STRICT_METS scale setter with a core scale of $\mu = m_{\mathrm{VV}}/2$. Electroweak parameters are set using the default EW_SCHEME=1 in Sherpa.

The Sherpa options EXCLUSIVE_CLUSTER_MODE=1 and METS_CLUSTER_MODE=16 are used in these samples to allow only strong splittings but unordered histories in the ME+PS clustering procedure, to correctly treat the hadronic decay products.

6.1.2 Sherpa v2.2

Another set of samples for semileptonic diboson production are generated with Sherpa v2.2 using the same factorised approach. The following differences apply compared to the samples described in the last section:

- The production accuracy is raised to $pp \to VV$ + 0,1j@NLO + 2,3j@LO for all final states.
- The vector boson decay branching ratios are adjusted to match PDG values to avoid sensitivity to missing QCD corrections for the hadronic partial widths.
- The electroweak parameters are set in the G_F scheme (Sherpa parameter EW_SCHEME=3) with $G_F = 1.166397 \cdot 10^{-5}$ GeV^{-2}.
- The option AMEGIC_CUT_MASSIVE_VECTOR_PROPAGATORS=0 is used to stabilise the matrix elements for $pp \to VV$ + 1j@NLO from the Amegic matrix element generator in all final states.

6.1.3 PowhegBox+PYTHIA8

Semileptonic diboson samples are furthermore produced with the PowhegBox v2 generator, interfaced to the Pythia parton shower model. The CT10 NLO PDF set is used for the hard-scattering process, while the CTEQ6L1 set is used for the parton shower. The non-perturbative effects are modelled using the AZNLO tune. The EvtGen v1.2.0 program is used for properties of the bottom and charm hadron decay. The PowhegBox generator provides NLO QCD accuracy for diboson production.

The samples are split according to semi-leptonic final-states ($2lqq$, $lvqq$, $2\nu qq$). NLO corrections to the hadronic decay processes are not included, but the hadronic V decays are generally well modeled by showering Monte Carlos. All final-states include the effect of off-shell singly resonant amplitudes, and the WZ and ZZ samples include the effects of Z/γ^* interference.

The dynamic scale of the mass of the boson pair is used for both the factorisation and renormalisation scales. The withdamp and bornzerodamp flags were set in PowhegBox for each sample to ensure that any phase-space region in which the Born cross section vanishes is properly handled.

A matrix element level generator cut is placed on the Z boson decay products in the case that they are charged leptons or quarks, requiring the mass of the charged lepton or quark pair to be greater than 20 GeV.

6.1.4 PowhegBox+HERWIG ++

A final set of semileptonic diboson samples has been produced by changing the parton shower model for the events generated with PowhegBox, described in Section 6.1.3. The same set of events is thus showered with HERWIG ++ v2.7.1 with the UE-EE-5 tune and the corresponding CTEQ6L1 PDF set.

The main purpose of this sample is to provide a comparison with a different parton shower model, while maintaining the same hard scattering simulation with PowhegBox.

6.2 Cross sections

The generator cross sections and filter efficiencies for each sample can be found in Table 27. It can be seen, that the generator cross section for the Sherpa samples is typically about 10% larger than for the PowhegBox samples. This difference stems from additional contributions from higher multiplicity matrix elements present in the Sherpa samples as can be seen in Figure 21(b).

Further differences between different decay channels of the same process must be attributed to the branching ratios used in the generators. For example the ratio $R \equiv \frac{\sigma(W(\to\ell\nu)Z(\to qq))}{\sigma(W(\to qq)Z(\to\ell\ell))} = \frac{\mathcal{B}(W\to\ell\nu)\mathcal{B}(Z\to qq)}{\mathcal{B}(W\to qq)\mathcal{B}(Z\to\ell\ell)}$ is given by:

$$
\begin{aligned}
R^{\text{PDG}} &= \frac{0.3246 \cdot 0.6991}{0.6754 \cdot 0.1010} = 3.327 \\
R^{\text{Sherpa v2.2}} &= \frac{11.413}{3.437} = 3.321 \\
R^{\text{PowhegBox}} &= \frac{10.086}{3.2777} = 3.077
\end{aligned}
$$

Table 27: Diboson samples used for this study. The MC generator, production cross section, k-factor, filter efficiency and total number of generated events are shown. The same values are valid for `PowhegBox+PYTHIA8` and `PowhegBox+HERWIG`, since the same hard-scattering events are re-used with different parton shower.

Process	Generator	$\sigma \times$ BR [pb]	k-factor	ϵ_{filter}	Events
WlvZqq	`Sherpa v2.1.1`	11.5	0.91	1.0	1952000
WqqZll	`Sherpa v2.1.1`	3.4258	0.91	1.0	490000
WqqZvv	`Sherpa v2.1.1`	6.7758	0.91	1.0	973000
ZqqZll	`Sherpa v2.1.1`	16.432	0.91	0.14352	487000
ZqqZvv	`Sherpa v2.1.1`	16.434	0.91	0.28245	493000
WlvZqq	`Sherpa v2.2`	11.413	1.0	1.0	7200000
WqqZll	`Sherpa v2.2`	3.437	1.0	1.0	5400000
WqqZvv	`Sherpa v2.2`	6.7973	1.0	1.0	6000000
ZqqZll	`Sherpa v2.2`	15.563	1.0	0.13961	5400000
ZqqZvv	`Sherpa v2.2`	15.564	1.0	0.27976	5400000
WlvZqq	`PowhegBox`	10.086	1.0	1.0	9693000
WqqZll	`PowhegBox`	3.2777	1.0	1.0	1469000
WqqZvv	`PowhegBox`	5.7576	1.0	1.0	2921000
ZqqZll	`PowhegBox`	2.2699	1.0	1.0	3933000
ZqqZvv	`PowhegBox`	3.9422	1.0	1.0	9591000

6.3 Generator comparisons

6.3.1 Analysis description

The semileptonic diboson processes are an important irreducible background for the search of the Higgs boson in the $VH(H \to b\bar{b})$ channel [69]: although their cross sections are significantly lower than other background processes (such as V+jets or $t\bar{t}$ production), they can mimic very closely the $VH(\to b\bar{b})$ signature with a cross section approximately 5 times larger than the signal.

In this section some studies aimed at understanding the impact of the semileptonic diboson modeling are reported, considering kinematic regions typical for the $VH(\to b\bar{b})$ analysis.

In the particle-level analysis applied for these studies, the main objects are defined as follows. Electrons and muons with $p_{\text{T}} > 7$ GeV and within $|\eta| < 2.47$ (for electrons) or $|\eta| < 2.7$ (for muons) are retained if the p_{T} sum of all charged particles (excluding the lepton candidate) within a cone of $\Delta R = 0.2$ around the lepton is less than 10 % of the lepton p_{T}. These are referred to as 'loose' selection criteria. For leptons passing 'tight' selection criteria the isolation cut is reduced to 4 % in addition to passing the loose selection, and they are required to have $p_{\text{T}} > 25$ GeV.

Jets are reconstructed using the anti-k_t clustering algorithm with a jet-radius parameter of $R = 0.4$. The jet transverse momentum is required to be greater than 20 GeV for central jets ($|\eta| < 2.5$) and greater than 30 GeV for forward jets ($2.5 < |\eta| < 5$). Jets with $|\eta| > 5$ are ignored. An overlap removal procedure is applied between selected jets and leptons. A jet is rejected if an electron passing the loose identification criteria can be matched to it in η-ϕ space ($\Delta R = 0.4$). Similarly a muon-jet overlap removal procedure is applied, provided that at most three charged particle tracks are pointing to the primary vertex associated with an overlapping muon candidate. No requirement on the flavor composition of the selected jets is applied.

The missing transverse energy ($E_{\mathrm{T}}^{\mathrm{miss}}$) is reconstructed by taking the transverse momentum of the negative sum of the four-momenta of all the visible particles, and the missing transverse momentum ($p_{\mathrm{T}}^{\mathrm{miss}}$) is defined consistently summing over all the charged particles.

Three separate event selections are implemented: the 0-, 1- and 2-lepton channels, targeting the different leptonic decays of one of the vector bosons ($Z \to \nu\nu$, $W \to \ell\nu$ and $Z \to \ell\ell$ respectively). All selections require at least 2 central jets, corresponding to the hadronic decay of one of the two vector bosons. In the following, the hadronically decaying vector boson is reconstructed by ordering the selected central jets in transverse momentum, and taking the leading two selected central jets (named j_1 and j_2). In the 0-lepton selection exactly 0 charged leptons passing the 'loose' selection are required, the transverse momentum of the leptonically decaying vector boson is reconstructed from the missing transverse momentum. The 1-lepton selection contains events with exactly 1 'tight' lepton and no additional 'loose' leptons, the vector boson is reconstructed from the missing transverse energy and the selected lepton. In the 2-lepton selection exactly 2 same-flavour (in case of muons also opposite charge) leptons passing the 'loose' selection, of which at least 1 passing the 'tight' selection are required, while the vector boson is reconstructed from the two selected leptons.

Additional selection cuts for the different lepton-channels are reported in Table 28, reflecting the analysis strategy from [69].

These selection strategies are considered for the different semileptonic diboson processes in order to obtain the results shown in Section 6.3.2: the 0-lepton selection is applied to $Z(\to qq)Z(\to \nu\nu)$ and $W(\to qq)Z(\to \nu\nu)$ samples, the 1-lepton selection is applied to $Z(\to qq)W(\to l\nu)$ and the 2-lepton selection is applied to $Z(\to qq)Z(\to ll)$ and $W(\to qq)Z(\to \nu\nu)$ samples.

Table 28: Semileptonic diboson event selection for the different lepton-channels.

Variable	Selection
0-lepton	
$E_{\mathrm{T}}^{\mathrm{miss}}$ [GeV]	>150
$p_{\mathrm{T}}^{\mathrm{miss}}$ [GeV]	>30
$p_{\mathrm{T}}(j_1)$	> 45
$\Delta\phi(E_{\mathrm{T}}^{\mathrm{miss}}, p_{\mathrm{T}}^{\mathrm{miss}})$	$< \pi/2$
$\min[\Delta\phi(E_{\mathrm{T}}^{\mathrm{miss}}, jets)]$	$< 20°$
$\sum p_T(jets)$ [GeV]	> 120(150) [2-jet(3-jet)]
$\Delta\phi(j_1, j_2)$	$< 140°$
$\Delta\phi(E_{\mathrm{T}}^{\mathrm{miss}}, j_1 + j_2)$	$< 120°$
#(central and forward jets)	≤3
1-lepton	
p_T^W [GeV]	> 150
$p_T(j_1)$ [GeV]	> 45
#(central and forward jets)	≤3
2-lepton	
71 GeV $< m_{ll}$ [GeV]	< 121
$p_T(j_1)$ [GeV]	> 45

6.3.2 Results

In this section the result of the comparisons between the generators introduced in Sections 6.1.1, 6.1.2, 6.1.3 and 6.1.4 are shown. Figure 21 shows these comparisons for a specific set of variables, chosen to describe kinematic and topology for one of the semileptonic diboson processes, $Z(\rightarrow qq)Z(\rightarrow ll)$: $p_T(V)$, number of central and forward jets, $\Delta\phi(j_1, j_2)$, $\Delta R(j_1, j_2)$, $\Delta\phi(V, j_1 j_2)$ and $m(j_1, j_2)$. Figure 22 focuses on the comparison among different generators for the invariant mass of the reconstructed hadronically decaying boson, $m(j_1, j_2)$, for all diboson processes considered.

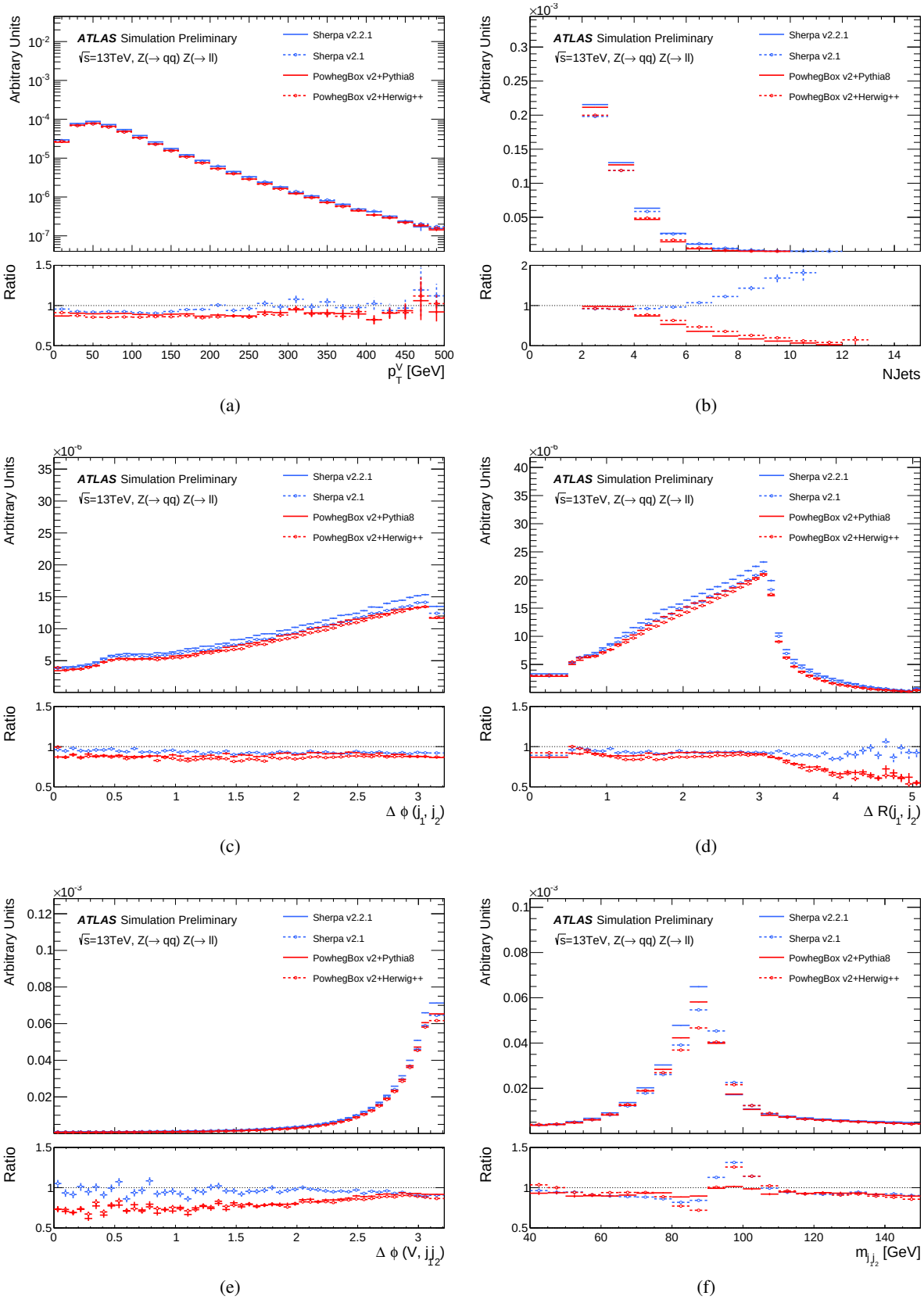

Figure 21: Comparison of differential distributions in $Z(\rightarrow qq)Z(\rightarrow \ell\ell)$ production at 13 TeV. The lower panel shows the ratio of each distribution with respect to the `Sherpa v2.2` prediction.

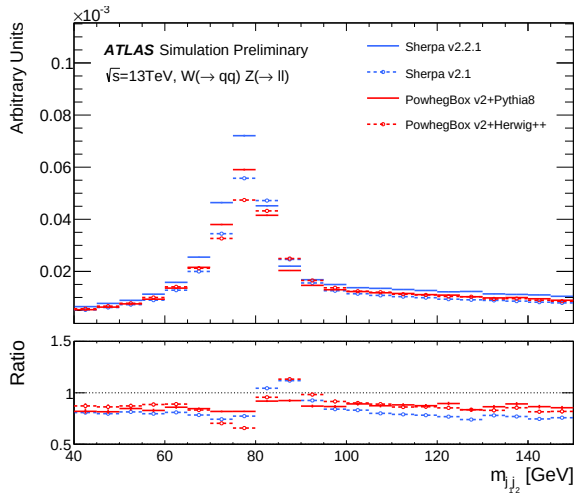

(a) $W(\to qq)Z(\to \ell\ell)$

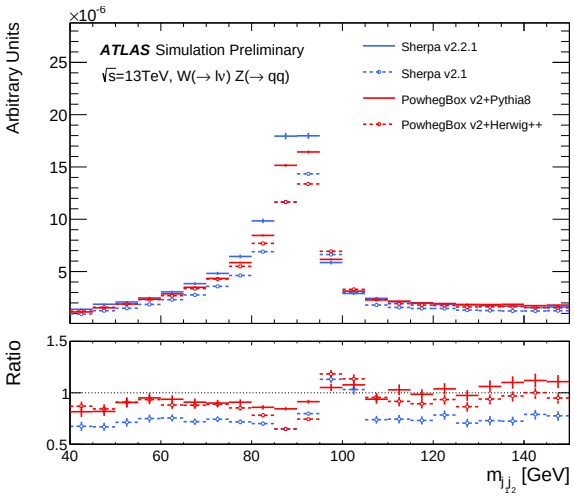

(b) $W(\to \ell\nu)Z(\to qq)$

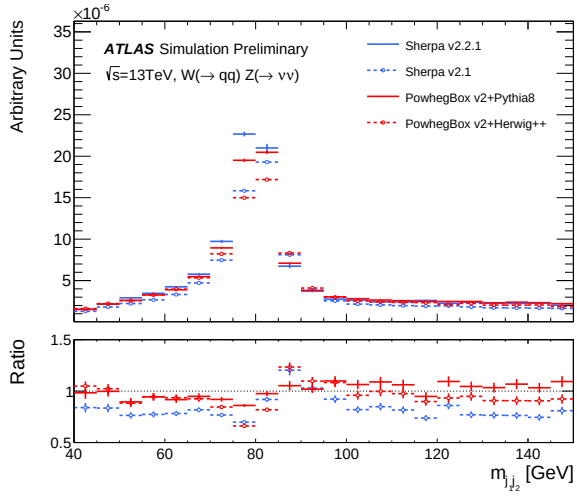

(c) $W(\to qq)Z(\to \nu\nu)$

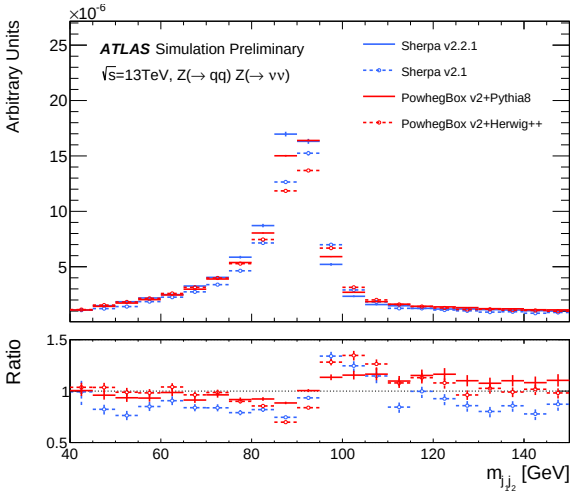

(d) $Z(\to qq)Z(\to \nu\nu)$

Figure 22: Comparison of the invariant dijet mass $m(j_1, j_2)$ distribution in four different semileptonic final states at 13 TeV. The lower panel shows the ratio of each distribution with respect to the `Sherpa v2.2` prediction.

7 Triboson production processes

7.1 Generator setup

This section describes the generator setup used for triboson production. An overview of the accuracy achieved with the chosen generators is given in Table 29.

Table 29: Overview of process accuracies for the chosen generators.

		$VVV + 0j$	$VVV + 1j$	$VVV + 2j$	$VVV + \geq 3j$
VVV on-shell	Sherpa v2.2	NLO	LO	LO	PS
$6\ell, 5\ell 1\nu, 4\ell 2\nu, 3\ell 3\nu, 2\ell 4\nu$	Sherpa v2.2	LO	LO	PS	PS
$3\ell 3\nu$	VBFNLO+PYTHIA8	LO	PS	PS	PS

7.1.1 Sherpa

Matrix elements for all combinations of $pp \to VVV$ with $V = W^{\pm}, Z$ have been generated using Sherpa v2.2.2 with up to two additional partons in the final state, including full NLO accuracy for the inclusive process. The setup is based on the one used in Reference [70]. All diagrams with three electroweak couplings are taken into account, including diagrams involving Higgs propagators. However, since these samples use factorised decays with on-shell vector bosons, the resonant contribution from those diagrams can not be reached from the 125 GeV Higgs. Processes with bottom quarks in the hard scattering process are ignored, to avoid contributions from top-quark mediated processes.

Leptonic decay channels have been enabled exclusively, using a factorised on-shell approach. The LO branching ratios are corrected to comply with the values given by the PDG [71]. No parton-level cuts are imposed on the generated phase space.

In addition, LO-accurate samples for final states containing two or more charged leptons have been generated with Sherpa v2.2.1 including off-shell contributions. Matrix elements with up to one additional real emission are considered for these LO samples.

The NLO-accurate as well as the LO-accurate samples have been generated using the NNPDF3.0nnlo PDF set and a matching scale of 30 GeV is chosen. Both setups use the G_μ scheme, making use of the tree-level relations between the electroweak input parameters. The factorisation and renormalisation scales were set using the STRICT_METS scale setter with a core scale of $\mu = m_{VVV}$.

7.1.2 VBFNLO

The VBFNLO v2.7.0 Monte Carlo program [72–74] can generate vector boson fusion, double and triple vector boson production events at LO and it can also compute the corresponding process cross sections at NLO in QCD. VBFNLO is used to generate WWW events at LO using the CTEQ6L1 PDF and the dynamic scale of the mass of the three bosons for both the factorisation and renormalisation scales. The partonic events are processed by PYTHIA8 with the same PDF for parton showering. The A14 ATLAS tune [27] is used for the modeling of non-perturbative effects. The p_{T} of the three charged leptons in the final state is required to be greater than 5 GeV.

7.2 Cross sections

7.2.1 Generator cross sections

A summary of the cross sections predicted by Sherpa and VBFNLO is given in Table 30 using a setup for LO-accurate triboson production including off-shell contributions. Table 31 shows the Sherpa cross sections for NLO-accurate triboson production using a factorised decay setup, which excludes the off-shell contributions and hence also the contribution from on-shell Higgs-strahlung production.

Table 30: Summary of the generator cross sections at $\sqrt{s} = 13$ TeV predicted by Sherpa and VBFNLO for 6-lepton final states, i.e. LO VVV production including off-shell contributions.

	Predicted cross sections	
Final state	Sherpa (fb)	VBFNLO (fb)
$2\ell 4\nu$	5.837	—
$3\ell 3\nu$	15.85	11.03
$4\ell 2\nu$	4.368	—
$5\ell 1\nu$	0.568	—
$6\ell 0\nu$	0.102	—

Table 31: Summary of the generator cross sections at $\sqrt{s} = 13$ TeV predicted by Sherpa for triboson production at NLO accuracy using factorised on-shell decays.

	Predicted cross sections
Final state	Sherpa (fb)
$WWW \to 3\ell 3\nu$	7.193
$ZWW \to 2\ell 4\nu$	3.543
$ZWW \to 4\ell 2\nu$	1.796
$ZZW \to 3\ell 3\nu$	0.748
$ZZW \to 5\ell 1\nu$	0.188
$ZZZ \to 2\ell 4\nu$	0.172
$ZZZ \to 4\ell 2\nu$	0.086
$ZZZ \to 6\ell 0\nu$	0.014

7.3 Generator comparisons

The 3-charged-lepton selection of the Rivet [75] routine ATLAS_2016_I1492320 for the recently published ATLAS search for triboson production at 8 TeV [76] has been used as a template in order to compare the different generator predictions at 13 TeV. In this phase space, three charged leptons with $p_{\mathrm{T}} > 20\,\mathrm{GeV}$ are selected and a cut on the missing transverse momentum in the event, $p_{\mathrm{T}}^{\mathrm{miss}}$, of 45 GeV and 55 GeV is placed depending whether one or two same-flavour opposite-sign pairs can be formed from the three leptons, respectively. A Z-boson veto is enforced by requiring that the mass of the same-flavour opposite-charge pair is sufficiently far away from the resonance. The jet veto that is placed in the original routine has been removed in order to be able to study distributions sensitive to the jet activity. The anti-k_t algorithm with a jet-radius parameter of 0.4 is used to construct jets, which are then required

to satisfy $p_{\mathrm{T}} > 25$ GeV and $|\eta| < 4.5$ for the pseudorapidity. The selection requirements are summarised in Table 32.

Table 32: Summary of the selection cuts to construct the three-charged-leptons fiducial phase space.

Selection requirement	0 SFOS	1 SFOS	2 SFOS
Leptons	Exactly three charged leptons with $p_{\mathrm{T}} > 20$ GeV		
$p_{\mathrm{T}}^{\mathrm{miss}}$	—	$p_{\mathrm{T}}^{\mathrm{miss}} > 45$ GeV	$p_{\mathrm{T}}^{\mathrm{miss}} > 55$ GeV
Same-flavour dilepton mass	$m_{\ell\ell} > 20$ GeV	—	
Angle between triboson and $\vec{p}_{\mathrm{T}}^{\mathrm{miss}}$	$\lvert\phi^{3\ell} - \phi^{\vec{p}_{\mathrm{T}}^{\mathrm{miss}}}\rvert > 2.5$		
Z-boson veto	$\lvert m_{ee} - m_Z\rvert > 15$ GeV	$\lvert m_Z - m_{\mathrm{SFOS}}\rvert > 35$ GeV or $\lvert m_{\mathrm{SFOS}} - m_Z\rvert > 20$ GeV	$\lvert m_{\mathrm{SFOS}} - m_Z\rvert > 20$ GeV

Generator uncertainties have been estimated using scale and PDF variations of the LO-accurate `Sherpa v2.2.1` predictions. An uncertainty band is constructed from the quadrature sum of the statistical uncertainty, 7-point scale variations of the factorisation and the renormalisation scales, two α_{S} variations by ± 0.002 around the nominal value of 0.118 as well as a PDF uncertainty estimated using the NNPDF3.0nnlo replicas using LHAPDF [77]. The statistical uncertainty component is indicated by the error bars.

Figure 23 shows both the inclusive and the exclusive jet multiplicity distributions. The NLO-accurate `Sherpa` prediction (in blue) uses a factorised boson-decay setup that misses off-shell contributions and is therefore smaller than the LO-accurate predictions in the lowest multiplicity bins. At large jet multiplicities where triboson contribution can be considered an electroweak correction to multijet production, the differences between the two `Sherpa` setups become less relevant. `VBFNLO` is not expected to model the jet multiplicity very well as it does not include additional parton-emissions at matrix-element level.

Figure 24 shows the p_{T} distributions for the two highest-p_{T} jets in the event. Differences between the two `Sherpa` setups are noticable in the soft regime of the leading jet p_{T} spectrum, while the agreement is generally better in the hard region of the leading jet p_{T} spectrum. The two setups give fairly similar results for the second and third jet p_{T} spectra where they both have LO accuracy. The three lepton p_{T} distributions are shown in Figure 25. The ratio of the two LO predictions from `VBFNLO` and `Sherpa` are quite flat for all three lepton p_{T} spectra. The difference in normalisation between the two is presumably due to the additional matrix elements included in the `Sherpa` prediction. Significant differences between the NLO-accurate `Sherpa` prediction and the LO-accurate predictions can be seen in the soft lepton p_{T} regions, which are likely due to the missing off-shell contributions in the NLO setup. The agreement generally improves at large lepton p_{T}, where the off-shell contributions become less relevant.

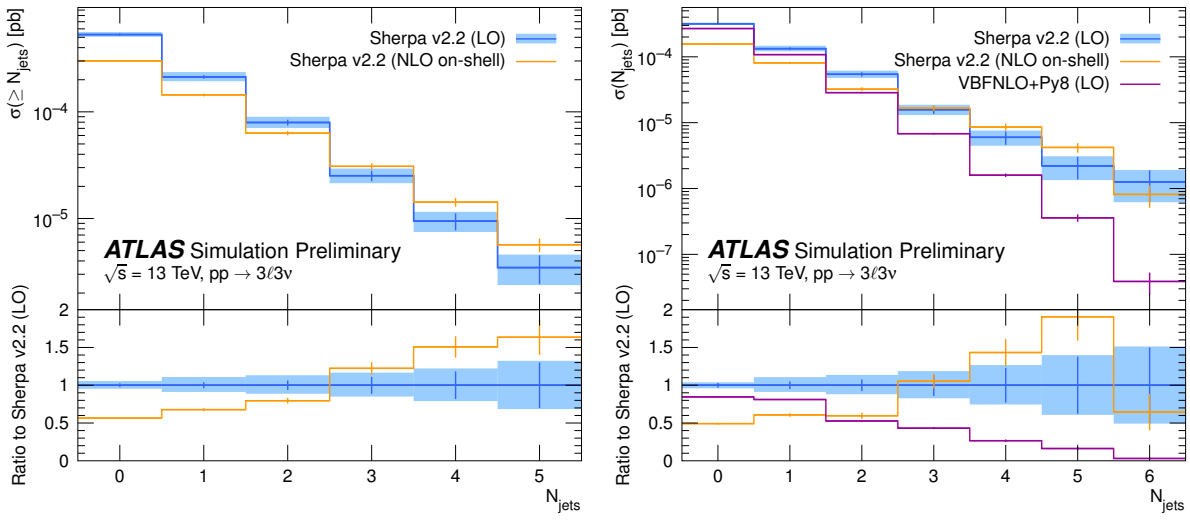

Figure 23: Distributions for the inclusive (left) and exclusive (right) jet multiplicity for $WWW \to 3\ell 3\nu$ production. A NLO-accurate prediction by `Sherpa v2.2` (in blue) for the VVV on-shell final state is compared to two LO-accurate predictions by `Sherpa v2.2` (in red) and `VBFNLO` (in green) for the full $3\ell 3\nu$ final state. The uncertainties indicated by the error bars are statistical only. The blue band in the ratio also includes scale and PDF uncertainties estimated using the LO-accurate `Sherpa v2.2` setup.

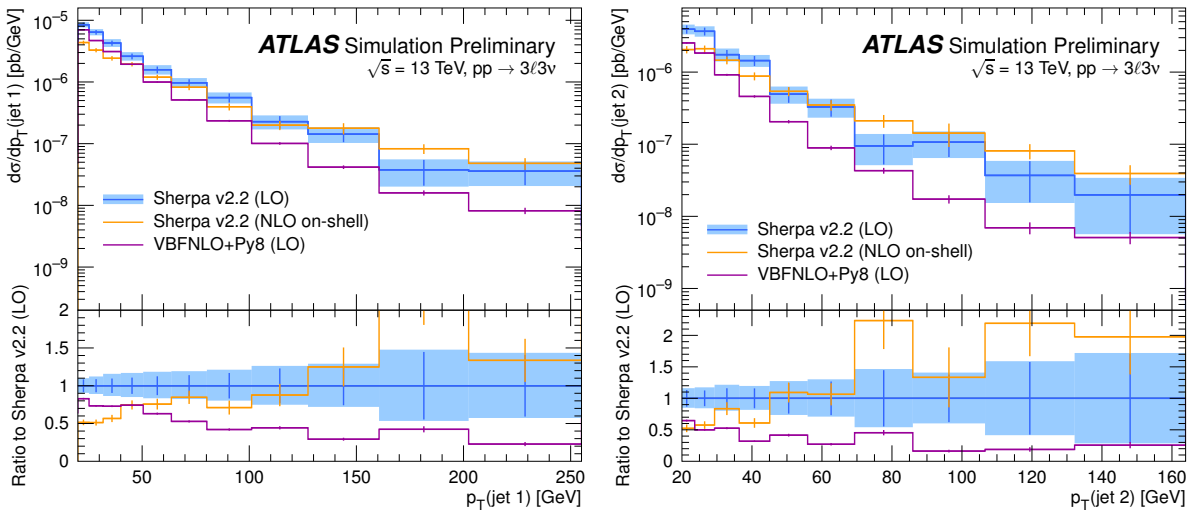

Figure 24: Transverse momentum distributions for the leading (left) and sub-leading (right) jet in the event. A NLO-accurate prediction by `Sherpa v2.2` (in blue) for the VVV on-shell final state is compared to two LO-accurate predictions by `Sherpa v2.2` (in red) and `VBFNLO` (in green) for the full $3\ell 3\nu$ final state. The uncertainties indicated by the error bars are statistical only. The blue band in the ratio also includes scale and PDF uncertainties estimated using the LO-accurate `Sherpa v2.2` setup.

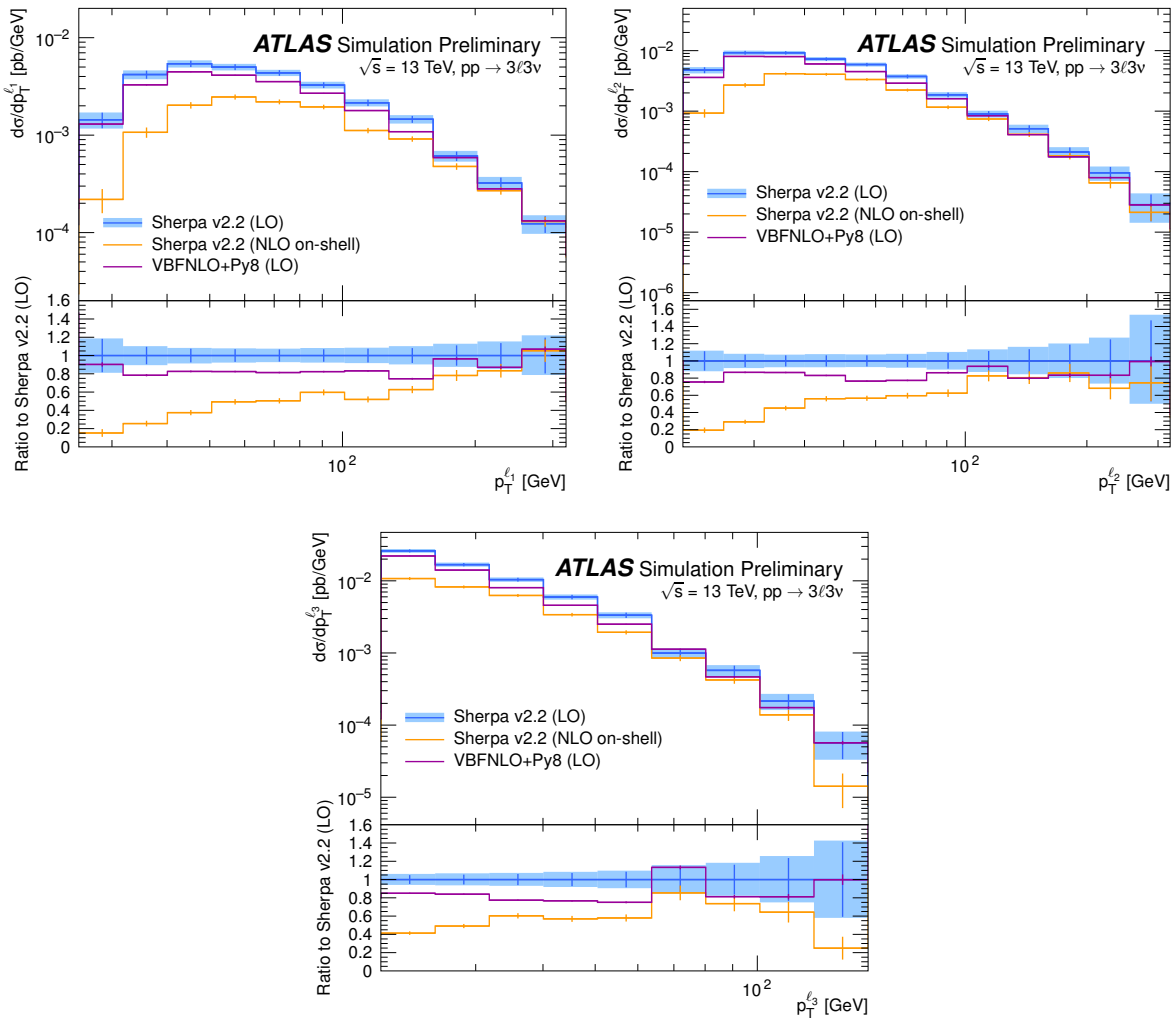

Figure 25: Transverse momentum distributions for the first (top left), second (top right) and third (bottom) lepton in the event. A NLO-accurate prediction by `Sherpa v2.2` (in blue) for the VVV on-shell final state is compared to two LO-accurate predictions by `Sherpa v2.2` (in red) and `VBFNLO` (in green) for the full $3\ell 3\nu$ final state. The uncertainties indicated by the error bars are statistical only. The blue band in the ratio also includes scale and PDF uncertainties estimated using the LO-accurate `Sherpa v2.2` setup.

8 V+γ production

8.1 Leptonic V+γ production

8.1.1 Generator setup

Table 33: Overview of process accuracies for the chosen generators.

		$V\gamma + 0j$	$V\gamma + 1j$	$V\gamma + 2j$	$V\gamma + 3j$	$V\gamma + \geq 4j$
$V = \ell\ell, \ell\nu, \nu\nu$	`Sherpa v2.1.1`	LO	LO	LO	LO	PS
	`Sherpa v2.2`	NLO	NLO	LO	LO	PS

Table 34: Parton-level cuts for the $V + \gamma$ samples

Cut		v2.1.1 LO ($p_\perp^\gamma$-sliced)	v2.1.1 LO ($m_{\ell\ell\gamma}$-sliced)	v2.2 NLO ($p_\perp^\gamma$-sliced)
$p_\perp^\gamma >$		10 GeV	40 GeV	7 GeV
$\Delta R(\gamma, \ell) >$		0.1	0.1	0.1
Photon isolation [55]	$n =$	2	2	2
	$\epsilon =$	0.025	0.025	0.1
	$\delta =$	0.3	0.3	0.1
(for $\ell\ell\gamma$) $m_{\ell\ell} >$		10 GeV	40 GeV	10 GeV

LO samples with `Sherpa v2.1.1` Samples for $\ell\ell\gamma$, $\ell\nu\gamma$ and $\nu\nu\gamma$ final states (collectively called $V+\gamma$ in this subsection) are produced using `Sherpa v2.1.1` in the configuration described in Sec. 2. All off-shell contributions are taken into account. Leading order matrix elements for $V + \gamma + 0, 1, 2, 3$ jets are merged with the parton shower using an ME+PS merging scale of $Q_{\text{cut}} = 20$ GeV.

The parton level cuts are given in Table 34. Additionally, to ensure sufficient MC statistics in relevant regions, the samples are sliced at the parton level in $p_\perp^\gamma$. A second set of $\ell\ell\gamma$ samples for high-mass searches is available with slicing in $m_{\ell\ell\gamma}$ but otherwise identical configuration.

NLO samples with `Sherpa v2.2` Additional samples for $\ell\ell\gamma$, $\ell\nu\gamma$ and $\nu\nu\gamma$ are produced using `Sherpa v2.2` in the configuration described in Sec. 2. Matrix elements including all off-shell contributions are generated for $V + \gamma + 0$, 1jet@NLO+, 2, 3jet@LO, where the given accuracy refers to the QCD accuracy in each parton-level final state. The different final-state multiplicities are merged using the MEPS@NLO method with a merging scale of $Q_{\text{cut}} = 20$ GeV. One-loop matrix elements are provided by the `OpenLoops` library [6].

The parton level cuts are given in Table 34. Additionally, to ensure sufficient MC statistics in relevant regions, the samples are sliced at the parton level in $p_\perp^\gamma$.

8.1.2 Cross sections

All Monte Carlo predictions for $V+\gamma$ production are normalised according to the cross sections provided by the generator. The `Sherpa v2.1.1` LO samples are listed with their cross sections in Table 35.

No higher-order calculations (K-factors) are used to scale these samples.

Table 35: Summary of the generator cross sections at $\sqrt{s} = 13$ TeV predicted by `Sherpa v2.1.1` at LO for some examples of $V+\gamma$ final states, including the number of events expressed as equivalent integrated luminosity.

Final state	$p_{\perp}^{\gamma}$ slice	`Sherpa` [pb]	$L_{equivalent}$ [1/fb]
$ee\gamma$	$10 \to 35$	52.7	$9.49 \cdot 10^1$
$ee\gamma$	$35 \to 70$	5.24	$9.54 \cdot 10^1$
$ee\gamma$	$70 \to 140$	0.385	$6.50 \cdot 10^2$
$ee\gamma$	>140	0.0472	$5.30 \cdot 10^3$
$e\nu\gamma$	$10 \to 35$	200	$1.45 \cdot 10^1$
$e\nu\gamma$	$35 \to 70$	15.3	$3.26 \cdot 10^1$
$e\nu\gamma$	$70 \to 140$	1.53	$1.64 \cdot 10^2$
$e\nu\gamma$	>140	0.242	$1.03 \cdot 10^3$
$\nu\nu\gamma$	$35 \to 70$	4.04	$1.24 \cdot 10^2$
$\nu\nu\gamma$	$70 \to 140$	0.972	$2.57 \cdot 10^2$
$\nu\nu\gamma$	>140	0.171	$1.46 \cdot 10^3$

8.1.3 Generator comparisons

A selection of comparison plots between the LO and NLO samples for the $W(\to e\nu)\gamma$ final state are shown in Figure 26. The fiducial phase space selection for these comparisons is summarised in Table 36.

Table 36: Definitions of the event selection employed for studies of $W(\to e\nu)\gamma$ production.

Object/event selection	
Electrons	$E_{\mathrm{T}} > 25\,\mathrm{GeV}$, $\lvert\eta\rvert < 2.47$, $R_{e,\gamma}^{\mathrm{dress}} < 0.1$
Photons	$E_{\mathrm{T}} > 15\,\mathrm{GeV}$, $\lvert\eta\rvert < 2.37$
Missing energy	$E_T^{\mathrm{miss}} > 35\,\mathrm{GeV}$
Jets	anti-k_t, $R = 0.4$, $p_{\perp} > 30\,\mathrm{GeV}$, $\lvert\eta\rvert < 4.4$
Overlap removal	$\Delta R(e, j) > 0.3$, $\Delta R(\gamma, j) > 0.3$, $\Delta R(e, \gamma) > 0.7$

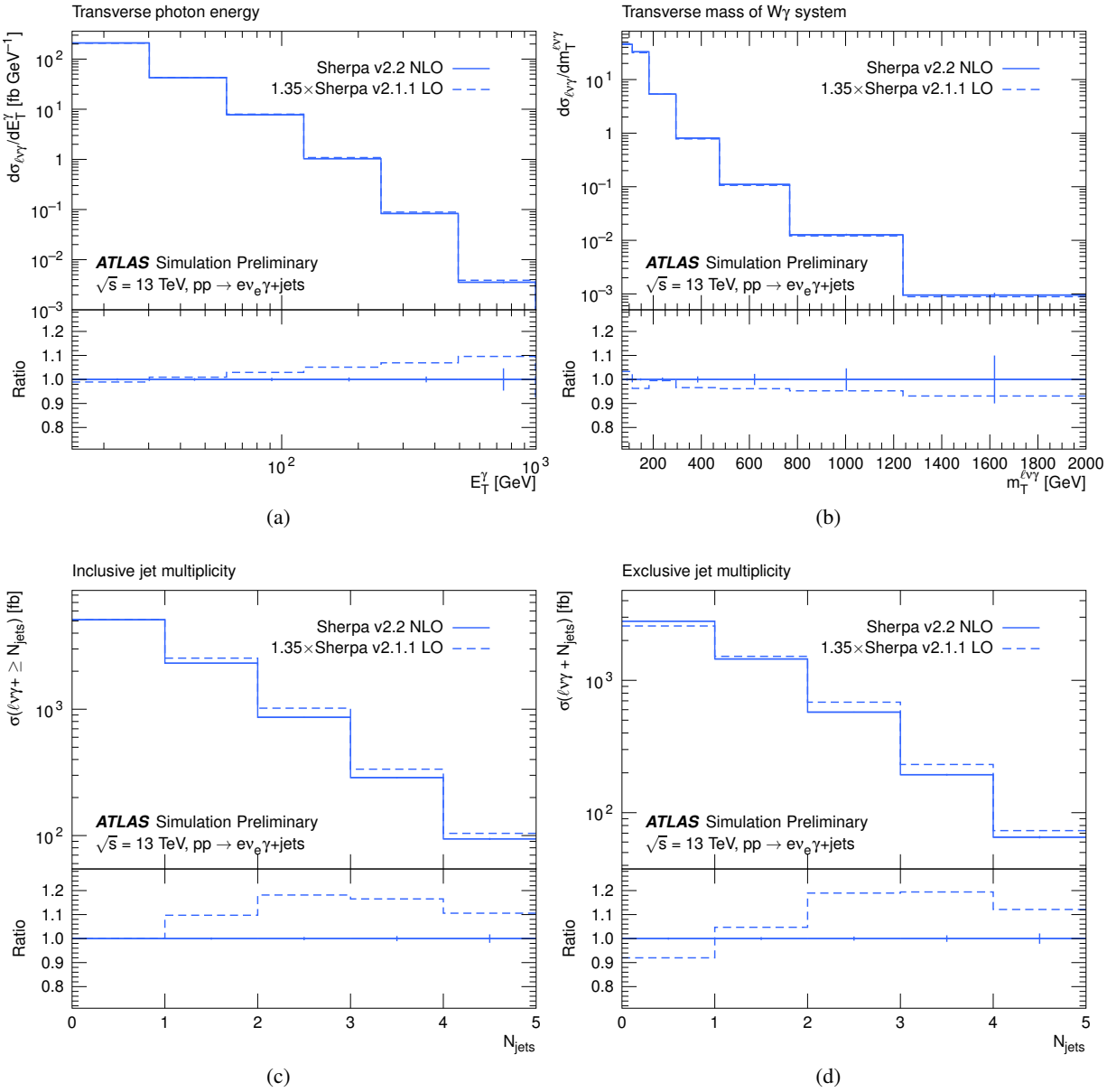

Figure 26: Comparison of differential distributions in $W^{\pm}\gamma$ production at 13 TeV.

8.2 $V(\rightarrow qq')+\gamma$ production

8.2.1 Generator setup

The processes of $V+\gamma$ ($V = W^{\pm}/Z$) in the final states of W/Z bosons decaying into hadrons are modeled using `Sherpa v2.1.1` and `MadGraph5_aMC@NLO v5.2.3.3` generators. The modeling is performed at LO with only on-shell W/Z bosons taken into account.

Both `Sherpa v2.1.1` and `MadGraph5_aMC@NLO v5.2.3.3` generate LO matrix elements for $V + \gamma +$ $0, 1, 2, 3$ jets. `Sherpa` merge the matrix elements with the parton shower using an ME+PS merging scale of $Q_{\text{cut}} = 20$ GeV. `MadGraph5_aMC@NLO` matrix elements are parton showered by `PYTHIA8` with `A14` tune and the `NNPDF2.3LO` PDF set and merged with CKKW scale. The Monte Carlo are produced for both `Sherpa` and `MadGraph5_aMC@NLO` in bins of Matrix Element level photon E_{T}: [140, 240], [240, 500], [500, 1000], [1000, 2000], [2000, E_{CMS}] GeV. A smooth isolation [55] with $n = 2$, $\epsilon = 0.025$, $\delta = 0.3$ is applied to the photons.

8.2.2 Generator comparisons

The modeling of $V\gamma$ hadronic final states by `MadGraph5_aMC@NLO` and `Sherpa` are investigated and compared in various kinematics truth observables of anti-k_t $R = 1.0$ boosted boson jets and truth isolated photon. The pre-selections applied to truth stable particles with HEPMC status code equal to 1 and in detail:

- At least one isolated photon, with $p_{\text{T}} > 140$ GeV and $|\eta| < 2.5$.
- At least one anti-k_t $R = 1.0$ truth jet with $p_{\text{T}} > 200$ GeV, $|\eta| < 2.1$, $\Delta R_{j\gamma} > 1.0$.

Figure 27 shows the `Sherpa` and `MadGraph5_aMC@NLO` $Z(\rightarrow q\bar{q}) + \gamma$ sample comparison in terms of both jet and photon kinematics for two specific photon E_{T} (GeV) slices: [140, 280], [280, 500] combined. The shapes are generally in good agreement except for the truth jet masses.

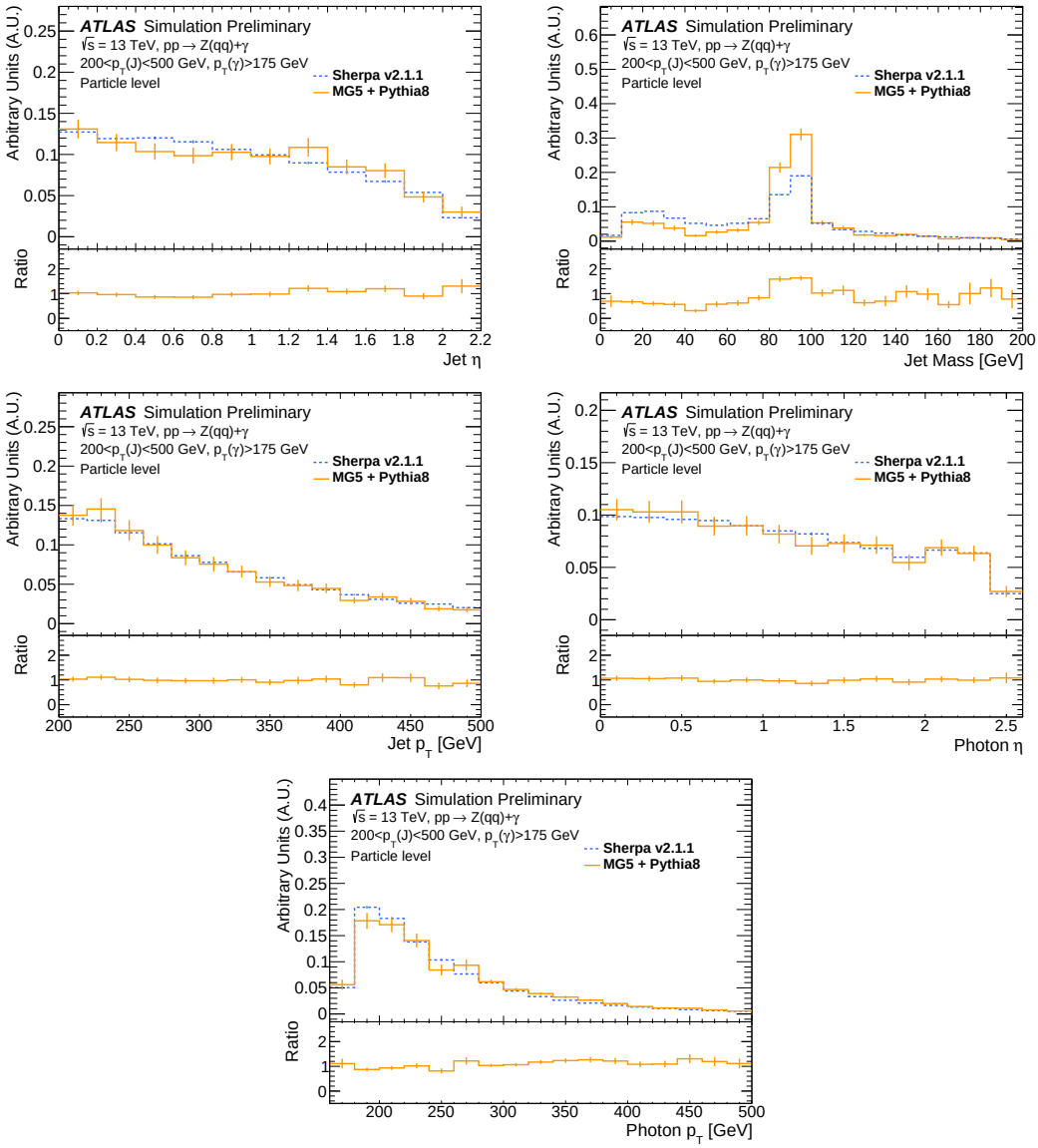

Figure 27: Differential normalised distributions of `MadGraph5_aMC@NLO` (Red) and `Sherpa` (Blue) $Z(\rightarrow q\bar{q}) + \gamma$ with matrix element photon E_{T} of [140, 500] GeV are compared for the observables of: truth jet η (upper left), mass (upper right), p_{T} (middle left) and photon η (middle right), E_{T} (bottom left). The shapes are compared after normalising both distributions to unity.

9 Conclusion

The Monte Carlo setup used by ATLAS to model multi-boson processes in 13 TeV pp collisions was described. State-of-the-art generators are utilised which were thoroughly validated and compared with each other in key kinematic distributions of the processes under study. The sample normalisations used by ATLAS were given as well and are generally based on the native generator cross-sections. Systematic uncertainties such as scale and PDF variations were described for the generators used as well as based on fixed-order cross section calculations to give an impact on sample normalisation.

References

[1] T. Gleisberg et al., *Event generation with SHERPA 1.1*, JHEP **02** (2009) 007, arXiv:0811.4622 [hep-ph].

[2] T. Gleisberg and S. Höche, *Comix, a new matrix element generator*, JHEP **0812** (2008) 039, arXiv:0808.3674 [hep-ph].

[3] S. Schumann and F. Krauss, *A Parton shower algorithm based on Catani-Seymour dipole factorisation*, JHEP **03** (2008) 038, arXiv:0709.1027 [hep-ph].

[4] S. Hoeche et al., *A critical appraisal of NLO+PS matching methods*, JHEP **09** (2012) 049, arXiv:1111.1220 [hep-ph].

[5] S. Hoeche et al., *QCD matrix elements + parton showers: The NLO case*, JHEP **04** (2013) 027, arXiv:1207.5030 [hep-ph].

[6] F. Cascioli, P. Maierhofer and S. Pozzorini, *Scattering Amplitudes with Open Loops*, Phys. Rev. Lett. **108** (2012) 111601, arXiv:1111.5206 [hep-ph].

[7] A. Denner, S. Dittmaier and L. Hofer, *Collier: a fortran-based Complex One-Loop LIbrary in Extended Regularizations*, Comput. Phys. Commun. **212** (2017) 220, arXiv:1604.06792 [hep-ph].

[8] H.-L. Lai et al., *New parton distributions for collider physics*, Phys. Rev. **D82** (2010) 074024, arXiv:1007.2241 [hep-ph].

[9] R. D. Ball et al., *Parton distributions for the LHC Run II*, JHEP **04** (2015) 040, arXiv:1410.8849 [hep-ph].

[10] S. Dulat et al., *New parton distribution functions from a global analysis of quantum chromodynamics*, Phys. Rev. **D93** (2016) 033006, arXiv:1506.07443 [hep-ph].

[11] L. A. Harland-Lang et al., *Parton distributions in the LHC era: MMHT 2014 PDFs*, Eur. Phys. J. **C75** (2015) 204, arXiv:1412.3989 [hep-ph].

[12] P. Nason, *A New method for combining NLO QCD with shower Monte Carlo algorithms*, JHEP **11** (2004) 040, arXiv:hep-ph/0409146 [hep-ph].

[13] S. Frixione, P. Nason and C. Oleari, *Matching NLO QCD computations with Parton Shower simulations: the POWHEG method*, JHEP **11** (2007) 070, arXiv:0709.2092 [hep-ph].

[14] S. Alioli et al., *A general framework for implementing NLO calculations in shower Monte Carlo programs: the POWHEG BOX*, JHEP **06** (2010) 043, arXiv:1002.2581 [hep-ph].

[15] E. Boos et al., 'Generic user process interface for event generators', *Physics at TeV colliders. Proceedings, Euro Summer School, Les Houches, France, May 21-June 1, 2001*, 2001, arXiv:hep-ph/0109068 [hep-ph], URL: http://lss.fnal.gov/archive/preprint/fermilab-conf-01-496-t.shtml.

[16] J. Alwall et al., *A Standard format for Les Houches event files*, Comput. Phys. Commun. **176** (2007) 300, arXiv:hep-ph/0609017 [hep-ph].

[17] T. Sjöstrand et al., *An Introduction to PYTHIA 8.2*, Comput. Phys. Commun. **191** (2015) 159, arXiv:1410.3012 [hep-ph].

[18] K. Nakamura et al., *Review of particle physics*, J. Phys. **G37** (2010) 075021.

[19] D. E. Groom et al., *Review of particle physics. Particle Data Group*, Eur. Phys. J. **C15** (2000) 1.

[20] T. Melia et al., *W+W-, WZ and ZZ production in the POWHEG BOX*, JHEP **11** (2011) 078, arXiv:1107.5051 [hep-ph].

[21] P. Nason and G. Zanderighi, W^+W^- , *WZ and ZZ production in the POWHEG-BOX-V2*, Eur. Phys. J. **C74** (2014) 2702, arXiv:1311.1365 [hep-ph].

[22] ATLAS Collaboration, *Measurement of the $Z/\gamma*$ boson transverse momentum distribution in pp collisions at $\sqrt{s}$ = 7 TeV with the ATLAS detector*, JHEP **2014** (2014) 55, arXiv:1406.3660 [hep-ex].

[23] J. Pumplin et al., *New generation of parton distributions with uncertainties from global QCD analysis*, JHEP **07** (2002) 012, arXiv:hep-ph/0201195 [hep-ph].

[24] D. J. Lange, *The EvtGen particle decay simulation package*, Nucl. Instrum. Meth. **A462** (2001) 152.

[25] J. Bellm et al., *Herwig 7.0 / Herwig++ 3.0 Release Note*, (2015), arXiv:1512.01178 [hep-ph].

[26] J. Alwall et al., *The automated computation of tree-level and next-to-leading order differential cross sections, and their matching to parton shower simulations*, JHEP **07** (2014) 079, arXiv:1405.0301 [hep-ph].

[27] ATLAS Collaboration, *ATLAS Pythia 8 tunes to 7 TeV data*, ATL-PHYS-PUB-2014-021, 2014, URL: http://cdsweb.cern.ch/record/1966419.

[28] R. Frederix et al., *Merging meets matching in MC@NLO*, JHEP **12** (2012) 061, arXiv:1209.6215 [hep-ph].

[29] S. Frixione and B. R. Webber, *Matching NLO QCD computations and parton shower simulations*, JHEP **06** (2002) 029, arXiv:hep-ph/0204244 [hep-ph].

[30] J. M. Butterworth, J. R. Forshaw and M. H. Seymour, *Multiparton interactions in photoproduction at HERA*, Z. Phys. **C72** (1996) 637, arXiv:hep-ph/9601371 [hep-ph].

[31] K. Hagiwara et al., *Probing the Weak Boson Sector in $e^+e^- \to W^+W^-$*, Nucl. Phys. B **282** (1987) 253.

[32] J. M. Campbell and R. K. Ellis, *An Update on vector boson pair production at hadron colliders*, Phys. Rev. **D60** (1999) 113006, arXiv:hep-ph/9905386 [hep-ph].

[33] J. M. Campbell, R. K. Ellis and C. Williams, *Vector boson pair production at the LHC*, JHEP **07** (2011) 018, arXiv:1105.0020 [hep-ph].

[34] J. M. Campbell, J. W. Huston and W. J. Stirling, *Hard Interactions of Quarks and Gluons: A Primer for LHC Physics*, Rept. Prog. Phys. **70** (2007) 89, arXiv:hep-ph/0611148 [hep-ph].

[35] M. Grazzini et al., *$W^\pm Z$ production at the LHC: fiducial cross sections and distributions in NNLO QCD*, (2017), arXiv:1703.09065 [hep-ph].

[36] M. Grazzini et al., *$W^\pm Z$ production at hadron colliders in NNLO QCD*, Phys. Lett. **B761** (2016) 179, arXiv:1604.08576 [hep-ph].

[37] M. Grazzini et al.,
W^+W^{--} production at the LHC: fiducial cross sections and distributions in NNLO QCD,
JHEP **08** (2016) 140, arXiv:1605.02716 [hep-ph].

[38] M. Grazzini, S. Kallweit and D. Rathlev,
ZZ production at the LHC: fiducial cross sections and distributions in NNLO QCD,
Phys. Lett. **B750** (2015) 407, arXiv:1507.06257 [hep-ph].

[39] Bothmann, Enrico and Schonherr, Marek and Schumann, Steffen,
Reweighting QCD matrix-element and parton-shower calculations, Eur. Phys. J. **C76** (2016) 590,
arXiv:1606.08753 [hep-ph].

[40] A. D. Martin et al., *Parton distributions for the LHC*, Eur. Phys. J. **C63** (2009) 189,
arXiv:0901.0002 [hep-ph].

[41] M. Cacciari, G. P. Salam and G. Soyez, *The Anti-k(t) jet clustering algorithm*,
JHEP **04** (2008) 063, arXiv:0802.1189 [hep-ph].

[42] ATLAS Collaboration, *Measurements of the Higgs boson production cross section at* 7, 8 *and* 13 *TeV centre-of-mass energies and search for new physics at* 13 *TeV in the $H \to ZZ^* \to \ell^+\ell^-\ell'^+\ell'^-$ final state with the ATLAS detector*, ATLAS-CONF-2015-059, 2015, URL: https://cds.cern.ch/record/2114825.

[43] ATLAS Collaboration, *Study of the Higgs boson properties and search for high-mass scalar resonances in the $H \to ZZ^* \to 4\ell$ decay channel at $\sqrt{s} = 13$ TeV with the ATLAS detector*, ATLAS-CONF-2016-079, 2016, URL: https://cds.cern.ch/record/2206253.

[44] ATLAS Collaboration, *Measurement of the ZZ Production Cross Section in pp Collisions at $\sqrt{s}$ = 13 TeV with the ATLAS Detector*, (2015), arXiv:1512.05314 [hep-ex].

[45] B. Biedermann et al.,
Electroweak corrections to $pp \to \mu^+\mu^-e^+e^- + X$ at the LHC: a Higgs background study,
Phys. Rev. Lett. **116** (2016) 161803, arXiv:1601.07787 [hep-ph].

[46] B. Biedermann et al., *Next-to-leading-order electroweak corrections to the production of four charged leptons at the LHC*, JHEP **01** (2017) 033, arXiv:1611.05338 [hep-ph].

[47] S. Gieseke, T. Kasprzik and J. H. Kühn,
Vector-boson pair production and electroweak corrections in HERWIG++,
Eur.Phys.J. **C74** (2014) 2988, arXiv:1401.3964 [hep-ph].

[48] ATLAS Collaboration, *Measurement of the $W^\pm Z$ boson pair-production cross section in pp collisions at $\sqrt{s} = 13$ TeV with the ATLAS Detector*, Phys. Lett. B **762** (2016) 1,
arXiv:1606.04017 [hep-ex].

[49] ATLAS Collaboration,
Measurement of $W^\pm Z$ boson pair-production in pp collisions at $\sqrt{s} = 13$ TeV with the ATLAS Detector and confidence intervals for anomalous triple gauge boson couplings,
ATLAS-CONF-2016-043, 2016, URL: https://cds.cern.ch/record/2206093.

[50] ATLAS Collaboration, *Measurement of total and differential W^+W^- production cross sections in proton–proton collisions at $\sqrt{s} = 8$ TeV with the ATLAS detector and limits on anomalous triple-gauge-boson couplings*, JHEP **09** (2016) 029, arXiv:1603.01702 [hep-ex].

[51] ATLAS Collaboration, *Measurement of W^+W^- production in association with one jet in proton–proton collisions at $\sqrt{s} = 8$ TeV with the ATLAS detector*, (2016),
arXiv:1608.03086 [hep-ex].

[52] ATLAS Collaboration,
Observation and measurement of Higgs boson decays to WW^* with the ATLAS detector,
Phys. Rev. D **92** (2015) 012006, arXiv:1412.2641 [hep-ex].

[53] B. Jager and G. Zanderighi, *NLO corrections to electroweak and QCD production of W^+W^+ plus two jets in the POWHEG BOX*, JHEP **11** (2011) 055, arXiv:1108.0864 [hep-ph].

[54] ATLAS Collaboration, *Measurement of $W^\pm W^\pm$ vector-boson scattering and limits on anomalous quartic gauge couplings with the ATLAS detector*, (2016), arXiv:1611.02428 [hep-ex].

[55] S. Frixione, *Isolated photons in perturbative QCD*, Phys. Lett. **B429** (1998) 369, arXiv:hep-ph/9801442 [hep-ph].

[56] S. Alioli et al., *ZZ production in gluon fusion at NLO matched to parton-shower*,
Phys. Rev. **D95** (2017) 034042, arXiv:1609.09719 [hep-ph].

[57] N. Kauer and G. Passarino,
Inadequacy of zero-width approximation for a light Higgs boson signal, JHEP **08** (2012) 116, arXiv:1206.4803 [hep-ph].

[58] N. Kauer, *Interference effects for $H \to WW/ZZ \to \ell\bar{\nu}_\ell\bar{\ell}\nu_\ell$ searches in gluon fusion at the LHC*, JHEP **12** (2013) 082, arXiv:1310.7011 [hep-ph].

[59] F. Cascioli et al., *Precise Higgs-background predictions: merging NLO QCD and squared quark-loop corrections to four-lepton + 0,1 jet production*, JHEP **01** (2014) 046, arXiv:1309.0500 [hep-ph].

[60] K. Melnikov and M. Dowling,
Production of two Z-bosons in gluon fusion in the heavy top quark approximation,
Phys. Lett. B **744** (2015), arXiv:1503.01274 [hep-ph].

[61] F. Caola et al., *QCD corrections to W^+W^- production through gluon fusion*,
CERN-PH-TH-2015-276 (2015), arXiv:1511.08617.

[62] F. Caola et al., *QCD corrections to ZZ production in gluon fusion at the LHC*,
Phys. Rev. D **92** (2015) 094028, arXiv:1509.06734 [hep-ph].

[63] G. Passarino, *Higgs CAT*, Eur. Phys. J. **C74** (2014) 2866, arXiv:1312.2397 [hep-ph].

[64] M. Bonvini et al.,
Signal-background interference effects for $gg \to H \to W^+W^-$ beyond leading order,
Phys. Rev. D **88** (2013), arXiv:1304.3053 [hep-ph].

[65] C.S. Li et al.,
Soft gluon resummation in the signal-background interference process of $gg(\to h^*) \to ZZ$,
JHEP **08** (2015), arXiv:1504.02388 [hep-ph].

[66] F. Caola et al., *QCD corrections to vector boson pair production in gluon fusion including interference effects with off-shell Higgs at the LHC*, JHEP **07** (2016) 087,
arXiv:1605.04610 [hep-ph].

[67] J. M. Campbell et al., *Two loop correction to interference in $gg \to ZZ$*, JHEP **08** (2016) 011,
arXiv:1605.01380 [hep-ph].

[68] ATLAS Collaboration, *Search for new phenomena in the $Z(\to \ell\ell) + E_{\mathrm{T}}^{\mathrm{miss}}$ final state at $\sqrt{s} = 13$ TeV with the ATLAS detector*, ATLAS-CONF-2016-056, 2016,
URL: https://cds.cern.ch/record/2206138.

[69] ATLAS Collaboration, *Search for the Standard Model Higgs boson produced in association with a vector boson and decaying to a $b\bar{b}$ pair in pp collisions at* 13 *TeV using the ATLAS detector*, ATLAS-CONF-2016-091, 2016, URL: https://cds.cern.ch/record/2206813.

[70] S. Hoeche et al.,
Triple vector boson production through Higgs-Strahlung with NLO multijet merging,
Phys. Rev. **D89** (2014) 093015, arXiv:1403.7516 [hep-ph].

[71] K. A. Olive et al., *Review of Particle Physics*, Chin. Phys. **C38** (2014) 090001.

[72] K. Arnold et al., *VBFNLO: A Parton level Monte Carlo for processes with electroweak bosons*, Comput. Phys. Commun. **180** (2009) 1661, arXiv:0811.4559 [hep-ph].

[73] K. Arnold et al., *VBFNLO: A Parton Level Monte Carlo for Processes with Electroweak Bosons – Manual for Version 2.5.0*, (2011), arXiv:1107.4038 [hep-ph].

[74] J. Baglio et al., *Release Note - VBFNLO 2.7.0*, (2014), arXiv:1404.3940 [hep-ph].

[75] A. Buckley et al., *Rivet user manual*, Comput. Phys. Commun. **184** (2013) 2803, arXiv:1003.0694 [hep-ph].

[76] ATLAS Collaboration, *Search for triboson $W^{\pm}W^{\pm}W^{\mp}$ production in pp collisions at $\sqrt{s} = 8$ TeV with the ATLAS detector*, Eur. Phys. J. **C77** (2017) 141, arXiv:1610.05088 [hep-ex].

[77] A. Buckley et al., *LHAPDF6: parton density access in the LHC precision era*,
Eur. Phys. J. C **75** (2015) 132, arXiv:1412.7420 [hep-ph].